DOI:10.15774/PPKE.ITK.2023.004

Dynamical Analysis of Biological Feedback & Feedforward Systems

A Thesis Submitted For the Degree of Doctor of Philosophy

By

Suchana Chakravarty

Supervisor: Prof. Dr. Attila Csikász-Nagy, DSc

Pázmány Péter Catholic University
Faculty of Information Technology and Bionics
Roska Tamás Doctoral School of Sciences and Technology

Budapest, 2023

DOI:10.15774/PPKE.ITK.2023.004

Table of Contents

DOI:10.15774/PPKE.ITK.2023.004

DOI:10.15774/PPKE.ITK.2023.004

DOI:10.15774/PPKE.ITK.2023.004

DOI:10.15774/PPKE.ITK.2023.004

List of Figures

DOI:10.15774/PPKE.ITK.2023.004

DOI:10.15774/PPKE.ITK.2023.004

DOI:10.15774/PPKE.ITK.2023.004

List of Tables

DOI:10.15774/PPKE.ITK.2023.004

“If we knew what it was we were doing, it would not be called research, would it?”

— Albert Einstein

This thesis is dedicated to my beloved parents.

DOI:10.15774/PPKE.ITK.2023.004

Acknowledgements

Since so many people have helped me with my PhD, the acknowledgements end up being longer than the thesis abstract.

First and foremost, I'd like to thank my supervisor, Professor Attila Csikász-Nagy, for all of his assistance, comments, advice, and guidance over the years in regard to my professional work, scientific publications, presentations, and a general navigation through the world of research, as well as for his patience with me. From him, I have learnt patience and perseverance. Thank you for understanding me and my concerns and for assisting me in a variety of ways with my thesis work and in life. I'd also want to thank Professor Luca Cardelli and Professor Christian I. Hong for their help with my research.

I would like to extend my sincere thanks to Professor Zoltán Gáspári for putting his faith in me and letting me teach the preparatory chemistry and biology courses in the faculty and also to Professor Péter Szolgay for his useful comments and guidance during the Friday Program . I sincerely extend my gratitude to the Head of our Doctoral School, Professor Gábor Szederkenyi, and my program leader, Professor Sándor Pongor, for their academic support during my research. I am also grateful to current Dean Professor Cserey György and former Dean Professor Iván Kristóf for their assistance in a variety of areas. I am thankful to Mrs. Vida Tivadarné because, without her, getting my Ph.D. would have been a lot more challenging. She has a kind heart and is always willing to provide help when I'm in need. I'd want to thank all the professors and non-teaching staff members who helped me in many ways. Many thanks to András Serf for assisting me at the library.

I am grateful to Juhász János, Luca Laurenti and Ágnes Szabó for allowing me to approach them at any moment with questions, since the following dissertation would not have been accomplished without their chats, assistance, and advice. I'd like to thank Dr. Debashis Barik,UoH, for his guidance and for introducing me to this subject back in India. I'd want to convey my heartfelt thanks to my university (Visva Bharati University) professors in India, particularly Pranab Sarkar, Bidhan Chandra Bag, and Sudip Kumar Mondal, who helped me mould into the person I am today.

DOI:10.15774/PPKE.ITK.2023.004

For me, Budapest has been a fantastic environment for developing new skills and expanding my horizons. When I initially arrived in Budapest, the first person I met was Alexandra Venczel. I'm grateful to her for all the support she gave me when I first arrived in Hungary. My other dorm friends, Jalal Alafandi, Ayşegül Sayin, and Obada Muhammad are all very important to me, and I'd want to express my gratitude to them as well. Additionally, I'd want to express my admiration for my housemates, Ismat Ara Roksana, Shuaa Bhatti, and Livia Pelepciuc, with whom I've had a lot of wonderful experiences. Pallavi Majumder is a wonderful friend and companion I met in Budapest. Our trip adventures in many countries and developing new experiences together have been fantastic. I am thankful to her for all of our shared experiences. I'd also want to thank Prabal Dutta, who has always been there for me as a guardian. I feel blessed to have them both in my life.

I consider myself very blessed to have childhood best friends like Ushasi Ghosh and Debraj Bhattacharya. They are the first people I call when I have a problem. They are always there for me, no matter what. I gratefully appreciate them for their support in many different ways.

I would also like to extend my thanks to Soutrick Das, Archana GR, Hafizur Rahaman, Ananya Pal, Prakash Majee, Milan Singh, Sanjib Barui, Jyotirmoy Ruidas, Sinchan Banerjee, Geetanjali Singhania, Shreya Bera, Adrija Roy, and Sugata Goswami for being in my life and adding so much essence at various points in my life.

I would want to express my heartfelt thanks to my parents, Sumantra Chakravarty (baba) and Sukanya Chakravarty (ma), for embedding values in me and raising me to be a better person, as well as for their unwavering support in allowing me to fly in a broader sky and never limiting my wings. I'd also want to thank my sister Suchetana Chakravarty for being my rock. I appreciate my paternal grandpa, Subrata Chakravarty, and maternal grandma, Dipa Dey, for always wanting to hear my voice and staying in touch with me no matter how far away I was from them. My heartfelt gratitude to my late maternal grandpa, Bibhuti Bhusan Dey, and late paternal grandma, Gita Chakravarty, who would have been overjoyed to see me receive a doctoral degree today. I would want to express my gratitude to my Uncle Joy Roy Chowdhury for being a part of my life. Anupam Dey has been an integral part of everything I've been working on. I am grateful to him for always being there for me and for providing such strong support.

DOI:10.15774/PPKE.ITK.2023.004

I acknowledge the Tempus Public Foundation in Hungary and the University Grant Commission in India for awarding me the Stipendium Hungaricum Scholarship. My work was partially funded by the EFOP-3.6.3-VEKOP-16-2017-00002 grant, the Thematic Excellence Programme - TKP2020-NKA-11 and Tempus Public Foundation's Stipendium Hungaricum Dissertation Scholarship. I certainly could not have gone on this path without the help of my defense committee, who generously shared their knowledge and skills.

DOI:10.15774/PPKE.ITK.2023.004

Abstract

The tiny regulatory network motifs that make up bigger, more complicated signaling pathways are the fundamental units of any physiological pathways. There are mainly two types of regulatory motifs known as feedforward and feedback loops. While a feedback loop operates in both ways, the feedforward loop only operates in single direction. Because feedforward loops are such efficient network motifs inside a living system, they are able to alter the behavior of the system such that it can react to a set of predetermined criteria. In contrast, feedback loops are designed to operate in such a manner that they modify the dynamic behavior of the individual components in order to keep the behavior of the system stable. Furthermore, a feedback loop can appear in the form of either a switch or an oscillator. Significant biological circuits, for instance, the cell cycle, gene regulation, circadian rhythms, and so on, make application of the qualities of these two dynamical network motifs.

Given the enormity of network topologies, many ways to investigate their dynamical features have been proposed. In my thesis, I examine the small basic networks to get a better understanding of these complicated dynamics.

Because of the biochemical noise, a live cell normally functions in a noisy environment, and the influence of the noise might potentially modify the dynamics and outcomes. Despite various stochastic sources, physiological processes work accurately. What makes signaling pathways accurate and robust despite noise? Do regulatory motif topologies play an important role? In my thesis, I investigate how various kinds of feedforward and feedback loops generate robust reactions. I elaborate on the unique qualities of circadian oscillations such as temperature compensation and noise resilience. I also made steps in uncovering the key controllers of the circadian oscillatory network enabling temperature compensation.

A theoretical approach has been followed during the course of this study. Consequently, in order to investigate the dynamical properties of these tiny motifs, I have carried out mathematical modeling and simulations with the aid of the software programs MATLAB and Kaemika. A systematic approach has been carried out to understand the dynamical behavior of small regulatory network motifs like feedforward and feedback loops.

DOI:10.15774/PPKE.ITK.2023.004

List of Abbreviations

TF : Transcription Factor

FFL : Feedforward Loop

isolated FFLs : isolated Feedforward Loops

coupled FFLs : coupled Feedforward Loops

PFB : Positive Feedback

NFB : Negative Feedback

DNFB : Double Negative Feedback

SN : Saddle-Node

DNFL-d : Double Negative Feedback loop at the degradation

cFFL : coherent Feedforward Loop

iFFL : incoherent Feedforward Loop

ODE : Ordinary Differential Equation

CRN : Chemical Reaction Network

CME : Chemical Master Equation

SSA : Stochastic Simulation Algorithm

CLE : Chemical Langevin Equation

LNA : Linear Noise Approximation

MAPK : Mitogen Activated Protein Kinases

CV : Coefficient of Variation

minp-FFLs : multi-input coupled Feedforward Loops

mint-FFLs : multi-intermediate coupled Feedforward Loops

AU : Arbitrary Unit

TTFL : Transcription-Translation Feedback Loop

DOI:10.15774/PPKE.ITK.2023.004

PTO: Post-Translational Oscillator

ATP : Adenosine Triphosphate

T432 : Threonine 432

S431: Serine 431

BIC : Bayesian Information Criterion

DOI:10.15774/PPKE.ITK.2023.004

Chapter 1

Introduction

DOI:10.15774/PPKE.ITK.2023.004

1.1. Overview

Computational and systems biology nowadays largely rely on biological network analysis. Physiological functions may now be better understood because of systems analysis, which gives a unified understanding to explain the interrelationships between various parts of complex networks. In the biological context, cells include a variety of mechanisms to carry out certain physiological functions. Furthermore, biological pathways are dynamic on both the evolutionary timescale and the much shorter physiological timescale [1]. Different metabolites, including genes, mRNAs, proteins, etc., encompass the biological process at diverse spatial and temporal domains [2,3].

With the advent of high-throughput technology, biologists now see the cell as a big and complex system made up of many smaller systems that are widely interconnected. "Network motifs," which are tiny biological repeating units [4,5], form a core regulatory network. The dynamical activity that is responsible for global biochemical functions is intimately linked to the architecture of these network motifs. Thus, it is evident that studying these network topologies is crucial to comprehending the intricate dynamic nature of biological processes.

In nature, the interaction time of any biological process is random [6,7]. Cells often modify the outcomes due to the presence of chemical noise. In order to govern metabolic pathways, it is necessary to understand numerous sources of stochasticity and how the network topology responds to the noise. Thus, stochastic modeling is the ideal way to depict dynamic network analysis [8].

1.2. Scope of the Research

Cells, combine many processes in order to execute distinct functions. To coordinate with external signals, these systems adapt or transform their responses through a succession of molecular events such as chemical reactions. Cell signaling is a fundamental mechanism that all biological systems employ to communicate to their surroundings [9]. Multicellular organisms operate effectively because of the well-coordinated signaling pathways. In signaling pathways, biomolecules such as genes, mRNAs, transcription factors (TFs), and proteins interact with each other and lead to functional and structural variations in expression levels [10].

DOI:10.15774/PPKE.ITK.2023.004

Small regulatory network motifs are the building blocks of larger, more complex signaling pathways. Feedforward loops (FFLs) [4,5] and feedback loops [11,12] are two distinct forms of regulatory motifs that are categorized according to the type of regulation that exists between the two regulators involved. It is important to note that whereas the feedforward loop works in one direction, a feedback loop works in both directions. Motifs' dynamical behavior may be altered by their connections to one another in a bigger network [13,14]. This shows that the study of the isolated network motifs is not adequate to explain the overall dynamic characteristics of a biological function.

FFLs are such an effective network motifs in a biological system that they change the system’s behavior in order to respond to a preset criteria. FFLs are not always isolated; instead, they are paired with other FFLs (coupled FFLs) [15,16] and this changes their noise-reduction abilities, making them a better noise reducer.

On the other hand, feedback loops function in such a way that they adjust the dynamics of the individual units so that the system's behavior can be maintained. Depending on the network's design, feedback loops may either be a switch or an oscillator. There are various biological processes that depend on oscillators, including the cell cycle and the circadian clock [17]. Temperature compensation [18] is one of the most well-known essential features of circadian oscillator. The exact mechanisms by which the clock maintains a temperature-compensated and a robust circadian oscillatory network are still a mystery.

Furthermore, the mathematical modelling and representation of dynamical systems makes it feasible to conduct research on the analysis of the dynamical properties of networks. Computer science and biology work hand in hand to cope with the growing volume of biological data. To describe biological systems, certain algorithms and statistical analysis can be useful.

Stochasticity, also known as chemical noise, is inherent in chemical processes and may interfere with and influence the result. The purpose of this thesis is to comprehend the dynamic characteristics of various regulatory networks and their behavioral changes towards the noisy environment. In this thesis, robustness of these networks has been tested systematically. This dissertation includes an in-depth investigation of the robustness of feedback loops in a circadian oscillator as well as an understanding of how

DOI:10.15774/PPKE.ITK.2023.004

temperature compensation works. This thesis tries to unravel the mystery associated with the dynamical features of various regulatory networks.

1.3. Outline of the Thesis

The study objectives and views have been laid forth in this first chapter. It describes how network architecture influences their biological function. An interdisciplinary approach to dynamic network analysis has been suggested. Furthermore, the scope of this study and the contributions to this research have been outlined in this chapter as well.

The second chapter briefly describes about the earlier studies related to this thesis. It has depicted different network architectures associated with various biological functions. The description of a biological dynamical system has been presented in terms of inter-disciplinary subjects including mathematics, physics, chemistry, biology, statistics, and computer simulations.

The methods are explained in the third chapter. This section discusses the theoretical approaches used and the commercial software programs MATLAB and Kaemika, which were used to perform analyses on the models presented in chapters 4 and 5.

The first result section, chapter 4, investigates feedforward loops systematically when they are present in isolated or coupled form. Extensive research has been conducted to determine whether or not these systems have the capacity to reduce noise without compromising their signal transducing capabilities. It is shown that the network topology and logical gate of some isolated and coupled feedforward loops are advantageous for signal transduction and noise reduction. Both temperature compensation and robustness to cellular noise, two fundamental properties of the circadian clock, are discussed in the second result section, chapter 5. The existence of such time-delayed negative feedback mechanisms in the regulatory pathway causes the majority of circadian oscillations. Cyanobacteria's circadian rhythm, on the other hand, is governed by an oscillator with a powerful positive feedback loop. The purpose is to look at the robustness and temperature adjustment capabilities of circadian clocks using network design with positive and negative feedbacks.

In conclusion, this work is summarized in chapter 6, which also discusses the importance of the aforementioned research to the overall project. In its final section, it provides an overview of potential future research avenues that are a direct result of this dissertation.

DOI:10.15774/PPKE.ITK.2023.004

1.4. List of Publications

[J1] **S. Chakravarty** and A. Csikász-Nagy, "Systematic analysis of noise reduction properties of coupled and isolated feedforward loops," *PLOS COMPUTATIONAL BIOLOGY*, vol. 17, no. 12, pp. e1009622, 2021.

[J2] **S. Chakravarty**, C. I. Hong , and A. Csikász-Nagy, "Systematic analysis of negative and positive feedback loops for robustness and temperature compensation in circadian rhythms," *NPJ SYSTEMS BIOLOGY AND APPLICATIONS*, vol. 9, no. 1, pp. 5, 2023.

[C1] **S. Chakravarty** and A. Csikász-Nagy, "Biological noise can be reduced by coupled feed forward loops," *JEDLIK LABORATORIES REPORTS*, vol. 7, no. 4, pp. 78–80, 2019. (Poster)

[C2] **S. Chakravarty**, "Reducing the Effects of Biological Noise by Coupled Feed Forward Loops," *PHD PROCEEDINGS ANNUAL ISSUES OF THE DOCTORAL SCHOOL FACULTY OF INFORMATION TECHNOLOGY AND BIONICS*, vol. 14, pp. 13, 2019.

[C3] **S. Chakravarty**, "Feed forward loops towards potential noise reduction," *PHD PROCEEDINGS ANNUAL ISSUES OF THE DOCTORAL SCHOOL FACULTY OF INFORMATION TECHNOLOGY AND BIONICS*, vol. 15, pp. 13, 2020.

[C4] **S. Chakravarty**, "Studying the robustness of biological oscillators," *PHD PROCEEDINGS ANNUAL ISSUES OF THE DOCTORAL SCHOOL FACULTY OF INFORMATION TECHNOLOGY AND BIONICS*, vol. 16, pp. 13, 2021.

[C5] **S. Chakravarty**, "Investigating the robustness of biological oscillators," *PHD PROCEEDINGS ANNUAL ISSUES OF THE DOCTORAL SCHOOL FACULTY OF INFORMATION TECHNOLOGY AND BIONICS*, vol. 17, pp. 14, 2022.

1.5. Oral Presentations

[O1] **S. Chakravarty** and A. Csikász-Nagy, "Noise reducing capabilities of feed-forward loops," *Information and Computation special issue (not published yet)*, HSB 2020: 7th International Workshop on Hybrid Systems Biology. (Oral Presentation)

DOI:10.15774/PPKE.ITK.2023.004

Chapter 2

Background

DOI:10.15774/PPKE.ITK.2023.004

2.1. Dynamics of Biological Processes

The cell is the smallest and the most fundamental unit of life. Multicellular organisms are just as common as single-celled ones. Humans, for example, contain around 10^{14} cells arranged into approximately 200 tissues [3]. Biological operations are regulated by chemical reactions that take place in molecular networks. These wireless molecular networks enable proteins, RNA, DNA, and small molecules to interact with one another and carry out signaling and energy transfer processes. A comprehensive understanding of the dynamical behaviors and properties of biological processes is always challenging. The complexity arises when cells integrate a multitude of activities to perform specialized roles.

The individual functions of discrete entities cannot explain the overall behavior of biological processes [19]. Integrative insights are a valuable tool for comprehending the function of biological processes. Technological advancements and increased cross-talk across many disciplines of study are driving the integrated approach. The amalgamation of the concepts of physics, chemistry, biology, and mathematics along with technology helps to unveil the properties of dynamical biological networks. The representation of biological networks as dynamical mathematical models, in fact, facilitated the analysis of their dynamical characteristics [8]. Theoretical computer science and algorithmic applications [20,21] can also be used to shed insight on the problem of understanding biological systems.

The biological molecular networks exhibit strong non-linear behavior due to a large number of coupled interactions between molecular species [22]. Certain small recurrent patterns of interactions between entities resulted in the same dynamical behaviors, but not always in the same biological functions [4,23,24]. These recurrent patterns are known as network motifs. Network motifs are frequently used to build the main regulatory networks that govern cellular processes. As a result, studying these network motifs is critical for understanding the wider complex network pathways of the biological system and its activities.

Feedback [11,12] and feedforward loops [4,5] are the most typical network motifs. These are depicted as dynamic phenomena in which quantities like protein, RNA, metabolites, and other cell substances are considered as functions of time. The numerous components of a system and their interactions are best described as networks, which are primarily

DOI:10.15774/PPKE.ITK.2023.004

depicted as graphs with thousands of nodes connecting to thousands of vertices. Nodes in these networks represent any type of biological units, such as proteins, while edges describe biochemical interactions, such as activation or inhibition [25]. Interactions between nodes can be either unidirectional or bidirectional. The dynamical aspects of complex biological networks can be deciphered by knowing the dynamical properties of such building blocks.

2.2. Classifications of Network Motifs

This section focuses on network motif classifications. All of these motifs are important in biological systems. It is worthwhile to investigate regulatory motifs in molecular control systems and their potential functional importance in signal processing and output creation.

2.2.1. Simple Regulations

Production and decay interactions are the most basic kind of rules. Production is continually increasing the amount of a molecular species X in the system, whereas decay is consistently removing this species from the system (Figure 2.1).

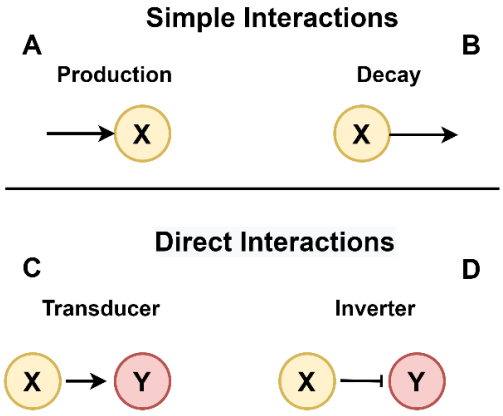

Figure 2.1: Illustration of simple interactions.
Production (A) and decay (B) processes are shown in the top panel. The bottom panel represents two fundamental modes of direct interactions- the activation process (known as a transducer) (C) and the inhibition process (known as an inverter) (D). The pointed arrow represents activation, whereas the blunt-headed arrow denotes inhibition.

There is another kind of simple regulation, which is termed direct interaction. Direct interactions occur when two molecular species, such as X and Y, interact with unfixed

DOI:10.15774/PPKE.ITK.2023.004

concentrations. This mechanism of direct interaction is separated into two subcategories: transducer and inverter. In the case of a transducer, X activates Y, but in the case of an inverter, X inhibits Y (Figure 2.1). The sign of the signal is retained for transducers, whereas it is reversed for inverters. In signal-transduction and transcription processes, both transducer and inverter systems are prevalent [4,24].

2.2.2. Feedback Loops

The autoregulation process is one of the most basic types of feedback regulation. A molecular species X auto-activates or auto-inhibits its own activity. An example of auto-activation (Figure 2.2A, B) is when a transcription factor induces the transcription of its own gene. In the post translational modifications, auto-inhibition is a common example.

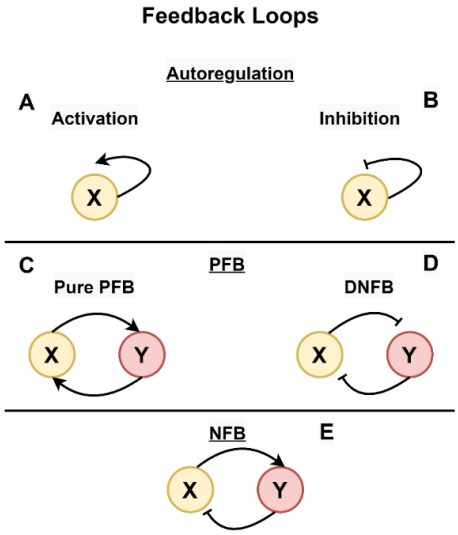

Figure 2.2: Influence diagram of feedback loops.

In the upper panel, the autoregulation processes are shown. Autoregulation refers to either autoactivation (A) or autoinhibition (B). The middle panel shows two forms of Positive Feedback Loops (PFB): pure PFB (C) with all positive interactions and a double negative feedback loop (DNFB) (D) with two mutual inhibitory interactions resulting in an overall positive effect. The schematic diagram of a Negative Feedback Loop (NFB) is shown in the lower panel (E), with two species linked by activatory and inhibitory interactions. The pointed arrow indicates activation, whereas the blunt-headed arrow implies inhibition.

The two molecular species that promote each other's activity are classic examples of feedback loops. There are two different kinds of feedback loops: positive (Figure 2.2C, D) and negative (Figure 2.2E). Positive feedback loops (PFB) boost the production of the species engaged in the loop. That is, molecular species govern production in the same way that they are regulated. This PFB can be either a mutual activatory (known as a

DOI:10.15774/PPKE.ITK.2023.004

purely positive feedback loop) or mutual inhibitory (known as double negative feedback (DNFB) loop). A negative feedback loop (NFB) is one, in which the output and input nodes provide opposing functions.

The feedback loop can function as a switch or as an oscillator. Because of the presence of an ultrasensitive signal and a positive feedback loop, two stable steady states (known as ON/OFF states) can be formed. This will lead to a switch like behavior, known as Bistable switches. These PFB loops play critical roles in cell fate decisions. Negative feedback loops (NFB) maintain homeostasis and can cause oscillations. Sustained oscillation is produced by the combination of PFB and NFB loops.

Time course simulations provide a visualization of the dynamical nature of these network motifs. Biological processes progress from a transitory to a stable state. These stable states can be of two types: sustained oscillators, often known as limit cycles in mathematics, or steady states. A steady behavior means that the system's state does not change over time. According to Lyapunov functions [26], this is known as a fixed attractor. A sustained oscillator has steady behavior since it repeats the same pattern throughout time and is known as a periodic attractor [26,27].

2.2.2.1. Bistable Switch

Non-linearity and PFB loops are essential for a system to be a bistable switch [26]. Bistable systems are very important in molecular signaling pathways. These switches can convert a gradient signal to a binary (on / off) response. Along with the signal level changes the response of a bistable switch shifts between the high and low activation states [27]. A bistable switch has both stable and unstable states [26]. Bifurcation points are the precise locations where a system's stability shifts, i.e. when a molecular species transitions from being stable to unstable or vice versa. In bistable systems, these points are known as saddle-nodes (SN), where a saddle is an unstable state, and a node is a stable state. Hysteresis is a significant feature observed in bistable systems. Hysteresis maintains the system in the switched state even in the absence of a continuous signal, making it resistant to signal perturbations or noise [26,27]. The diagram of a bistable switch has been shown in Figure 2.3. The equations for the DNFL-d [28] model and the parameter values are taken from the article published by Chakravarty, S.; Barik, D [28].

DOI:10.15774/PPKE.ITK.2023.004

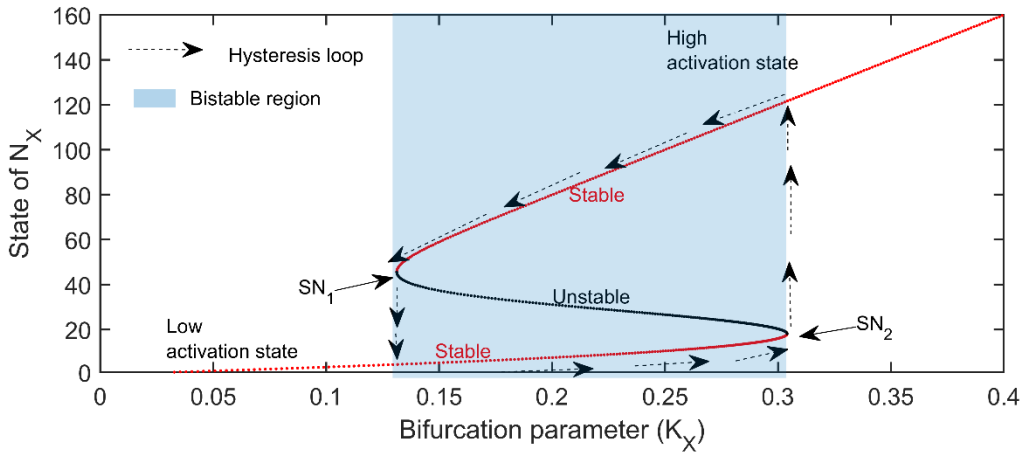

Figure 2.3: Bifurcation diagram of a bistable switch.

For a bifurcation parameter (K_X) the bifurcation diagram of a DNFL-d model is shown. The solid red lines represent N_X's stable state, while the black solid line represents the unstable state. The hysteresis loop is shown by the dashed arrow-line that circles the N_X states. The bistable zone is shown by the blue shade. Two saddle-node points SN_1 and SN_2 are indicated in the diagram. The mathematical model and the parameter values are chosen from the article by Chakravarty et al. [28].

2.2.2.2. Oscillators and Limit Cycles

There are many instances of oscillatory dynamics in the biological system. These oscillations are sometimes referred to as the limit cycle in mathematics [26,27]. Oscillatory behaviors result in periodicity since they are repetitive. In a biological context, non-linearity and NFB loops are directly connected to the formation of oscillatory dynamics. For biological systems, the emergence of an oscillatory rhythm is a very beneficial characteristic. Time and spatial oscillations are present all across nature and are essential to dynamic biological activities. Oscillations may be seen in a number of biological processes, including circadian rhythms, the cell cycle, and various metabolic activities [29].

One of these oscillators, the circadian oscillator [30], is important because it works as a biological timekeeper [31]. Almost every living creature has a 24-hour internal clock. Along with temperature compensation [18], the circadian clock has several other important characteristics such as tunability, entrainment, and robustness [32]. Temperature compensation refers to the general constancy of the period at various constant temperatures.

DOI:10.15774/PPKE.ITK.2023.004

There are two types of oscillators: sustained oscillations and damped oscillations [27]. The amplitude of damped oscillations decreases and finally converges to a steady state. This steady state is located between the higher and lower activity thresholds and represents an optimum intermediate value. This is called homeostasis. On the other hand, the repeating character and, consequently, the periodicity of a sustained oscillation persist sufficiently for longer time periods. Damped oscillations ideally need (i) a strong cooperative feedback regulations and (ii) equivalent timeframes on the two arrows. The dynamical equations and the time trajectory for the damped and the sustained oscillations are shown in Figure 2.4. This example has been taken from the book chapter written by Brian Ingalls [27].

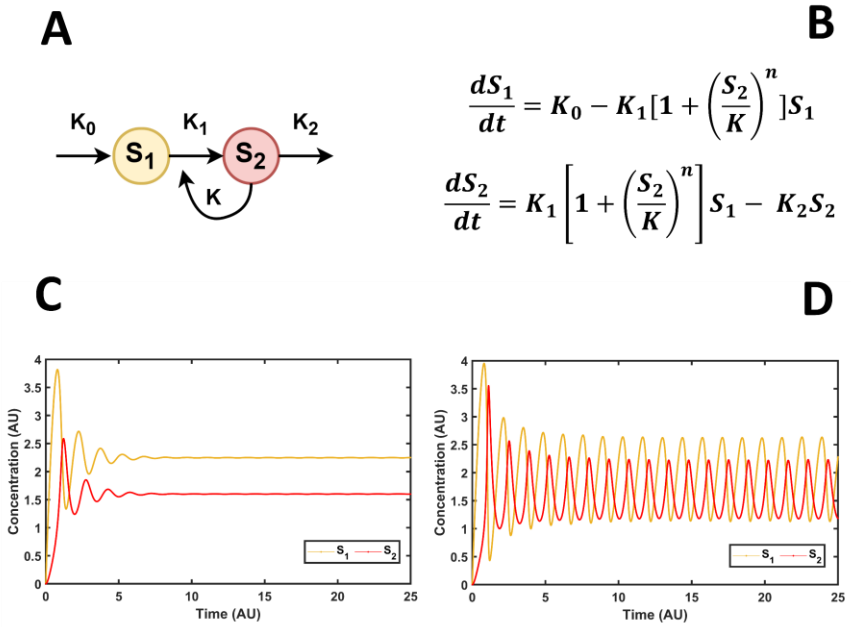

Figure 2.4: An oscillator's topology creates damped and sustained oscillations.
Wiring diagram of an oscillator is shown (A). This is an example of Selkov's substrate depletion network [33], which is a substrate depletion-driven oscillator with the simplest positive feedback loop caused by S_2's autocatalytic activity. Despite the fact that this is not a typical negative feedback loop, in this scenario, S_2 tends to remove S_1. The ODEs mathematically explain the network (B). Time course image for damped oscillation is shown (C). The parameter values for damped oscillation are : $K_0 = 8$, $K_1 = 1$, $K_2 = 5$, $K = 1$, $n = 2$ (AU). Time course trajectory for the sustained oscillation is shown (D). The parameters associated with sustained oscillation are : $K_0 = 8$, $K_1 = 1$, $K_2 = 5$, $K = 1$, $n = 2.5$ (AU).

Furthermore, sustained oscillations can be categorized into two types: delayed and relaxation oscillators. A positive feedback loop provides delay to a system. Positive feedback in biological systems may cause a two-node negative feedback loop to exhibit sustained oscillations. The lag in the delayed oscillators can be modeled by introducing

DOI:10.15774/PPKE.ITK.2023.004

multiple intermediatory steps. The durations for various steps in delayed oscillators are equal [27]. Whereas in the case of relaxation oscillators, the time scale of the NFB loop must be much slower than that of the PFB loop [27]. Unlike the more symmetrical pulses of delayed oscillators, this form of oscillation often features asymmetric pulse patterns with gradual building at beginning, then fast buildup when positive feedback starts to dominate, and a quick drop. The time course simulation of the relaxation and delayed oscillators are presented in Figure 2.5.

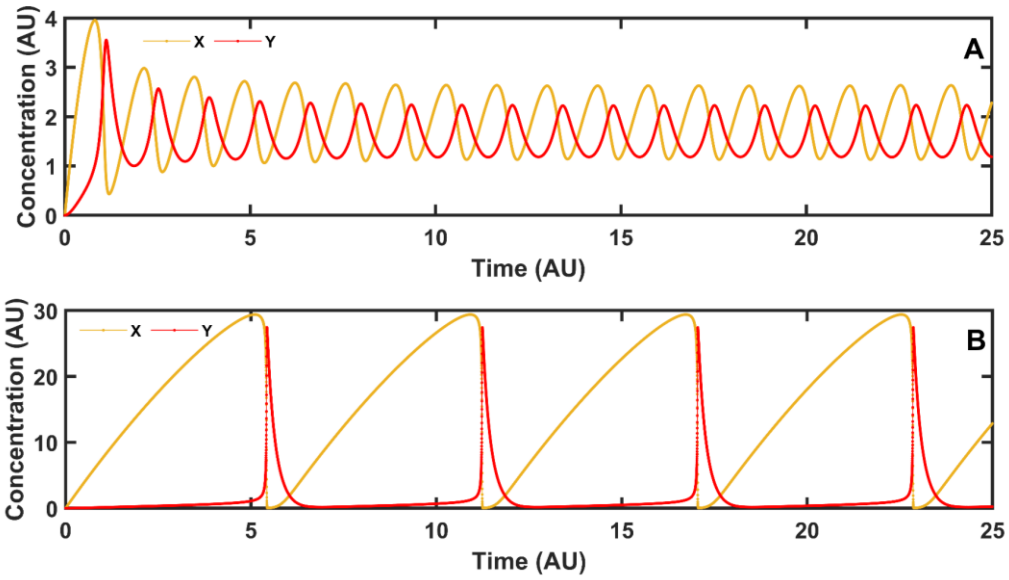

Figure 2.5: Two kinds of sustained oscillators.

Time course diagram for delayed oscillation is shown (A) with the parameter values: $K_0 = 8$, $K_1 = 1$, $K_2 = 5$, $K = 1$, $n = 2$ (AU). Time course diagram for a relaxation oscillator is represented (B). The parameters associated with relaxation oscillation are : $K_0 = 8$, $K_1 = 0.1$, $K_2 = 5$, $K = 1$, $n = 2.5$ (AU). The network topology and mathematical ODEs are same as shown in Figure 2.4A and 2.4B respectively.

2.2.3. Feedforward Loop

A feedforward loop (FFL) is a type of signaling network pattern in which a target gene Z is regulated directly (direct arm) by an input transcription factor (TF), X, or indirectly (indirect arm) by an intermediary TF, Y. There are two kinds of FFL – coherent (cFFL) and incoherent (iFFL). Coherent FFLs encompass themes in which the net impact of direct regulation (from X to Z) is the same as the net effect of indirect regulation (through Y). Incoherent FFLs are described as topologies in which the direct regulation (from X to Z) is the inverse of the indirect regulation (through Y). The FFLs are classified into eight types based on diverse combinations of positive and negative rules, four of which

DOI:10.15774/PPKE.ITK.2023.004

are coherent and four of which are incoherent shown in Figure 2.6. A coherent FFL can function as a noise filter while simultaneously displaying the delay mechanism. Incoherent FFLs are sign-sensitive accelerators with the ability to function as pulsers. These network topologies cannot be observed in isolation since they are seen in biology in coupled forms. These coupled feedforward loop topologies have been discussed in the chapter 4. Immune cells, for example, are governed by feedforward loops which are both coherent and incoherent [15]. Another example of coupling between particular FFLs in biology is the mitogen activated protein kinases (MAPK) pathway [16]. Noise may be reduced by using linear MAPK pathways [34]. According to earlier studies [35,36], a network containing posttranslational modification through phosphorylation and dephosphorylation reactions may also reduce noise. It has been discovered that c1FFL functions as a low-pass filter that reduces noise.

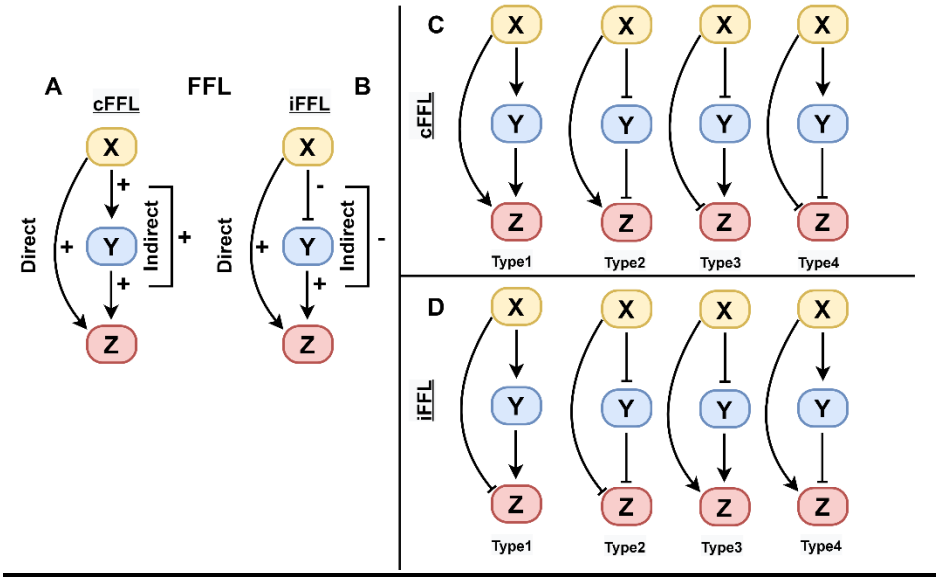

Figure 2.6: Feedforward loops.

The coherent feedforward loop (cFFL) and incoherent feedforward loop (iFFL) are presented in subplots (A and B), where cFFL has the same net effect on the direct and indirect arms (i.e. both arms are positive), whereas iFFL has the opposite net effect on the direct and indirect arms (i.e. one arm is positive while other is negative). The four possible coherent feedforward loops (cFFL) are shown at the top panel (C). The four different incoherent feedforward loops (iFFL) are shown at the bottom panel (D).

2.3. Understanding Network Topologies

In the next subsections I will discuss network topologies in depth and explain how to mathematically model such networks.

DOI:10.15774/PPKE.ITK.2023.004

2.3.1. Chemical Reaction Networks (CRN)

Chemical reaction networks offer a straightforward framework for representing complicated dynamical systems such as those found in inorganic chemistry, biochemistry, and systems biology [37,38]. A chemical reaction network is made up of a number of reactants, a number of products, and a number of reactions [39]. For a better understanding, a basic reaction scheme can be illustrated in Figure 2.7. In the following influence diagram, A and B are connected by the PFB loop, and A is synthesized from S. A, and B proceeds for self-degradation reactions.

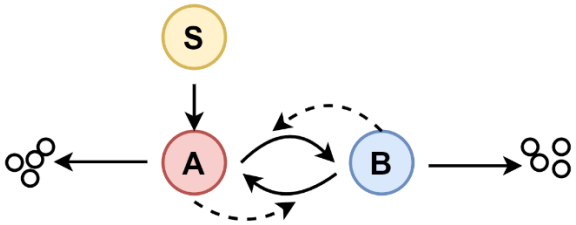

Figure 2.7: Wiring diagram of a network.

A and B are connected through a positive feedback loop (PFB). A is directly produced from S. B is influencing its own level positively by converting A to B, and A is doing the reverse, converting A to itself. This systems is a combination of these two pure positive feedback loops and the positive feedback, based on the antagonism of A and B, how they inhibit each other. This systems was termed as Direct Competition earlier [20]. A and B both can be degraded followed by mass action kinetics. The direct reactions (synthesis and degradation) are shown by solid arrows, while the indirect reactions (here, the positive influence) are represented by dashed arrows.

The set of chemical reactions connected with it is as follows:

$$S \xrightarrow{k_o} A$$

$$A + B \xrightarrow{k_1} 2B$$

$$B + A \xrightarrow{k_{-1}} 2A$$

$$A \xrightarrow{\Upsilon_1} \Phi$$

$$B \xrightarrow{\Upsilon_2} \Phi$$

DOI:10.15774/PPKE.ITK.2023.004

2.3.2. Mathematical Modeling and ODE

Dynamical mathematical modeling may easily convey mechanistic features of a network architecture. Ordinary Differential Equation (ODE) represents the dynamical properties of biological network topologies. The concentration of molecular species changes over time, and it is represented by ODEs. Each equation represents a molecular species, with positive values representing production and negative terms representing decay.

Rate of change of A = + rate of production of A – rate of degradation of A

An ODE is made up of parameters and state variables. State variable refers to molecular species that change throughout time. A chemical reaction has defined parameters that are generally reliant on biological variables such as temperature, activation energy, or reaction velocity (kinetic rates) [27]. This dependency can be easily understood from the mathematical expression of the Arrhenius Equation [18] (In section 3.1.2., the Arrhenius Equation is introduced in more details.).

For the above CRN the ODE for A can be represented as follows –

$$\frac{dA}{dt} = k_o \cdot S + k_{-1} \cdot B \cdot A - k_1 \cdot A \cdot B - \Upsilon_1 \cdot A \quad \textbf{(2.1)}$$

Where, S,B,A are the state variables and $k_o, k_1, k_{-1}, \Upsilon_1$ are the fixed parameters.

Steady state approximation can be used to determine the precise solution of state variables. Setting $\frac{dA}{dt} = 0$ yields the steady state (SS) equation of A.

2.3.3. Kinetics of Biological Processes

The kinetics of any biological process can be used to interpret it. The dynamical behavior of network motifs may be described using the network diagram and chemical kinetics. A series of chemical processes can be used to determine the network architecture. Chemical reactions describe the molecular species and their interactions. Mass-action kinetics, enzyme kinetics, and hill equations can all be used to describe the mathematical connection between molecular species.

The behavior of reactants and products in an elementary chemical reaction is described by mass action. This phenomenon is described by mass action kinetics as an equation in

DOI:10.15774/PPKE.ITK.2023.004

which the velocity or rate of a chemical reaction is exactly proportional to the concentration of the reactants [40,41]. According to the law of Mass-Action Kinetics, the rate of the reaction $A + B \xrightarrow{k_{rate}} C$, is $k_{rate} \cdot [A] \cdot [B]$.

Michaelis-Menten Kinetics is a model that accounts for enzyme kinetics. The model illustrates how an enzyme (E) can induce kinetic rate enhancement in a product (P) generation process and how reaction rates rely on the substrate (S) concentrations [42]. The substrate binding to the enzyme is a reversible process, but the product formation pathway is irreversible.

$$E + S \leftrightharpoons ES \xrightarrow{k_{cat}} E + P$$

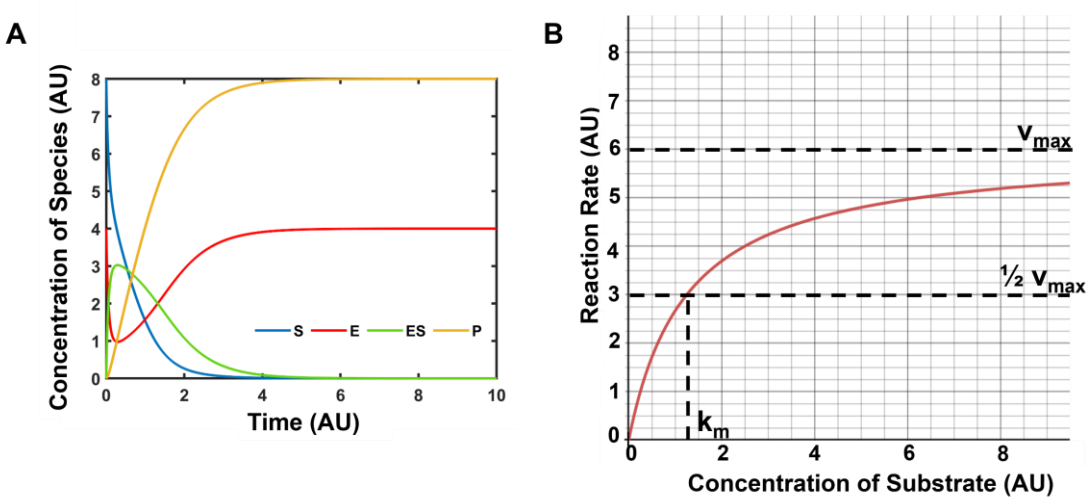

Figure 2.8: Michaelis-Menten kinetics.

In panel (A) time course simulation of substrate (S), enzyme (E), saturated enzyme (ES), and the product (P) has been shown in blue, red, green, and yellow colored lines, respectively. According to the Michaelis-Menten law, the saturation curve displays how the concentration of the substrate in enzyme kinetics changes over the reaction rate (B).

The product (P) formation can be mathematically expressed as follows (assuming that the concentration of enzymes is substantially lower than the concentration of substrates.):

$$\frac{d[P]}{dt} = k_{cat} \cdot [E_o] \cdot \frac{[S]}{k_m + [S]} \tag{2.2}$$

DOI:10.15774/PPKE.ITK.2023.004

Where k_{cat} denotes the catalytic rate constant, $[E_o]$ and $[S]$ represent the total amount of enzyme and the substrate concentration respectively. v_{max} can be represented as following:

$$v_{max} = k_{cat} \cdot [E_o]$$

(2.3)

The k_m value is the substrate concentration at which half of the enzymes bind the substrate (Figure 2.8B). The change in product concentration over time is hyperbolic in nature (Figure 2.8A).

For $[S] << [k_m]$, the rate of reaction is proportional to the concentration of the substrate, and it follows first-order kinetics. For $[S] >> [k_m]$, the rate of the reaction becomes independent of [S] and it follows zero-order kinetics.

The Hill equation is widely used to calculate the number of ligand molecules needed to bind to a receptor and cause a functional effect. Non-linear sigmoidal dose–response interactions are described by the Hill equation [43,44]. The rate of change of activity of Y can be described by the following ODE when a transcription factor X regulates the targeted gene Y either positively or negatively, as in X ->/| Y .

$$\frac{dY}{dt} = k_0 + f(X) - \Upsilon_Y \cdot Y$$

(2.4)

In the above equation k_0 is the basal synthesis rate of Y. This is also known as the non-zero minimal expression rate. $f(X)$ is the regulated synthesis rate of Y and Υ_Y is the self-degradation rate of Y. According to the Hill function, for X->Y situations

$$f(X) = \frac{k_{Max} \cdot X^n}{K^n + X^n}$$

(2.5)

For X-| Y situation, the $f(X)$ can be written as follows

$$f(X) = \frac{k_{Max}}{K^n + X^n}$$

(2.6)

DOI:10.15774/PPKE.ITK.2023.004

The maximum expression rate of the targeted gene Y is given by k_{Max}. The activation coefficient, or K, is the amount of X required to influence gene Y. The parameter n denotes the Hill coefficient, which governs the Hill function's steepness (Ultrasensitivity). With increasing n, the steepness of the Hill function rises (Figure 2.9). This n also describes the co-operativity effect. If n < 1, there is negative cooperation; if n > 1, there is positive cooperation; and if n = 1, there is no cooperativity. When cooperativity is absent (n = 1), the sigmoidal curve turns into a hyperbolic curve, and the Hill equation resembles Michaelis-Menten kinetics (Figure 2.9).

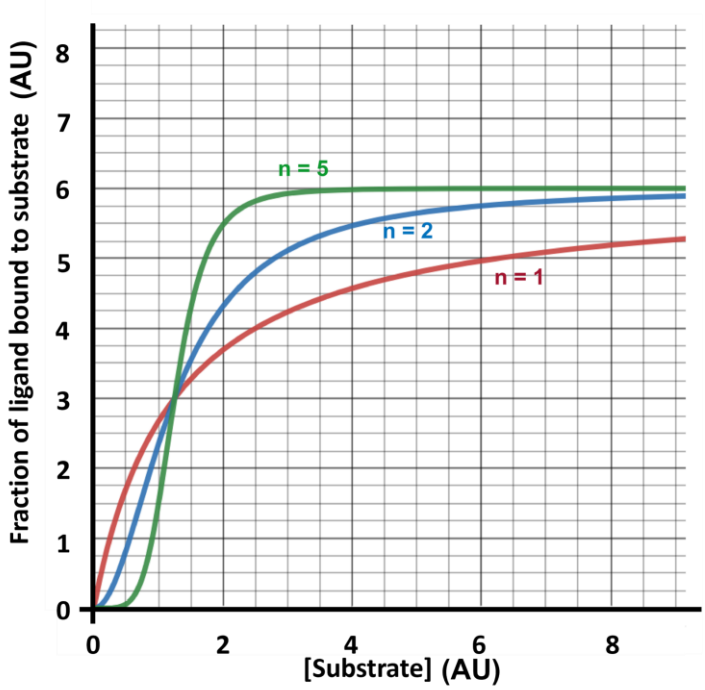

Figure 2.9: Hill kinetics.

As the substrate concentration rises, so does the proportion of ligand bound to it, as seen in the graph. Here n is the Hill co-efficient. In this graph each of these lines have different Hill co-efficient values (n). At n=1, the curve (in red color) resemblances with the Michaelis-Menten plot.

For multi-step post-translational modification processes [45–49], mass action kinetics can be implemented instead of the Hill equation. For a multi-step phosphorylation process like the following,

$$X \underset{k_{pp}}{\overset{k_p}{\rightleftarrows}} X^p \underset{k_{pp}}{\overset{k_p}{\rightleftarrows}} X^{pp}$$

the phosphorylation process is carried out by the kinase (k_p). As a result, each individual phosphorylation event can be modeled using the law of mass action, like $k_p \cdot X$, $k_p \cdot X^p$

DOI:10.15774/PPKE.ITK.2023.004

and $k_p \cdot X^{pp}$ [45–49]. The dephosphorylation reaction is carried out by the phosphates (k_{pp}). The mass action law for the dephosphorylation reaction will be , like $k_{pp} \cdot X^{pp}$ and $k_{pp} \cdot X^{p}$. Using mass action kinetics to a two site phosphorylation dephosphorylation process , the protein abundance curve has the shape of a sigmoid, which is the same as the "s-shaped" curve that comes from the Hill equation with a Hill coefficient of 2 [37].

2.4. Stochasticity in Biology

The biological processes are often influenced by the inherent stochasticity. Biological noise can be explained in terms of cell-to-cell variation found in groups of genetically identically cells. If two genetically identical cells are maintained under similar environmental circumstances, a gene will not yield the same quantity of mRNAs and proteins over time [44,50–54]. The low copy number of different biological metabolites like genes, mRNAs, proteins, transcription factors (TF) cause a biological process to be discrete and random (Figure 2.10).

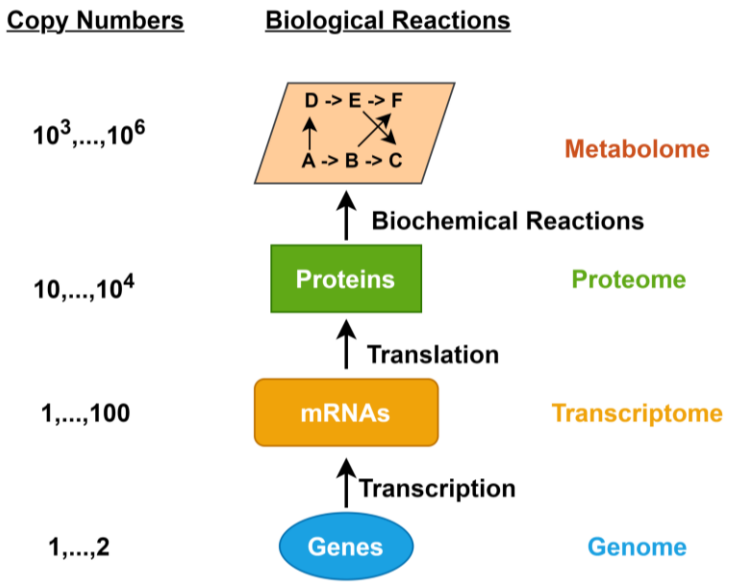

Figure 2.10: Numbers associated with biological process.

Copy number variation as an example throughout the metabolic hierarchy. Stochasticity makes it impossible to simulate accurately using ODEs the low copy numbers that occur at the genome to proteome levels. This graphic has been inspired from Martin Holub's page (https://www.martinholub.com/eth/code/2018/04/15/stochsim.html).

DOI:10.15774/PPKE.ITK.2023.004

The amplitude of the noise is governed by transcription rate, regulatory dynamics, and genetic variables. Significant amounts of the total variance are caused by stochasticity that is ingrained in the biochemical process of gene expression (intrinsic noise) and variations in other cellular components (extrinsic noise). The illustration of the cellular noise can be understood from Figure 2.11.

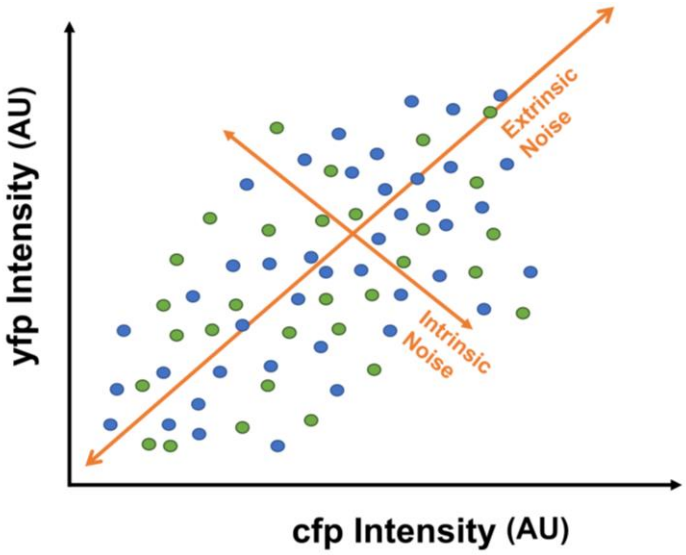

Figure 2.11: Interpretation of cellular noise.

Each data point represents the amount of expression of two in silico reporter genes, cyan fluorescent protein (cfp) (shown with green dots) and yellow fluorescent protein (yfp) (shown with blue dots). The scatter plot depicts the cell population. When two reporter genes become anti-correlated, intrinsic noise appears as a spread of dots perpendicular to the main diagonal. Extrinsic noise, on the other hand, makes the expression of the two reporter genes positively correlated and shows up along the main diagonal. The inspiration for this plot came from the publication by Ramsey et al. [55], which was influenced by the article by Elowitz et al. [51].

2.4.1. Extrinsic Noise

Extrinsic noise exists as a cause of variations or noise in the population of isogenic cells. These sources of noise differ in genetically similar cells in terms of shape, size, cell cycle stage, cytoplasm density, physical cellular environment (temperature, pressure, pH), and number of interacting molecules. Experiments in Escherichia coli reveal the presence of both external and intrinsic noise sources (Figure 2.12). In the presence of extrinsic noise, two distinct genes tagged with cyan (cfp) and yellow (yfp) alleles of the green fluorescent protein and regulated by identical promoters only show that each cell has the same

DOI:10.15774/PPKE.ITK.2023.004

quantity of both proteins, though the amount varies from cell to cell [51] (Figure 2.12, top panel).

2.4.2. Intrinsic Noise

The degree to which two identical copies of a gene do not correlate with each other when they are present in the same intracellular environment is known as the intrinsic noise for that gene. Due to the discrete chemical reactions and low copy number of the reacting species, intrinsic noise arises. The intrinsic noise in an isogenic cell population leads to population heterogeneity. As a result, a fraction of cells expresses more or less of one type of fluorescent protein than the other and the expression levels of the two different fluorescence strains become uncorrelated (Figure 2.12, bottom panel).

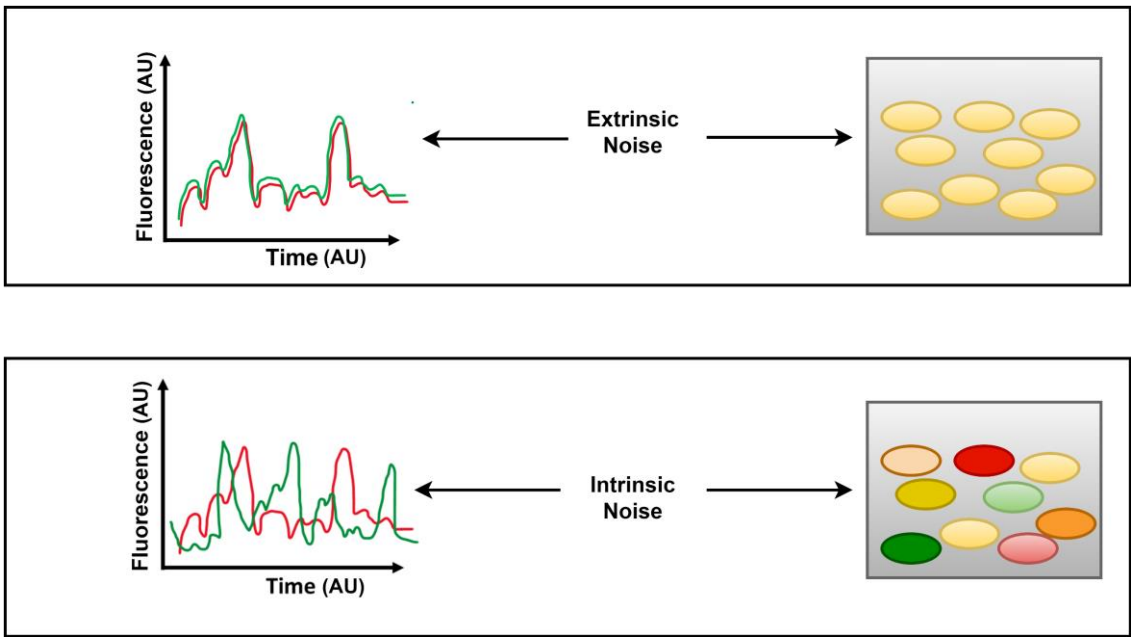

Figure 2.12: Illustrating extrinsic and intrinsic noise.

Two reporter genes yfp (shown in red) and cfp (shown in green) are regulated by the identical promoter. The fluorescence intensity of yfp and cfp is the same in the absence of intrinsic noise inside a single cell (indicated in yellow color, (top, right)). There will be overall variation in the fluorescence intensity due to the presence of extrinsic noise. The graph (top, left) suggests that the two promoter genes will be well coordinated. Intrinsic noise inside a single cell causes yfp and cfp fluorescence intensities to vary, leading in some green and some red colored cells (bottom, right). Due to the presence of intrinsic noise the graph will be also uncorrelated (bottom, left). The illustration has been borrowed from the article by Elowitz et al. [51].

DOI:10.15774/PPKE.ITK.2023.004

2.5. Mathematical Representation of Stochastic System

Because the reactions occur stochastically, there is no single solution that properly anticipates the population's evolution. There are several possibilities. Thus, in the presence of noise, the chemical reactions of a system can be represented by the Chemical Master Equation (CME) [56–58]. A CME is a representation of the probability that a system will be in a specific state. The CME is considered as a Markovian jump process because it accounts for two jump processes: achieving the current state from the prior state and departing the current state.

In a well stirred homogeneous mixture of molecular species $\{S_1,\ldots,S_N\}$, where $N \geq 1$, chemical interactions take place within a fixed volume Ω and at a constant temperature. The reactions and the dynamical states are represented as $\{R_1,\ldots,R_M\}$ (where $M \geq 1$) and $X(t) = \{X_1(t),\ldots, X_N(t)\}$ (where $X_i(t)$ = number of S_i molecules at time t). Here, a_j is the propensity (i.e. tendency) for the R_j reaction in the infinitesimal time interval dt. This value indicates how likely a reaction will occur at a particular time. Consider ν_{ji} = number of S_i molecules change when R_j reactions take place (where j =1,….,M and i=1,….,N). The CME can be represented as follows-

$$\frac{dP(X,t)}{dt} = \sum_{j=1}^{M}\left[a_j(X-\nu_j)P(X-\nu_j) - a_j(X)P(X)\right] \tag{2.7}$$

arriving term departing term

Here, *P(X, t)* is the probabilistic information of the state *X(t)* meaning that it is the probability of the system to attain a specific discrete state in an infinitesimal time interval between t and t + dt. Solving the CME is always challenging due to its high dimensionality that adds complexity to the system. There are several alternative approaches that bypass the problem, such as the Gillespie algorithm, Chemical Langevin Equation, Linear Noise Approximation, and so on.

2.5.1. Gillespie Algorithm

The Gillespie Algorithm [59] is also known as the Stochastic Simulation Algorithm (SSA) or the 'next reaction' method. Considering the reactions to be Markovian, the reason it is called the "next reaction" method is that it calculates the time of triggering

DOI:10.15774/PPKE.ITK.2023.004

the next reaction based on the current state. One way for numerically solving a CME is the Gillespie algorithm. For a stochastic equation system with known reaction rates, the Gillespie method generates alternative solutions (a collection of stochastic trajectories) and calculates the statistical mean of those stochastic trajectories.

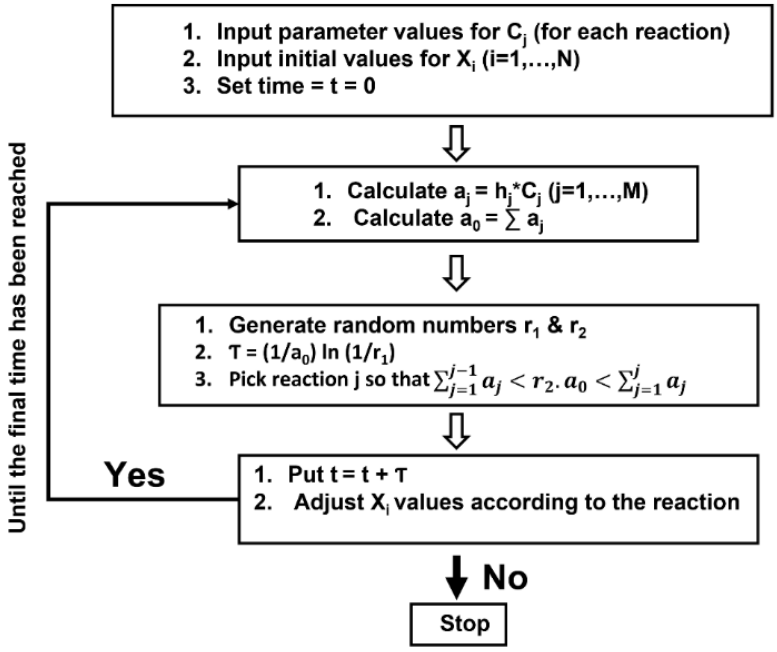

Figure 2.13: Gillespie algorithm.

The flow chart represents the simulation algorithm proposed by Gillespie for stochastic simulation and the idea of the flowchart have been borrowed from the article by Palanichamy et al. [60].

Consider M to be the total number of reaction channels; N to be the total number of chemical species; $a_j(X)$ to be the reaction propensities (displayed in the flowchart Figure 2.13); $X_i(t)$ to be the time evolved single-valued state function; C_j to be the intrinsic rate constant [61] that depends on the physicochemical properties of reactants, bond formation, temperature, reaction volume (for each reaction j); h_j to be the extrinsic reaction rate factor [61] that depends on the number of the reactant combinations (for each reaction j); and T to be the arbitrarily chosen time when the next reaction occurs. How the SSA functions may be readily explained using a simple flowchart shown in Figure 2.13.

2.5.2. Chemical Langevin Equation

Another alternative method for solving the CME is Chemical Langevin Equation (CLE) [56,62]. This comprises of a set of coupled stochastic differential equations that describe

DOI:10.15774/PPKE.ITK.2023.004

the time course of each molecular species. A feature of this approach is that it demonstrates that, as opposed to relying on a constant system size parameter, the equation's validity is dependent on the time varying propensities. CLE explains the accurate connection between the deterministic rate equations and the stochastic CME. If N is the number of molecular species, M is the total number of reactions, X(t) is the state variable ($X(t)=X_1(t),\ldots,X_N(t)$ i.e. $X_i(t)$ where i=1,2,…,N), $a_m(X(t))$ is the reaction propensity, ν_m is the vector that denotes the state change, dt is the macroscopic infinitesimal time, and $N_m(t)$ is the 'unit normal' random variable then the standard form of CLE can be represented as following [63]:

$$X(t+dt) - X(t) = \sum_{m=1}^{M} \nu_m a_m\big(X(t)\big)dt + \sum_{m=1}^{M} \nu_m \sqrt{a_m(X(t))} N_m(t)\sqrt{dt}\,, \tag{2.8}$$

Introducing a volume term (Ω) to express the above equation in terms of intensive variables (i.e. $Z_i(t) = \frac{X_i(t)}{\Omega}$), the chemical Langevin equation (CLE) can be written as follows:

$$Z(t+dt) - Z(t) = \sum_{m=1}^{M} \nu_m \widetilde{a_m}(Z(t))dt + \frac{1}{\sqrt{\Omega}} \sum_{m=1}^{M} \nu_m \sqrt{\widetilde{a_m}(Z(t))} N_m(t)\sqrt{dt}, \tag{2.9}$$

Here, $a_m(X) \to \Omega\, \widetilde{a_m}(Z)$ at thermodynamic limit.

So, the chemical Langevin equation (CLE) is a prominent approximation approach because it can represent temporal variations caused by the intrinsic stochasticity of the chemical process. In the next subsection, I am going to discuss the 'Linear Noise Approximation' method, which is another approximation method of the CME.

2.5.3. Linear Noise Approximation

Linear Noise Approximation (LNA) [63] is used to determine how a biological network propagates noise and how much it perturbs the system from a deterministic perspective. CME can be solved by LNA technique. The LNA of the CME is also known as the linear Fokker-Planck equation [64]. The LNA technique achieves a probabilistic logic for CRNs that allows reasoning about probability and expectation and indicates the variance of the linear combinations of the species population [65].

DOI:10.15774/PPKE.ITK.2023.004

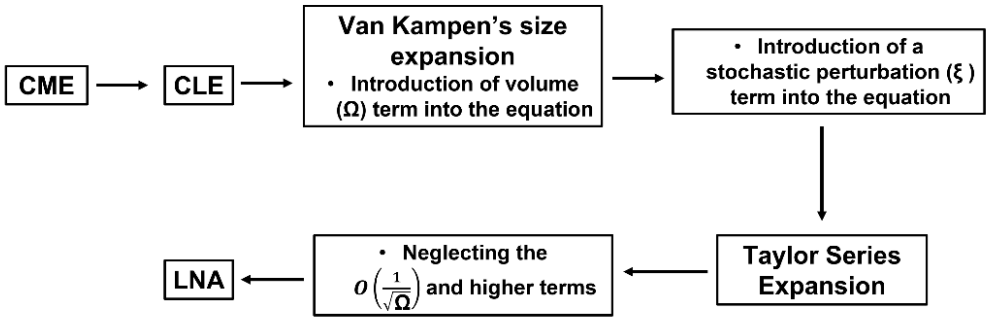

Figure 2.14: Linear Noise Approximation.

The flow chart represents the strategy of solving linear noise approximation (LNA).

A simple approach to deriving the LNA can be done by the system size expansion of Van Kampen. In this procedure, small parameters associated with the system's volume have been taken into consideration, such that it can represent the trajectory of a small stochastic fluctuation to a deterministic trajectory [66]. The infinite-order of Kramer's Moyal equation has not been considered in this straightforward method. The CLE, which is analogous to the Fokker Planck equation, was chosen as the starting point for this simplified LNA derivation approach. A flowchart can easily describe the simple derivation strategy for LNA calculation (Figure 2.14).

The works of Wallace et al. [63] and Cardelli et al. [65] offer an in-depth numerical solution of LNA from CLE, where random events are considered as Gaussian processes and happen in a continuous time. Thus, the noise ξ (t) in that approach is assumed to be white uncorrelated noise. Followed by the ansatz ($i.e. Z(t) = \hat{Z}(t) + \frac{1}{\sqrt{\Omega}}\xi(t)$), where the intensive state variable ($Z(t)$) can be represented in terms of a deterministic part $\left(\hat{Z}(t)\right)$ and a random part associated with volume terms ($\frac{1}{\sqrt{\Omega}}\xi(t)$), and plugging that into the CLE equation (Equation 2.9) gives the first step to solve LNA [63]. The extensive study by Wallace et al. [63] leads to the simple expression for LNA as:

$$[\xi(t+dt) - \xi(t)] =$$

$$\sum_{k=1}^{N}\left(\sum_{m=1}^{M} \nu_m \, \mathrm{f}_{mk}(t)\right)\xi_k(t)\mathrm{dt} + \sum_{\mathrm{m}=1}^{M} \nu_m \sqrt{\widetilde{\mathrm{a}_m}(\hat{Z}(t))} N_m(t)\sqrt{dt} \qquad \textbf{(2.10)}$$

DOI:10.15774/PPKE.ITK.2023.004

Here, $f_{mk}(t) = \frac{\partial \widetilde{a_m}(z)}{\partial z_k}|_{z=\hat{Z}(t)}$ (for m = 1,…., M; k = 1,…,N) is how the propensity of a particular reaction changes in the presence of noise, ν_m is the state change indicator, N_m is the independent white noise variable.

On this note, a successful computer simulation method for LNA of any chemical reaction network has been provided by Cardelli et al. [65].

Previous discussions have made it evident that identifying the tiny network motifs involved in the analysis of the dynamical biological network is the first step. The next step is to mathematically model these random biological processes. Analyzing the dynamical behavior of various network motifs is greatly aided by the use of various computer simulation techniques.

In the next chapter, I will discuss the commercial tools that can be used to analyze dynamical network motifs.

DOI:10.15774/PPKE.ITK.2023.004

Chapter 3

Methods

DOI:10.15774/PPKE.ITK.2023.004

The network analysis and the time course simulation covered in Chapters 4 and 5 have been carried out using various commercial tools. In this chapter, I am going to discuss about these tools that simulate the codes that I have written for the network motifs that are described in chapters 4 and 5.

3.1. Software Tools for Network Analysis

The computational study of complex networks provides approaches that are quick, reliable, and cost-effective [67]. The practice of modelling is a technique to solve problems that may be applied to real-world systems. The real challenge is in recreating and figuring out what happened based on what we know and what we don't know [68]. There has been a significant uptick in the use of ODE models for the investigation of biological systems. Various commercial applications provide a framework for doing fundamental dynamical analysis, including simulations, graphics, static perspective (object-oriented modelling, such as class diagrams or entity diagrams) [67] and stability analysis.

In this dissertation, Kaemika and MATLAB have been widely applied for network analysis. These two applications provide excellent deterministic as well as stochastic simulation results. In the upcoming sections, will provide a brief discussion of these two tools, Kaemika and MATLAB.

3.1.1. Kaemika

Kaemika is a functional programing language that provides a graphical interpretation of chemical reaction simulations [69]. It is an educational Microsoft tools, developed by Luca Cardelli. Kaemika is built up based on C# language [69]. In addition to deterministic and stochastic simulations, it provides techniques for visualizing digital microfluidics. Within the context of this framework, the mass action kinetics may be easily defined in terms of algebraic functions. On the other hand, the Hill equation, the Arrhenius equation, and other non-linear equations can be written in terms of basic transcendental functions. With the assistance of the Kaemika tools, it is possible to complete the linear noise approximation [63] (LNA) in a single shot in order to carry out stochastic simulation. The LNA simulation provides a variety of statistical measures

DOI:10.15774/PPKE.ITK.2023.004

[70], including standard deviations, coefficients of variation, variances, fano factors, and more.

The following examples provide a clear explanation of how to operate the Kaemika tools.

1. Kaemika Example-1 : Deterministic Simulation, Time Course Analysis

A. Reactions With Mass Action Kinetics

Consider an oscillatory network proposed by Selkov [33]. The network diagram is shown in Figure 2.4A. Earlier I have used non-linear equations (Figure 2.4B) to represent the network mathematically. Now I am going to use the simple mass action kinetics for the oscillatory network displayed in Figure 2.4A and simulate it with Kaemika tool.

```
// Define Rate Constant
number K0 = 0.01
number K1 = 0.001
number K = 5
number K2 = 0.1
// Define Species and Initial Conditions
species {S1,S2}
amount S1 @ 0.5 M
amount S2 @ 0.01 M
// Reactions
∅ -> S1  {K0} // background synthesis of S₁
S1 -> S2  {K1} // S₁ synthesizes S₂
S1 + S2 + S2 -> 3S2  {K} // S₂ activates its own synthesis and inhibits S₁
S2 -> ∅ {K2} // self-degradation of S₂
// Plot Species
report S1, S2
// Equilibrium Time
equilibrate for 1000
```

DOI:10.15774/PPKE.ITK.2023.004

Figure 3.1A depicts the time course of this network motif simulated by Kaemika. Kaemika also represents the chemical reaction influences graphically (bottom, right panel of Figure 3.1A).

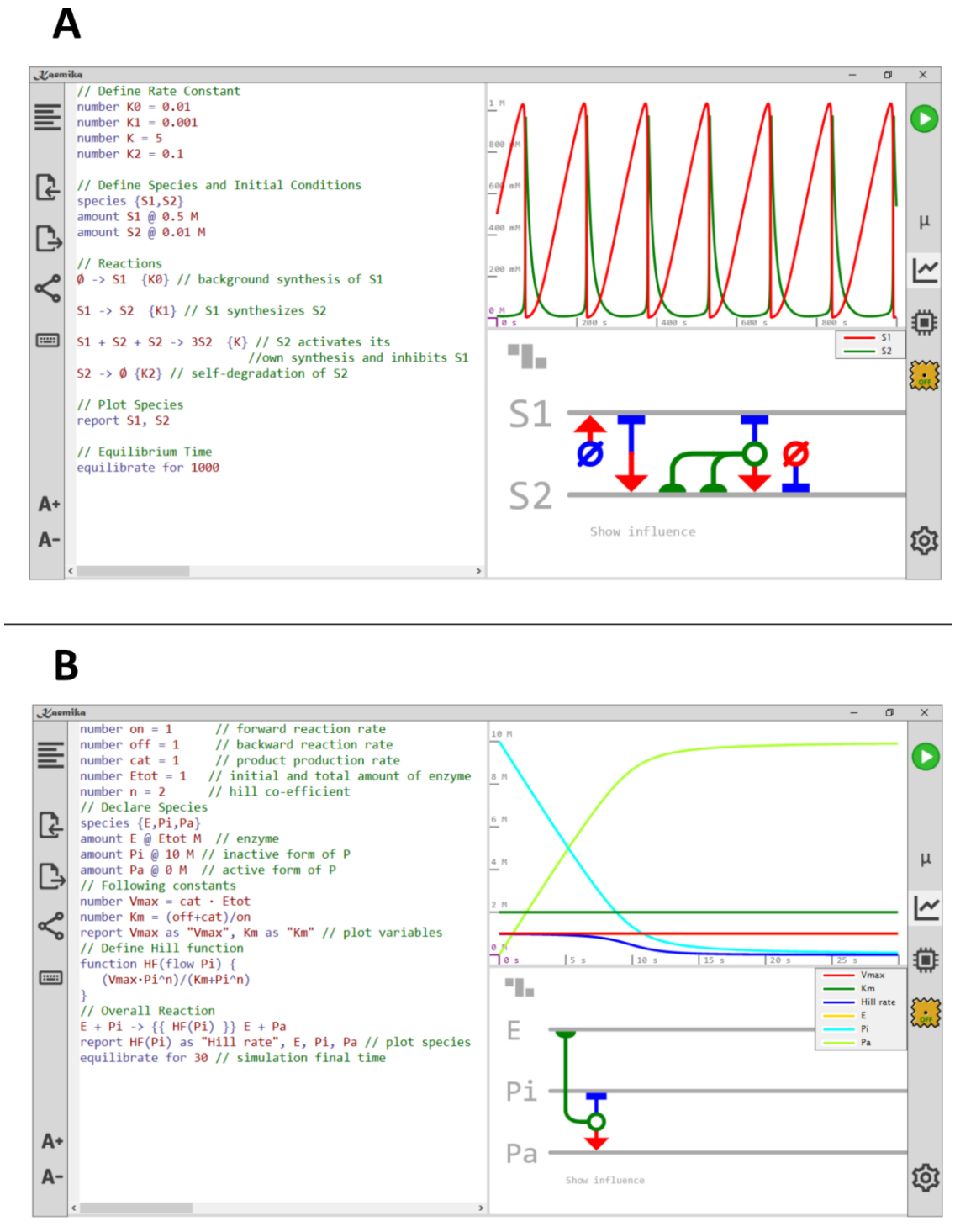

Figure 3.1: Implementing linear and non-linear kinetics on Kaemika.

(A) The code for the network motif shown in Figure 2.4A is displayed on the left-hand panel. The panel in the upper right-hand corner illustrates the oscillatory analysis of the model's time course. S_1 and S_2's oscillations are depicted in red and green color, respectively. The bottom right panel graphically represents

DOI:10.15774/PPKE.ITK.2023.004

the response score for both S_1 and S_2. The parameter values for the simulation is $K_0 = 0.01$, $K_1 = 0.001$, K = 5, $K_2 = 0.1$ (AU).

(B) The code displays how to implement non-linear kinetics in Kaemika. The panel in the upper right-hand corner shows the time course simulation results. Enzyme (E), P_i and P_a are plotted with yellow, cyan, and parrot-green color, respectively. The maximal reaction rate (V_{max}), Michaelis constant (K_m) and Hill rate are displayed with red, dark-green, and blue color, respectively. The bottom right panel graphically displays the influence of enzyme (E) on the variables. The parameter values for the simulation are on = 1, off = 1, cat = 1, Etot = 1, n = 2 (AU).

B. Reactions With Non-Linear Kinetics

Consider a network in which the inactive form of P (P_i) is converted into the active form of P (P_a) by an enzyme E, and it follows a non-linear Hill-like function. The reaction can be as follows:

$$P_i \underset{off}{\overset{on}{\rightleftarrows}} P_a$$

By using the Kaemika tool, the code can be written as follows:

```
number on = 1      // forward reaction rate
number off = 1     // backward reaction rate
number cat = 1     // product production rate
number Etot = 1   // initial and total amount of enzyme
number n = 2      // hill co-efficient
// Declare Species
species {E,Pi,Pa}
amount E @ Etot M  // enzyme
amount Pi @ 10 M // inactive form of P
amount Pa @ 0 M  // active form of P
// Following constants
number Vmax = cat · Etot
number Km = (off+cat)/on
report Vmax as "Vmax", Km as "Km" // plot variables
// Define Hill function
function HF(flow Pi) {
          (Vmax·Pi^n)/(Km+Pi^n)
}
```

DOI:10.15774/PPKE.ITK.2023.004


```
// Overall Reaction
E + Pi -> {{ HF(Pi) }} E + Pa
report HF(Pi) as "Hill rate", E, Pi, Pa // plot species
equilibrate for 30 // simulation final time
```

Figure 3.1B shows the simulation results of this network motif from Kaemika. Kaemika also displays the chemical reaction influence network graphically (bottom, right panel of Figure 3.1B).

Moving on to the next example, a demonstration of the use of Kaemika for LNA is shown, followed by the computation of a statistical quantities, such as the standard deviation (σ).

2. Example-2 : Stochastic Simulation via LNA calculations

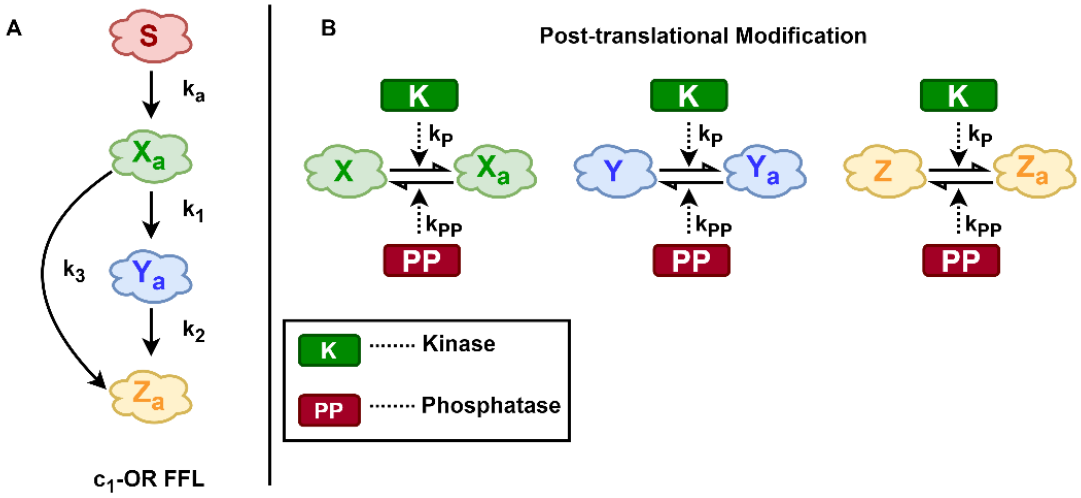

Figure 3.2: c1-OR-FFL diagram.

The diagram represents the type-1 coherent FFL in an OR connection (A). Here, Y and Z are phosphorylated by the kinase X_a. Y_a phosphorylates Z as well. (B) X, Y, and Z undergo post-translational modification in the presence of kinase (K) and phosphatase (PP).

Consider a coherent type-1 feedforward loop with OR type connections (c1-OR-FFL), shown in Figure 3.2. In this network, X_a is regulated by the noisy input (S). X_a influences Y_a. Both X_a and Y_a influence the output (Z_a) via direct and indirect arms, respectively. Here I consider FFLs, where regulation happens at the post-translational level. Post-translational modifications are considered for X_a, Y_a and Z_a. These contain activation and

DOI:10.15774/PPKE.ITK.2023.004

inactivation processes, but slower synthesis and degradation steps are omitted. In this example, the input (S) is changing with time. The FFL nodes X_a, Y_a, and Z_a will change over time and follow the input pattern as the input (S) changes over time (Figure 3.3).

Once again, the standard deviation can be calculated with a simple click of a button (Figure 3.4B). Figure 3.4A shows additional choices for each statistical quantity estimation.

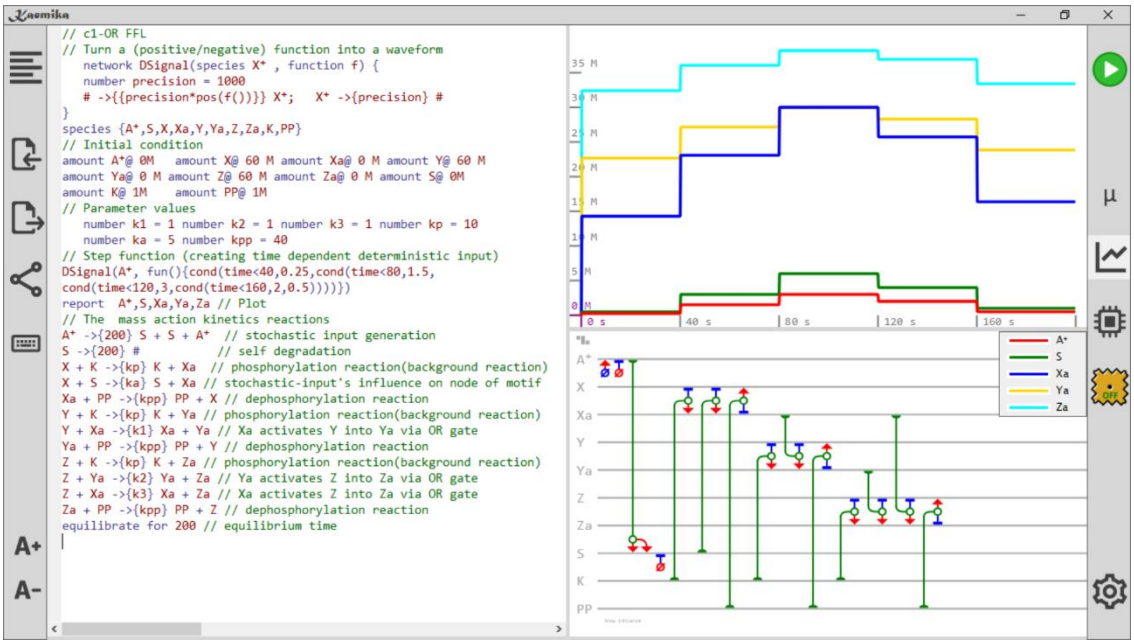

Figure 3.3: Variation of all variables with a staircase-like change in input (S) with time.

The reaction scheme for the network motif shown in Figure 3.2 is written on the left-hand panel. The right-hand panel shows the time evolution of the input (S, shown in red) and other FFL nodes X_a (shown in green), Y_a (shown in blue), and Z_a (output, shown in yellow) using Kaemika.

DOI:10.15774/PPKE.ITK.2023.004

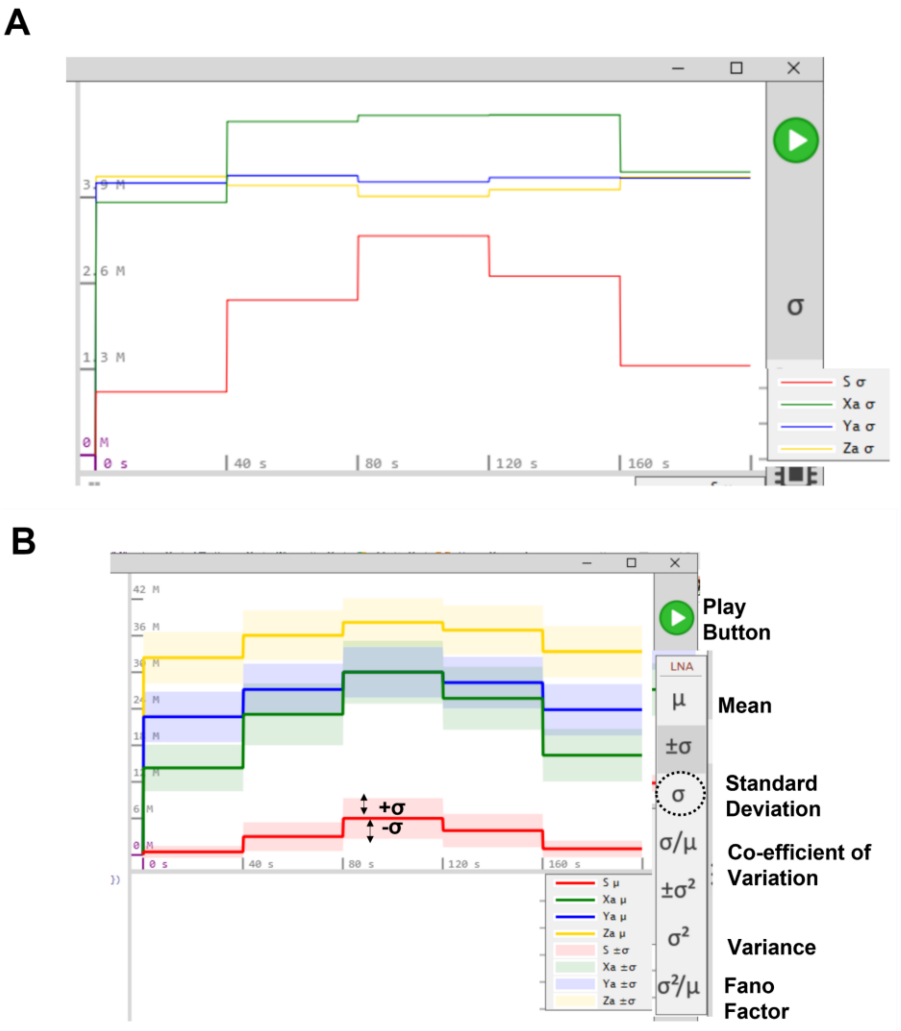

Figure 3.4: Statistical Analysis using Kaemika.

Panel A shows how the standard deviation (σ) changes at each layer for the network topology shown in Figure 3.2. Panel B shows the different statistical measurements that are available in Kaemika and plots mean ± standard deviation with shading for each variable.

3.1.2. MATLAB

The subjects like physics, chemistry, mathematics, and all branches of engineering make extensive use of the computational tool MATLAB. Its use may be found across the scientific and engineering communities. MATLAB is an acronym for "MATrix LABoratory" [71]. MATLAB was initially built to provide accessibility to matrix software created by the LINPACK (linear system package) and EISPACK (Eigen system package) projects. MathWorks developed MATLAB. MATLAB has a high level programing skill. It gives excellent graphic visualization in addition to programming and numerical computations. To assist in numerical calculations, numerical methods, and

DOI:10.15774/PPKE.ITK.2023.004

graphic representation, MATLAB has various built-in functions and commands. A toolbox is a collection of programs in MATLAB that are used for certain applications such as control theory, signal processing, optimizations, and so on. APIs (Application Program Interfaces) in MATLAB let users write codes in other programming languages, like C/C++ and Fortran, that interact directly with MATLAB [71].

1. Example-1: Deterministic simulation, and Period of Oscillation Calculation

In relation to this thesis, the following example clearly demonstrates the use of MATLAB. This is an example of a deterministic computation. Consider an NFB in which X facilitates in the synthesis of Y while Y inhibits the synthesis of X. The goal is to compute the period of oscillations at temperatures ranging from 283 to 313 Kelvin. To correlate the reaction rates with temperature, I used the Arrhenius equation [72] to represent the reaction rates as a function of temperature. The reaction rates increase with temperature, according to Arrhenius equations [73,74]. As temperatures increase, it is believed that oscillating periods would decrease [75]. The Arrhenius equation displayed in the following example of MATLAB function file can be expressed as follows:

$$reaction\ rate = A_e \cdot e^{\frac{-E}{R \cdot T}} \tag{3.1}$$

where A_e = pre-exponential factor for all rates (AU), R = universal gas constant = 8.3144598 $J.K^{-1}.mol^{-1}$, E = activation energy for the reaction, and T = Temperature is measured in Kelvin.

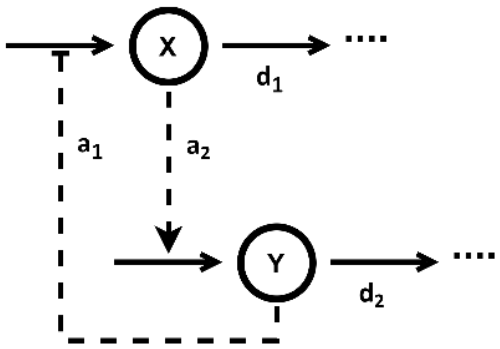

Figure 3.5: NFB Loop topology.

When X has a positive effect on the synthesis of Y while Y has an inhibitory effect on the synthesis of X, we have a NFB loop.

DOI:10.15774/PPKE.ITK.2023.004

For a NFB topology [76] (Figure 3.5) the ODEs are as following-

$$\frac{dX}{dt} = \frac{a_1 \cdot k}{k + Y} - \frac{d_1 \cdot X}{k_1 + X} \tag{3.2}$$

$$\frac{dY}{dt} = a_2 \cdot X - \frac{d_2 \cdot Y}{k_2 + Y} \tag{3.3}$$

To begin, a function environment has been constructed so that the models can be defined.

```
function dcdt = NFL(t,c,Temp)
% variables stored within array
X = c(1);
Y = c(2);
% parameters are defined based on Arrhenius Equation : rate = A_e.e^(-E_a×1000 / 8.3144598×Temp)
% A_e = pre-exponential factor, E_a = activation energy, Temp = Temperature in
Kelvin
k1 = 383.83.*exp(-(31.8565.*10^3)/(8.3144598.*Temp));
k2 = 383.83.*exp(-(31.8565.*10^3)/(8.3144598.*Temp));
d1 = 383.83.*exp(-(14.7420.*10^3)/(8.3144598.*Temp));
d2 = 383.83.*exp(-(14.7420.*10^3)/(8.3144598.*Temp));
k = 383.83.*exp(-(12.*10^3)/(8.3144598.*Temp));
a1 = 383.83.*exp(-(14.01.*10^3)/(8.3144598.*Temp));
a2 = 383.83.*exp(-(17.9420.*10^3)/(8.3144598.*Temp));
% initialization
dcdt = zeros(2,1);
% differential equations
dcdt(1) = (((a1.*k)./(k+Y)) - ((d1.*X)./(k1+X)));
dcdt(2) = ((a2.*X) - ((d2.*Y)./(k2+Y)));
```

DOI:10.15774/PPKE.ITK.2023.004

The main file calls function files and performs analysis and visualization. The main program file can be written as follows-

```
t0 = 0;                          % initial time
tf = 1150;                      % final time
tspan = t0:0.02:tf;      % Step length
css = [1 0]';                  % initial condition for X and Y
Temp = zeros(7,1);    % array for saving Temperature
X_val = zeros(length(tspan),7);    % array for X
Y_val = zeros(length(tspan),7);     % array for Y
% Iteration starts , Loop for the Temperature
for i=1:7
    i
    Temp(i,1)=278+5*i;
[t,c]=ode45(@(t,c) NFL(t,c,Temp(i,1)),tspan,css); % ODE solver
% Plot
figure(2)
plot(t,c(:,1),'.-','Color',[rand,rand,rand],'DisplayName','X')
hold on
plot(t,c(:,2),'.-','Color',[rand,rand,rand],'DisplayName','Y')
X_val(:,i) = c(:,1);
Y_val(:,i) = c(:,2);
% calculation of period of oscillation for each temperature value
[peakval,locval]=findpeaks(X_val(:,i),t);
period(:,i) = mean(diff(locval));
period1 = period;
end
```

The graphic visualization of the oscillatory behavior of X at seven different temperature is shown in Figure 3.6.

DOI:10.15774/PPKE.ITK.2023.004

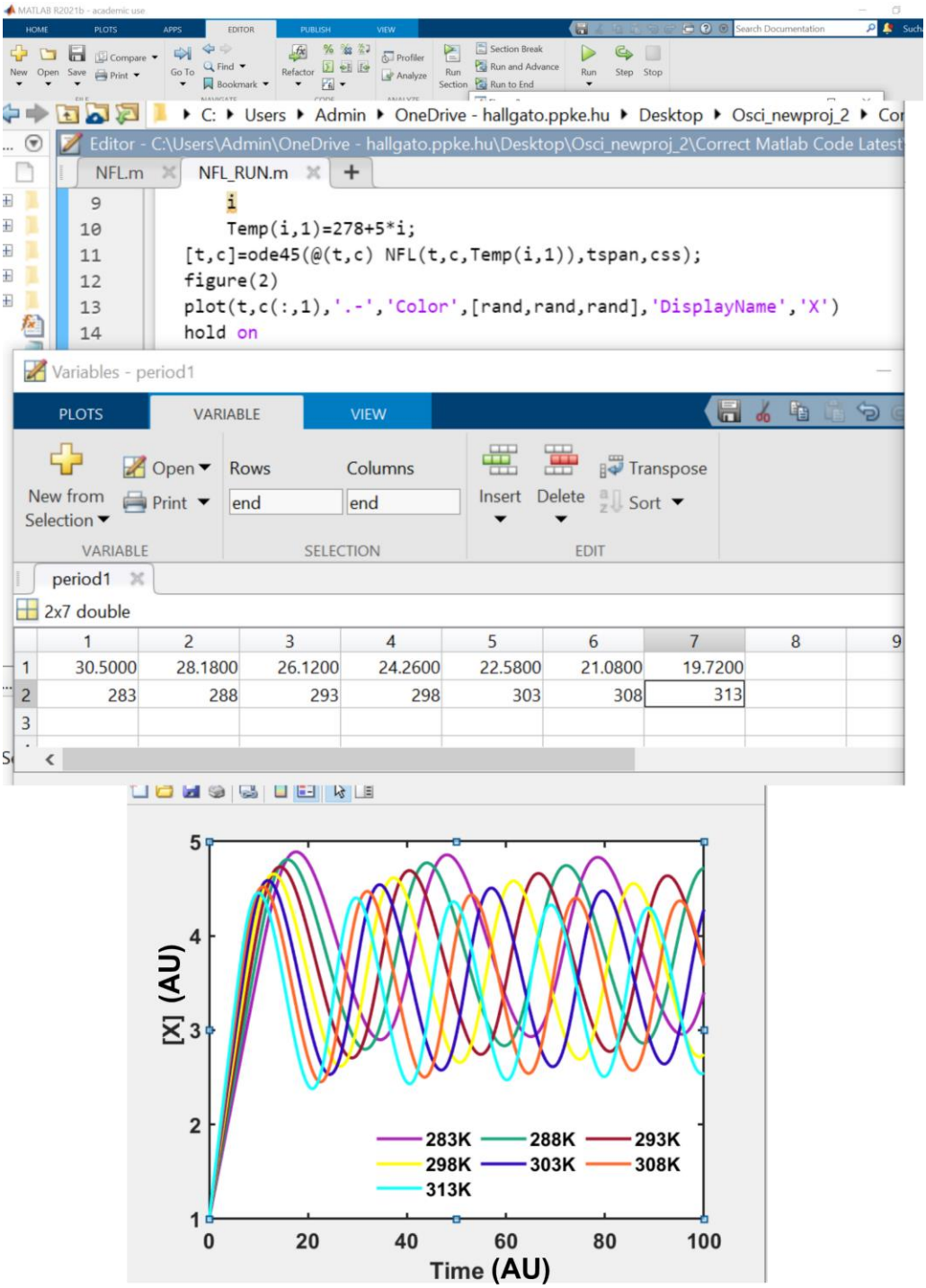

Figure 3.6: MATLAB screen.

MATLAB displays a panel in which the analysis is visualized (top). An array for the period of oscillations at various temperatures is provided on the middle panel (under a VARIABLE pop-up window). The oscillations associated with seven different temperatures are plotted with distinct colors (bottom panel, legend).

DOI:10.15774/PPKE.ITK.2023.004

2. Example-2: Analysis of Extrinsic Noise through parameter variations

In the following, I will describe the approach I used to add extrinsic noise to the model and solving it in MATLAB. In order to take into account extrinsic noise, I was checking how variability in parameter values perturb simulation outcome. Several simulations needed to be conducted, each with a different set of parameter values centered around the nominal value. To achieve this, a random generator is required to get the distribution of randomly chosen parameter values around the nominal value (from a log normal distribution).

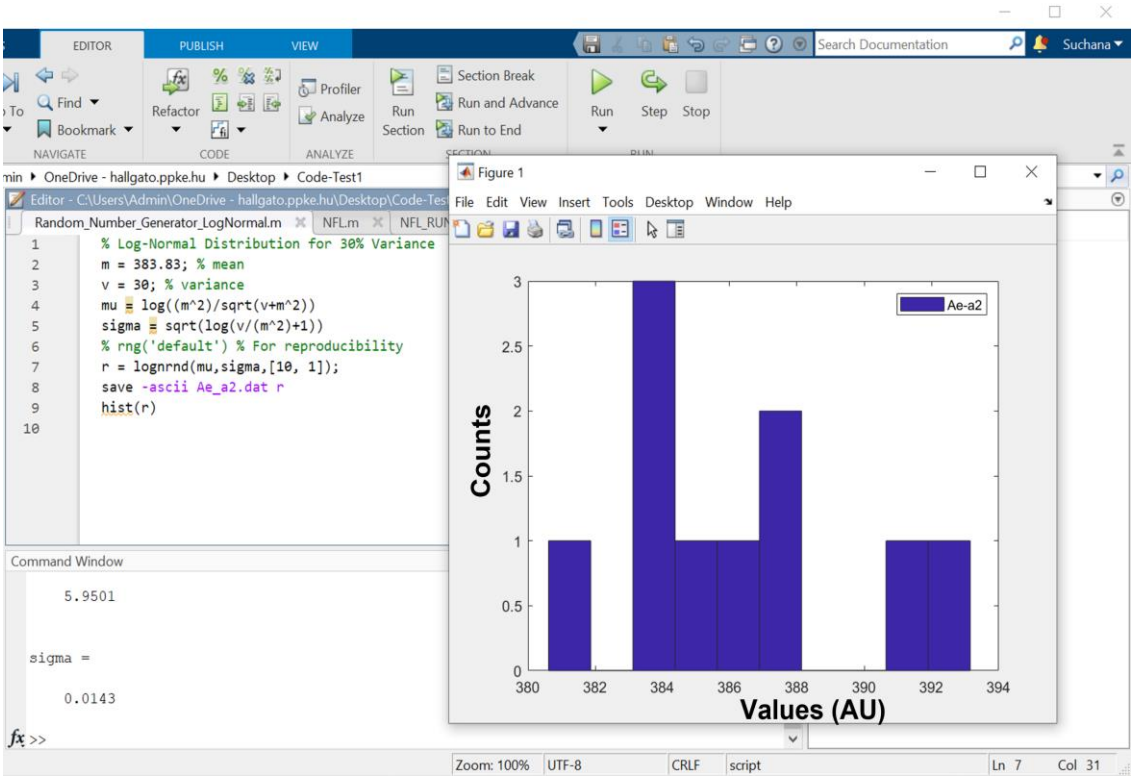

Figure 3.7: Random number generator.

The MATLAB code demonstrates how to produce 10 random numbers with 30 (AU^2) variance and a mean of 383.83 (AU) from a log normal distribution (left hand side). The histogram of these randomly distributed numbers is shown in the right panel.

To test the effects of extrinsic noise on this example, I have, produced for example 10 independent random sets of all parameters associated with the model shown in Figure 3.7. The numbers are drawn at random from a log normal distribution with a variance of 30 (AU^2) and a mean value of 383.83 (AU). The MATLAB code to create this is represented in Figure 3.7.

DOI:10.15774/PPKE.ITK.2023.004

In the main MATLAB file, these sets of random values and the function file have been called. The aim is to calculate the period of oscillations at seven different temperatures, with each parameter having ten randomly chosen values.

The function file can be written as follows:

```
function dcdt = NFL(t,c,Temp,...
    Ae_k1,Ae_k2,Ae_d1,...
    Ae_d2,Ae_k,Ae_a1,Ae_a2)
% variables stored within array
X = c(1);
Y = c(2);
% parameters are defined based on Arrhenius Equation : rate = A_e.e^(-E_a×1000/8.3144598×Temp)
% A_e = pre-exponential factor, E_a = activation energy, Temp = Temperature in
Kelvin, A_e is chosen randomly from a log normal distribution.
k1 = Ae_k1.*exp(-(31.8565.*10^3)/(8.3144598.*Temp)); %Ae_k1: random set
k2 = Ae_k2.*exp(-(31.8565.*10^3)/(8.3144598.*Temp)); %Ae_k2: random set
d1 = Ae_d1.*exp(-(14.7420.*10^3)/(8.3144598.*Temp)); %Ae_d1: random set
d2 = Ae_d2.*exp(-(14.7420.*10^3)/(8.3144598.*Temp)); %Ae_d2: random set
k = Ae_k.*exp(-(12.*10^3)/(8.3144598.*Temp)); %Ae_k: random set
a1 = Ae_a1.*exp(-(14.01.*10^3)/(8.3144598.*Temp)); %Ae_a1: random set
a2 = Ae_a2.*exp(-(17.9420.*10^3)/(8.3144598.*Temp)); %Ae_a2: random set
% initialization
dcdt = zeros(2,1);
% differential equations
dcdt(1) = (((a1.*k)./(k+Y)) - ((d1.*X)./(k1+X)));
dcdt(2) = ((a2.*X) - ((d2.*Y)./(k2+Y)));
```

The scheme for the main MATLAB file is described below:

```
t0 = 0;        % initial time
tf = 1150;     % final time
tspan = t0:0.02:tf;  % step length
css = [1 0]';      % initial conditions of X and Y
% load random parameters
load 'Ae_k1.dat';
load 'Ae_k2.dat';
load 'Ae_d1.dat';
load 'Ae_d2.dat';
load 'Ae_k.dat';
```

DOI:10.15774/PPKE.ITK.2023.004


```
load 'Ae_a1.dat';
load 'Ae_a2.dat';
% Loop for the parameter starts
for q=1:length(Ae_k)
    q
Ae_k1(q,1)=Ae_k1(q);
Ae_k2(q,1)=Ae_k2(q);
Ae_d1(q,1)=Ae_d1(q);
Ae_d2(q,1)=Ae_d2(q);
Ae_k(q,1)=Ae_k(q);
Ae_a1(q,1)=Ae_a1(q);
Ae_a2(q,1)=Ae_a2(q);
Temp = zeros(7,1);
X_val = zeros(length(tspan),7);
Y_val = zeros(length(tspan),7);
% Loop for the temperature starts
for i=1:7
    i
    Temp(i,1)=278+5*i;
[t,c]=ode45(@(t,c) NFL(t,c,Temp(i,1),Ae_k1(q,1),...
    Ae_k2(q,1),Ae_d1(q,1),Ae_d2(q,1),...
    Ae_k(q,1),Ae_a1(q,1),Ae_a2(q,1)),tspan,css); % ODE solve
X_val(:,i) = c(:,1);
Y_val(:,i) = c(:,2);
% Period of oscillation calculation
[peakval,locval]=findpeaks(X_val(:,i),t);
period(:,i) = mean(diff(locval));
end                 % End of temperature loop
period1(:,q) = period;
end                 % End of parameter loop
```

Finally, the output data (period of oscillation) is added into the diagrams in order to fully characterize the oscillatory behavior in the presence of extrinsic noise. The graphical representation for the calculation is shown in Figure 3.8. For extrinsic noise analysis shown in later chapters of this thesis I have created 1000 parameter sets to test the effects of extrinsic noise.

DOI:10.15774/PPKE.ITK.2023.004

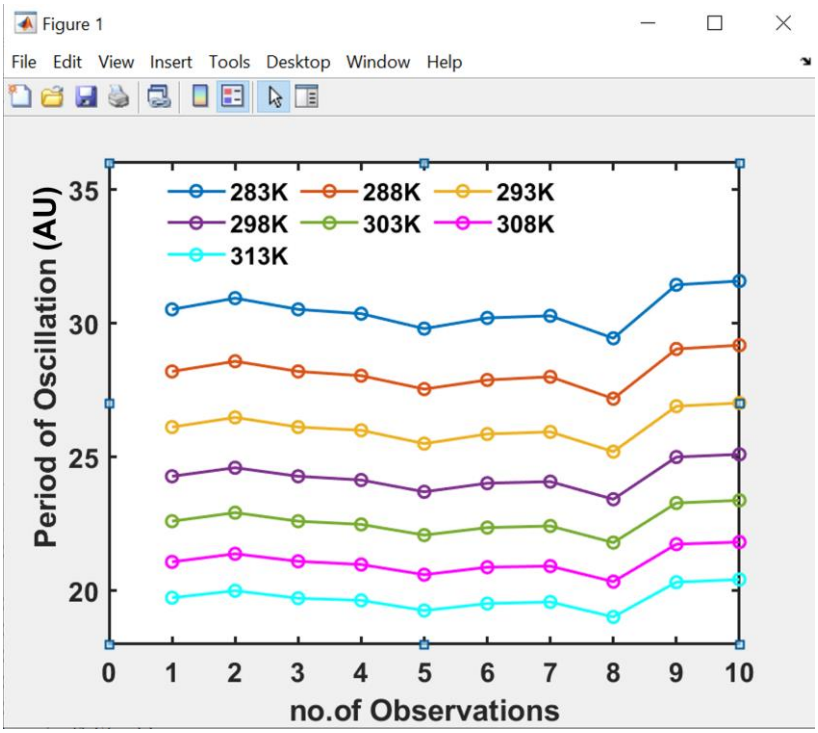

Figure 3.8: Calculation of period of oscillation for randomly chosen parameter set.

Here the period of oscillation has been plotted against the number of observations. Each of these observation points reflects parameter sets that were arbitrarily chosen. Different colored lines represent seven distinct temperatures.

3. Example-3: Stochastic Analysis for Intrinsic Noise

In this part, I will present the method I used to perform the Gillespie simulation on a NFB topology (Figure 3.5) and solve it in MATLAB in the presence of inherent noise. The ODEs (Equation 3.2, Equation 3.3) for this network are non-linear and do not follow mass action kinetics. So, this is not a classic example of Gillespie simulation because all the elementary reactions follow mass action kinetics. But here I want to simulate this network (Figure 3.5) in the classical Gillespie way, followed by the idea of an article by Gonze et al. [77]. Equations 3.2 and 3.3 are represented in terms of molecular numbers as below by introducing a volume scaling factor 'V_s':

$$\frac{dN_X}{dt} = \frac{a_1 \cdot k \cdot V_s^{\,2}}{k \cdot V_s + N_Y} - \frac{d_1 \cdot N_X \cdot V_s}{k_1 \cdot V_s + N_X} \tag{3.4}$$

DOI:10.15774/PPKE.ITK.2023.004

$$\frac{dN_Y}{dt} = a_2 \cdot N_X - \frac{d_2 \cdot N_Y \cdot V_s}{k_2 \cdot V_s + N_Y}$$

(3.5)

The scheme for the Gillespie simulation [59] in MATLAB is described below:

```
% Gillespie algorithm
% Rate constants declare
clear
clc
t = 0.0; % initial time
t_end = 1150.0; % final time
t_sample = 0.02; % sampling time
Nr = 4; % number of trajectory
Vs = 100; % scaling factor
t_run = t_end/t_sample+1;
k1=0.001;
k2=0.001;
d1=1.0003;
d2=1.0003;
k=3.0253;
a1=1.3442;
a2=0.2749;
% Initialization
j = 1.0; % counter for time
NX = 1.0*Vs; % initial X represented in numbers
NY = 0.0*Vs; % initial Y represented in numbers
% loop for trajectory starts
for q=1:Nr
%  Initial states before starting SSA
q
t_array(j,q)=t;
X_array(j,q)=NX;
Y_array(j,q)=NY;
% Reaction Propensities
while t < t_end
p1 = (a1.*k.*Vs.^2)./(k.*Vs+NY); % in numbers
p2 = (d1.*NX.*Vs)./(k1.*Vs+NX); % in numbers
p3 = a2.*NX; % in numbers
```

DOI:10.15774/PPKE.ITK.2023.004


```
p4 = (d2.*NY.*Vs)./(k2.*Vs+NY); % in numbers
h = [p1 p2 p3 p4];
%combined reaction propensities
    h0 = sum(h);
    if h0<=0
        h0=0.000000001;
    end
    r1=0+rand*(1-0);
            if (r1<=0)
                r1=0.00000001;
            end
%time update
     t_next = ((1/h0)*(log(1/r1)));
     t = t + t_next;
%determine next reaction
       i=1; mu=0; amu=0; r2=rand;
         while amu < r2*h0
              mu = mu + 1;
              amu = amu + h(i);
              i = i + 1;
         end
%reactions
if mu == 1
        NX = NX + 1;
    elseif mu == 2
        NX = NX - 1;
    elseif mu == 3
        NY = NY + 1;
    elseif mu == 4
        NY = NY - 1;
end
% avoid neg or zero values of the species
if NX<=0
NX=0.000001;
end
if NY<=0
NY=0.000001;
end
%store/output time and species
if t >= j*t_sample
```

DOI:10.15774/PPKE.ITK.2023.004


```
        j=j+1;
        t_array(j,q)=t;
        X_array(j,q)=NX;
        Y_array(j,q)=NY;
end
end % SSA ends here
j=1.0; % reset time counter
t=0.0; % reset initial time
NX=X_array(1,q); % NX update
NY=Y_array(1,q); % NY update
end  % trajectory loop ends
% Plot NX
figure(1)
hold on;
plot(t_array,X_array)
```

Oscillatory time evolutions from the four simulation runs have been plotted with distinct colors and shown in Figure 3.9.

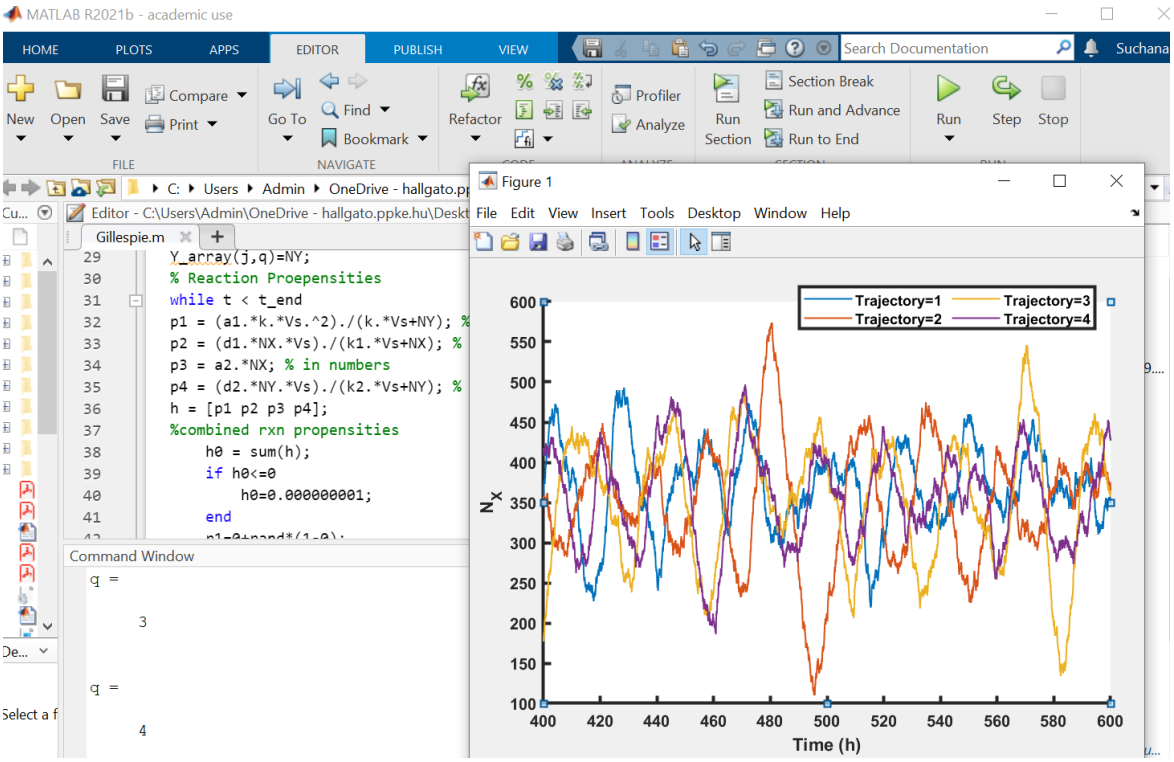

Figure 3.9: Gillespie simulation using MATLAB.

Here the oscillations have been plotted against the number of observations (four different observations). Each of these observation are represented with four different colors.

DOI:10.15774/PPKE.ITK.2023.004

Chapter 4

Comprehensive Study of Isolated and Coupled Feedforward Loops Towards Noise Reduction

DOI:10.15774/PPKE.ITK.2023.004

4.1. Biological Process and Cellular Noise

Noise in biological systems is caused by random variations in molecular levels [78–80]. In such a dynamic molecular environment, cells must make critical judgments, and their decision-making process must be capable of controlling stochastic fluctuations. When the random fluctuations are created by low-copy number molecules, it is called intrinsic noise. Extrinsic noises [81–83], on the other hand, can be generated by the dynamic environment that surrounds cells [84]. The intrinsic noise within a system correlate with the inverse of the square root of the number of molecules [85]. Because of the resulting changes in molecular numbers, systems regulated by low-abundant molecules may experience increased noise. A common example is gene expression, in which a small number of copies of transcription factors control the transcription of multiple genes [86]. Biochemical systems have also been shown to use signal processing techniques like low-pass filters that transduce lower-frequency signals and eliminate higher-frequency ones [87]. Following the idea of low-pass filters, I have explored how isolated and coupled feedforward loops reduce noise.

4.2. Isolated and Coupled FFLs

In a breakthrough study by Mangan et. al [88] revealed that feedforward loop (FFL) can be of two types: coherent FFL (cFFL) and incoherent FFL (iFFL). Type-1 coherent FFL (c1FFL), which includes activation steps only, is the most prevalent three-component FFL motif found across a wide range of biological systems. In fact, these network topologies can't be seen in isolated forms because they are found in coupled forms in biology. For example, immune cells are controlled by coherent and incoherent feedforward loops that are coupled to each other [15]. The mitogen activated protein kinase (MAPK) pathway is common in post-translational regulatory networks sometimes show examples of coupling between certain FFLs [16].

There are two types of coupled feedforward loops: multi-input coupled feedforward loops (minp-FFLs) (Figure 4.1C, 4.3C), and multi-intermediate coupled feedforward loops (mint-FFLs) (Figure 4.1D, 4.3D). It is possible for the coupled FFLs to be completely coherent, completely incoherent, or a combination of both coherent and incoherent, based upon the signs of interactions. Figure 4.1 presents 48 potential isolated FFL networks as well as coupled FFL networks that were identified. In order to conduct

DOI:10.15774/PPKE.ITK.2023.004

a systematic comparison analysis, four linear chain models with simple positive or negative influence running through the three-component topology were considered, as illustrated in Figure 4.1B.

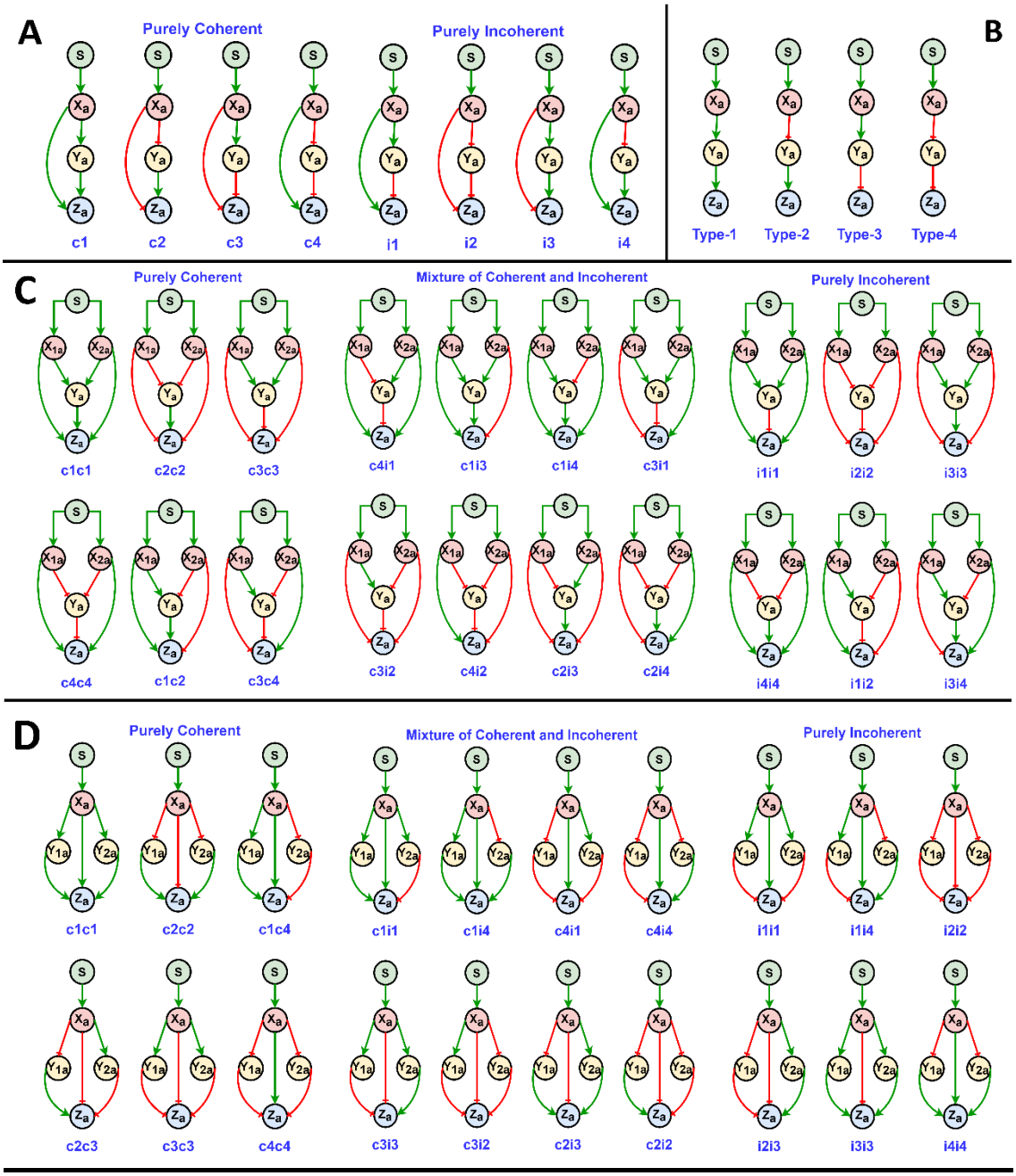

Figure 4.1: Coupled and Isolated FFL topologies.

(A) Isolated FFLs: The graphic depicts isolated feedforward loops that are fully coherent (left) or fully incoherent (right). Logical gates AND/OR are considered here. There are twelve different types of logical connection (Figure 4.2A). The letters 'c' and 'i' stand for coherent and incoherent, respectively. The number adjacent to 'c'/ 'I', denotes the model type. For example, c1 is a type 1 coherent model, whereas i4 is a type 4 incoherent model. Red and green arrows represent inhibition and activation processes,

DOI:10.15774/PPKE.ITK.2023.004

respectively. X_a is controlled by a noisy input S, which then affects the intermediate (Y_a) and the output (Z_a) through the direct and indirect pathways.

(B) Chain models: The graphic depicts all kinds of chain models that are feasible. The noisy input (S) acts as a regulator for X_a, which in turn has an influence on Y_a. The output (Z_a) is then regulated by Y_a.

(C) Multi-input coupled FFLs (minp-FFLs): All the possible minp-FFL topologies are shown here. Minp-FFL is divided into three types- fully coherent (left), mixed coherent and incoherent (middle), and fully incoherent (right) FFLs. Input (S) activates nodes X_{1a} and X_{2a} simultaneously. Through direct arms Y_a is influenced by X_{1a} and X_{2a}. The output (Z_a) is influenced by X_{1a} and X_{2a} through the indirect arms. By considering logical connectivity, there can be four types of gates: pure AND, pure OR, upper-AND-lower-OR (uAND-lOR), and upper-OR-lower-AND (uOR-lAND) (Figure 4.2C). In this diagram, green arrows indicate activation, while red arrows indicate inhibition.

(D) Multi-intermediate coupled FFLs (mint-FFLs): Here the networks are classified as either purely coherent (left), a combination of coherent and incoherent (middle), or purely incoherent (right). X_a is governed by the noisy input (S). Y_{1a}, Y_{2a}, and the output (Z_a) are controlled by X_a via direct and indirect arms respectively. The green arrows indicate activation, while the red arrows indicate inhibition. Only pure AND/OR types of logical gates can be constructed here (Figure 4.2D).

4.2.1. Description of Investigated Models

Posttranslational modifications involving activation and inhibitory processes were taken into account while developing the investigated networks. I consider, posttranslational modifications, including phosphorylation and dephosphorylation, that occur at various sites on biomolecules with rates equal to k_p and k_{pp}. Two varieties of each model are taken into account. In one-step posttranslational modification motifs, there exists a single mass-action transition from active to inactive forms, but in two-step posttranslational modification networks, the change occurs through an intermediary step. Back-and-forth enzyme kinetics, which are also called Goldbeter-Koshland switches [45,89,90], have the same kind of dynamics as these two-step processes.

Initially, a correlated noisy input signal is chosen that has a super-Poissonian [91] distribution (Fano factor > 1) (Figure 4.3F). To do this, two copies of a noisy input (S) has been created from a deterministic signal A^+, which has 5 steps as shown in Figure 4.3F. At a rate equals to k_a, the stochastic input signal (S) activates the node X into X_a. Then X_a influences Y with a rate equals to k_1. This might be either inhibitory or activatory. If activation takes place Y becomes Y_a and for inhibition Y_a becomes Y. The output (Z) is influenced by Y_a and X_a with the rate constants equal to k_2 and k_3

DOI:10.15774/PPKE.ITK.2023.004

respectively. When Z is turned on, it becomes Z_a, which is the active form of Z. When Z is turned off, it becomes Z, which is the inactive form of Z. All the reaction parameters are designed in such a way that no species approaches the minimum (0 AU) or maximum (60 AU) concentration values. This is done to avoid both the signal loss and noise cancellation from saturation.

4.2.2. Different Kinds of Logical Gates

When multiple molecules interact with a downstream component, the two inputs may impact the target either individually (known as OR gate) or jointly (known as AND gate). The only logical gates obtainable to mint-FFLs and isolated FFLs are AND/OR. For minp-FFLs there are four possible logical gates: completely AND, completely OR, upper-AND-lower-OR (uAND-lOR), and upper-OR-lower-AND (uOR-lAND) (Figure 4.3E). Both OR and AND gates may be considered if the incoming signals have the same sign impact upon the target molecule. In contrast, when the influences include opposite effects, only a single type of gate can be taken into consideration, which is not a true AND or a true OR gate but is functioning more like an OR gate.

In OR type of connectivity X_{1a} and X_{2a} can act independently to activate Y with a rate constant value k_1 as follows:

$$X_{1a} + Y \rightarrow \{k_1\}\, X_{1a} + Y_a$$

$$X_{2a} + Y \rightarrow \{k_1\}\, X_{2a} + Y_a$$

The ODE for the above-mentioned two reactions can be written as follows:

$$\frac{dY_a}{dt} = k_1 \cdot X_{1a} + k_1 \cdot X_{2a} \tag{4.1}$$

I include a complex formation step in the case of AND models, such that the overall conversion rate between both the AND and OR gated models would remain the same. For reference, instead of employing choosing a rate equals to 0.5· k1 rate (to fit with the maximum rate attainable in an OR model),, when X_{1a} and X_{2a} simultaneously activate Y with a rate constant parameter value k_1, I have included the complex formation step as follows:

$$X_{1a} + X_{2a}\{200\} \leftrightarrow \{200\}C1$$

DOI:10.15774/PPKE.ITK.2023.004

With a high conversion rate (equals to 200) the complex C1 is formed. Due to the fast reversable reaction, the equilibrium between the steady states of X_{2a}, X_{1a} and C1 are always maintained. Following that, the complex C1 operates on Y at a constant rate k_1 as follows:

$$Y + C1 \rightarrow \{k_1\}\, C1 + Y_a$$

Like this, the complex C1 carry forward the information of both X_{2a} and X_{1a}. The relevant ODEs for these two reactions are as follows:

$$\frac{dC1}{dt} = 200 \cdot X_{1a} \cdot X_{2a} - 200 \cdot C1 \tag{4.2}$$

$$\frac{dY_a}{dt} = k_1 \cdot C1 \tag{4.3}$$

In this chapter, I explored 68 potential FFL combinations and compared their behavior to 12 isolated FFLs and 4 linear chain models. Figure 4.2 depicts the possible logical gates for the network motifs shown in Figure 4.1.

DOI:10.15774/PPKE.ITK.2023.004

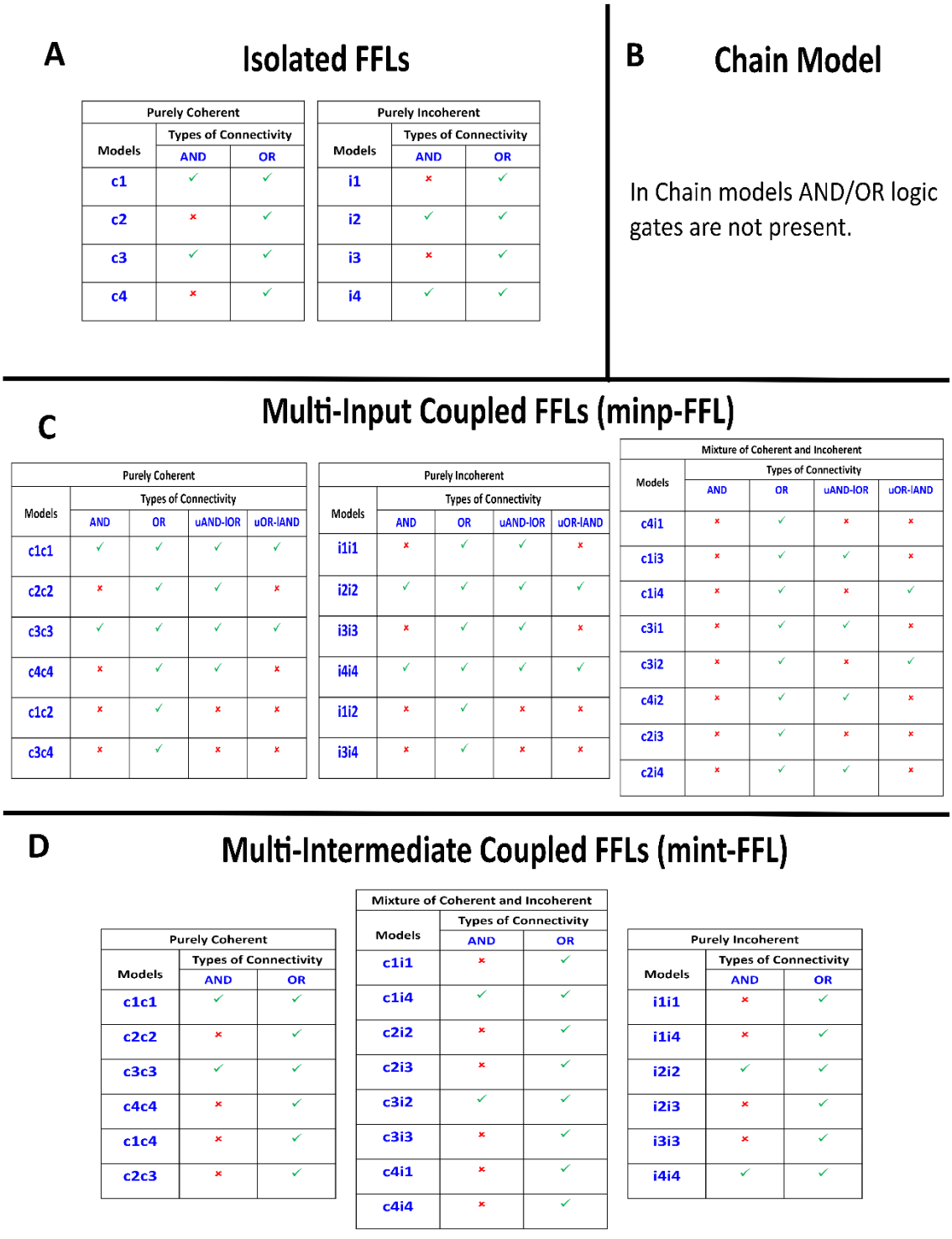

A — Isolated FFLs

Purely Coherent		
Models	Types of Connectivity	
	AND	OR
c1	✓	✓
c2	×	✓
c3	✓	✓
c4	×	✓

Purely Incoherent		
Models	Types of Connectivity	
	AND	OR
i1	×	✓
i2	✓	✓
i3	×	✓
i4	✓	✓

B — Chain Model

In Chain models AND/OR logic gates are not present.

C — Multi-Input Coupled FFLs (minp-FFL)

Purely Coherent				
Models	Types of Connectivity			
	AND	OR	uAND-IOR	uOR-IAND
c1c1	✓	✓	✓	✓
c2c2	×	✓	✓	×
c3c3	✓	✓	✓	✓
c4c4	×	✓	✓	×
c1c2	×	✓	×	×
c3c4	×	✓	×	×

Purely Incoherent				
Models	Types of Connectivity			
	AND	OR	uAND-IOR	uOR-IAND
i1i1	×	✓	✓	×
i2i2	✓	✓	✓	✓
i3i3	×	✓	✓	×
i4i4	✓	✓	✓	✓
i1i2	×	✓	×	×
i3i4	×	✓	×	×

Mixture of Coherent and Incoherent				
Models	Types of Connectivity			
	AND	OR	uAND-IOR	uOR-IAND
c4i1	×	✓	×	×
c1i3	×	✓	✓	×
c1i4	×	✓	×	✓
c3i1	×	✓	✓	×
c3i2	×	✓	×	✓
c4i2	×	✓	✓	×
c2i3	×	✓	×	×
c2i4	×	✓	✓	×

D — Multi-Intermediate Coupled FFLs (mint-FFL)

Purely Coherent		
Models	Types of Connectivity	
	AND	OR
c1c1	✓	✓
c2c2	×	✓
c3c3	✓	✓
c4c4	×	✓
c1c4	×	✓
c2c3	×	✓

Mixture of Coherent and Incoherent		
Models	Types of Connectivity	
	AND	OR
c1i1	×	✓
c1i4	✓	✓
c2i2	×	✓
c2i3	×	✓
c3i2	✓	✓
c3i3	×	✓
c4i1	×	✓
c4i4	×	✓

Purely Incoherent		
Models	Types of Connectivity	
	AND	OR
i1i1	×	✓
i1i4	×	✓
i2i2	✓	✓
i2i3	×	✓
i3i3	×	✓
i4i4	✓	✓

Figure 4.2: Logical gates.

All the possible logic gates for the isolated FFLs (A), chain models (B), minp-FFLs (C) and mint-FFL (D) are shown.

DOI:10.15774/PPKE.ITK.2023.004

4.3. FFLs Towards Noise Reduction

Numerous network topologies are effective in reducing noise in biology. Among them NFB loop has been often seen as a noise reducer [23,92,93]. There are several signaling pathways that may filter the noise through membrane receptor activation, therefore mRNA regulation is not the sole mechanism that can minimize noise [94]. One such signaling pathway that can reduce noise is the linear MAPK pathway [34]. MAPK pathway and other networks with posttranslational modification can also reduce noise [95,96]. Engineering concepts were brought into biology to demonstrate the potential low-pass filtering function of biological networks. Normal network patterns that could be used to filter out noise were found. Among these, FFL got a lot of attention [97]. It has been found that c1FFL works as a low-pass filter that minimizes noise [35,36]. The annihilation module consists of two molecules that have correlated synthesis and coordinated degradation (Figure 4.3B), which acts as an effective noise reducing motif but adds a delay to the system. The annihilation module coupled with an iFFL produces a very efficient noise cancelling annihilation filter with zero additional delays [87]. This idea has inspired to investigate the noise reduction properties in a coupled FFL system.

An effective strong noise reducer will remove noise from the system while also lowering signal transduction capabilities [98,99]. A signal processing pathway should limit the noise that affects cells while yet being able to react to important changes [100]. Low-pass filters will facilitate with this, but a proper application in biological context is still missing. In this chapter, all kinds of feasible coupled FFLs have been compared with the isolated FFL and linear chain models in terms of noise reduction and signal transduction abilities. The research takes into account posttranslational changes that can activate or inhibit molecules in every layer of the FFLs.

4.4. Estimation of Noise

The assessment of noise is crucial for a systematic study of the noise reduction capabilities of various FFLs. Numerous numerical simulation techniques exist for estimating noise. Among these methods, the LNA is a quick approach for approximating CRNs [65]. I performed LNA on the models to compute the distribution of every species using the 'Kaemika' software. The codes for each network have been uploaded in GitHub (https://github.com/SuchanaChakravarty/Noise-Reduction-Properties-of-Coupled-and-

DOI:10.15774/PPKE.ITK.2023.004

isolated-Feed-Forward-Loops.). The Kaemika tool is available for download from all application stores (http://lucacardelli.name/).

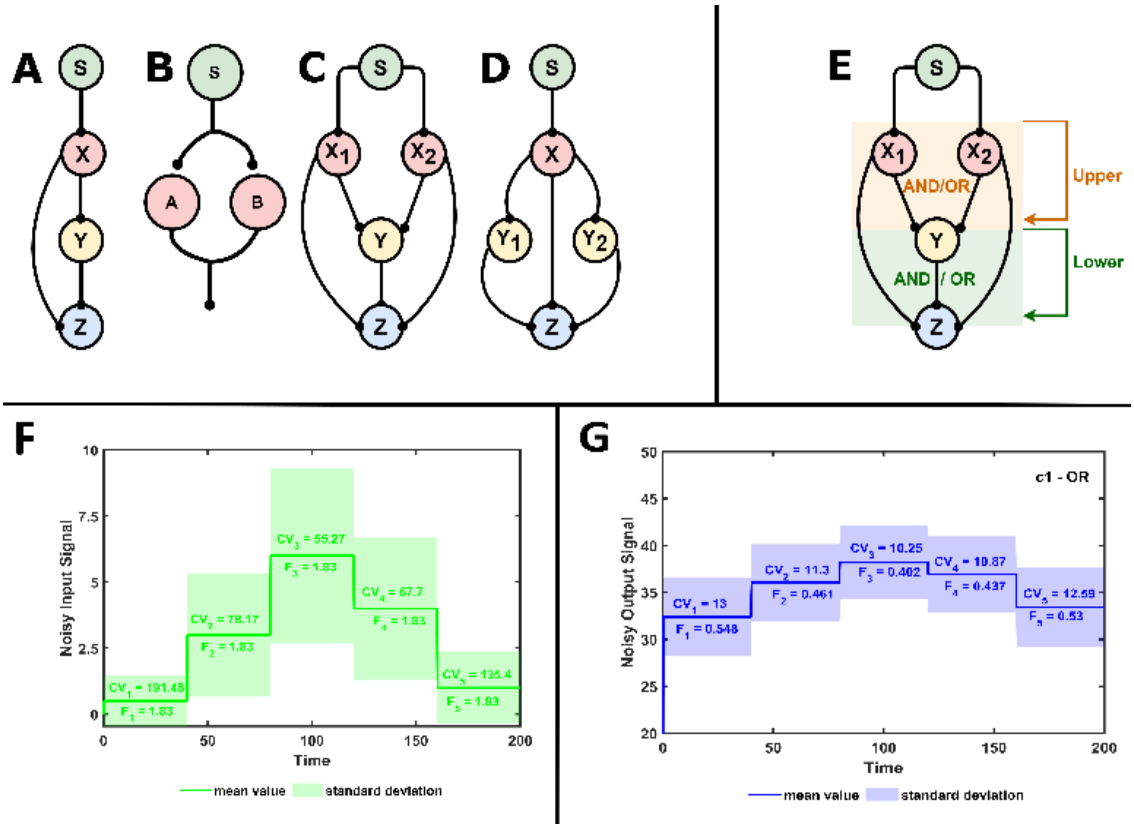

Figure 4.3: Networks and effects of noise on input and output.

Network topology of isolated FFL (A), annihilation motif (B), coupled minp-FFL (that partially resembles with annihilation module) (C) and coupled mint-FFL (D) are shown. 4 possible logical gates for coupled minp-FFL have been displayed (E). For the noisy input (S), the % CV and fano factor values at each of the 5 steps have been shown. (F). Across all the input levels, the mean output levels and the estimated noise for the output are recorded. This indicates a lower fano factor and % CV value for the output (G). parameters are $k_1=k_2=k_3=1$, kp=10, kpp=40, $k_a=5$.

For the purpose of quantifying noise, the percentile coefficient of variation (% CV) for each model has been evaluated. Fano factor quantifies signal's noise, however, CV is a more accurate indicator for the signal to noise ratio. This is really important in signal transduction; and hence, the values are displayed over the plots in Figure 4.3F, G. For any random process, standard deviation over the mean is known as coefficient of variation [70,101]. Poisson noise seems to have a fano factor equals to 1 and a CV equals to $(\text{mean value})^{-1/2}$. When the value for fano factor or CV is low, it means that the system is less noisy. The slope obtained from a mean output vs mean input plot is described as

DOI:10.15774/PPKE.ITK.2023.004

a signal transduction capacity. Signal transmission is better when the slope is higher, and signal inversion is what happens when the slope has negative value.

4.5. Comparison of Noisiness Among Isolated FFLs and Chain Models

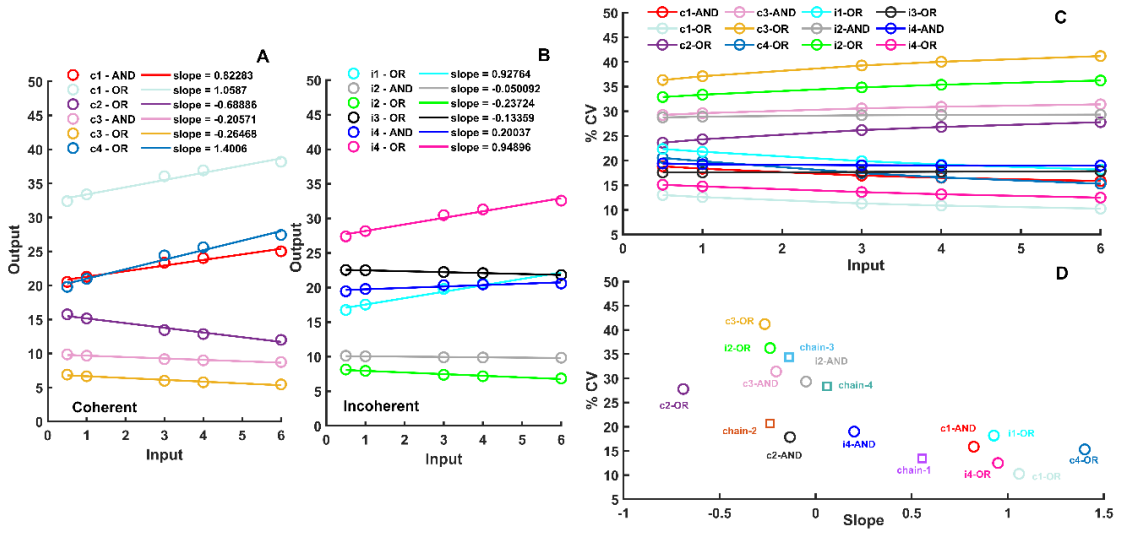

Figure 4.4: Noise attenuation and signal transduction abilities of linear chain models and isolated FFLs.

For all the species one-step posttranslational modification has been considered. Subplot (A) and (B) display the average input- average output relation of the coherent and incoherent isolated FFLs respectively. (C) To test the noise attenuation skills of the isolate FFLs, the % CV of the output has been plotted for each 5-step noisy input (Figure 4.3F). At input = 6, the slopes from panels A, B, and Figure 4.5 for isolated FFLs and chain models, respectively, are plotted against the % CV (D). This shows how well each network works at getting rid of noise and transmitting signals. Here the parameter values are : $k_1=k_2=k_3=1$, $k_p=10$, $k_{pp}=40$, $k_a=5$.

The linear chain models (Figure 4.1B) resemble the classical MAPK signaling pathways. This type of simple signaling cascades can also reduce noise to some extent. As a reference point, I compared these linear chain models to FFL networks. Both iFFL and cFFL may have negative or positive slopes based on the sign of the indicated interactions (Figure 4.4A, B). Lower % CV values of the outputs than the input suggests that these networks can act as a noise filter (Figure 4.4C). A higher input value leads to a lower % CV, as the mean of the molecules increases along with the input value, resulting in less noise. For an input value of 6, the %CVs of the isolated FFLs and linear chain models are plotted (Figure 4.4D) against the slopes obtained from Figure 4.4A, Figure 4.4B and

DOI:10.15774/PPKE.ITK.2023.004

Figure 4.5. This tells how to compare FFLs in terms of signal transduction and noise attenuation.

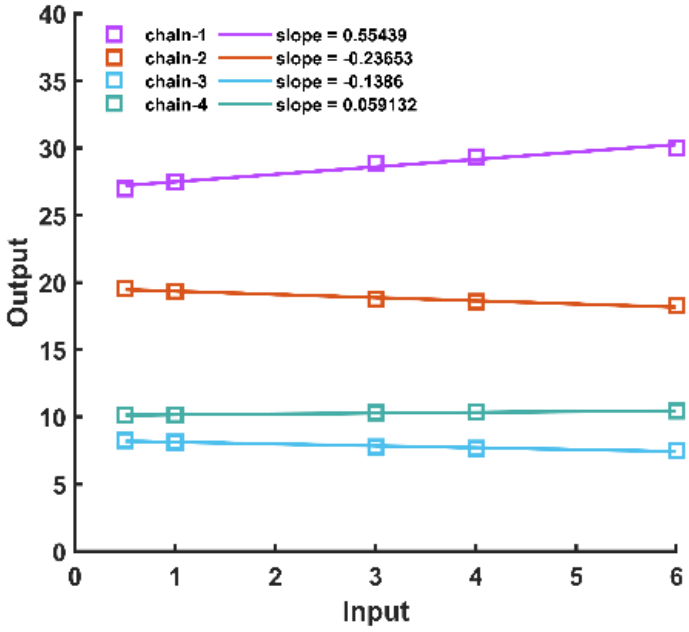

Figure 4.5: Correlation plot of linear chain models.

The graph shows the relationship between the output and the input for chain models. Figure 4.3F shows the noisy input that passed into the system. The plot indicates the slope values for each of the networks. Parameter values are : $k_1=k_2=k_3=1$, $k_p=10$, $k_{pp}=40$, $k_a=5$ and the species undergo one-step posttranslational modification.

It is intriguing that a lower CV value (less noise) correlates with greater signal transduction value (high slope value). The c1-OR network works the best in both cases, which is not surprising since it has been shown to work well, as both a low-pass filter [102] and a great signal transducer [99]. In a small network, the existence of non-linearity via active and inactive states might result in a noise filter. Among the chain models, only type-1 chain model demonstrates little signal transduction ability (Figure 4.4D). The rest are having negligible signal transmitting capacity. Type-1 chain motif resembles with MAPK regulation. Type-1 chain model exhibits ultra-sensitivity [103], and can minimize noise. It can also convert a signal transducer to an analog-digital converter.

4.6. Comparison of Noisiness Among Coupled FFLs

Often, signaling pathways do not work alone. There is the possibility of having various combinations of FFLs that can act as a noise filter modules while simultaneously having

DOI:10.15774/PPKE.ITK.2023.004

good signal transduction capacity. In order to have a systemic analysis, I have tested the signal transduction and noise reduction abilities of all the possible combinations of FFLs.

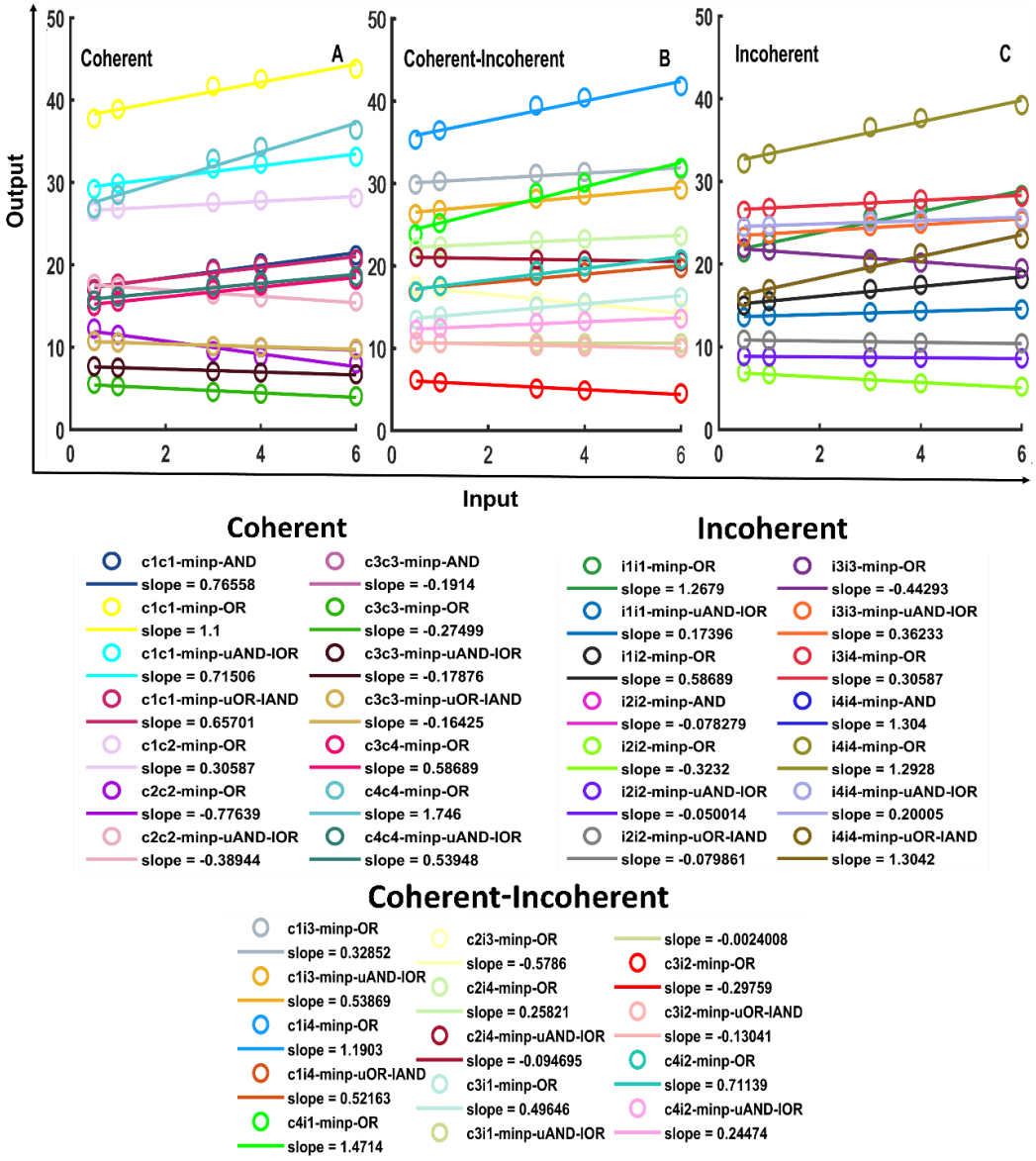

Figure 4.6: Correlation plot of coupled minp-FFLs.

The graph displays the relationship between the output and the input for minp-FFLs. Figure 4.3F depicts the stochastic input that passed into the models. The plot indicates the slope values for each of the networks calculated by linear regression process. Parameter values are : $k_1=k_2=k_3=1$, $k_p=10$, $k_{pp}=40$, $k_a=5$ and the species undergo one-step posttranslational modification. Each model falls into one of three categories: completely coherent (A), combined coherent and incoherent (B), and completely incoherent (C). All 4 possible logical gates (OR, AND, upper-OR-lower-AND (uOR-lAND), and upper-AND-lower-OR (uAND-lOR)) are taken into consideration.

By taking into account different permutation combinations, I've been able to model 42 different coupled minp-FFLs and 26 different coupled mint-FFLs. Output input

DOI:10.15774/PPKE.ITK.2023.004

correlation plots have been shown for these 42 coupled minp-FFLs (Figure 4.6) and 26 mint-FFLs (Figure 4.7).

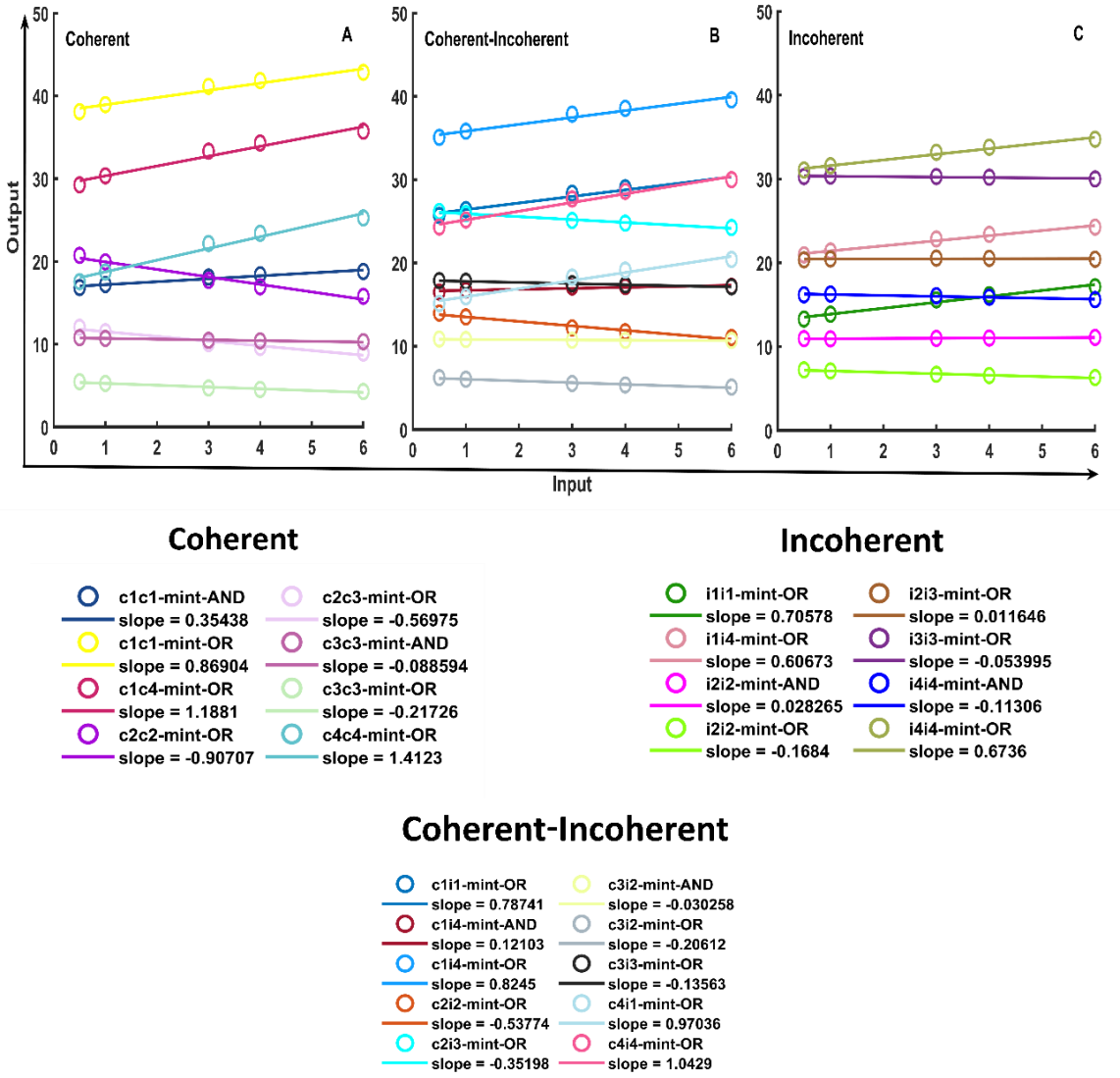

Figure 4.7: Correlation plot of coupled mint-FFLs.

The correlation plot displays the relationship between the output and the input for mint-FFLs. Figure 4.3F shows the noisy input that passed into the networks. The plot indicates the slope values for each of the networks calculated by linear regression process. Parameter values are : $k_1=k_2=k_3=1$, $k_p=10$, $k_{pp}=40$, $k_a=5$ and the species undergo one-step posttranslational modification. Each model falls into one of three categories: truly coherent (A), mixed coherent and incoherent (B), and truly incoherent (C). All 2 possible logical gates (OR, AND) are considered here.

The percentile coefficient of variation (% CV) has been displayed (Figure 4.8) against the slope values of these network motifs obtained from the input-output relationship plots (Figure 4.6, Figure 4.7). This also given an essence of the behavioral changes of signal transduction capacity towards noise for the coupled FFLs. Notably, there is a typical

DOI:10.15774/PPKE.ITK.2023.004

negative relation between the % CV and the slope values. For the fact, networks with greater noise reduction also exhibit higher signal transduction. Coherent minp-FFLs are the highest-performing network architectures. A system in which all responses activate their targets species, and both the arms act independently is the most effective noise suppressor (c1c1-minp-OR FFL). The best signal transducer is also a coherent minp-FFL. However, in this case, the longer branch consists of two inverted inhibitory responses (c4c4-minp-OR FFL). Further, it can be inferred that coupling two FFLs at an input level results in stronger noise suppression than coupling the similar FFLs at an intermediate step (Figure 4.8A and Figure 4.8B).

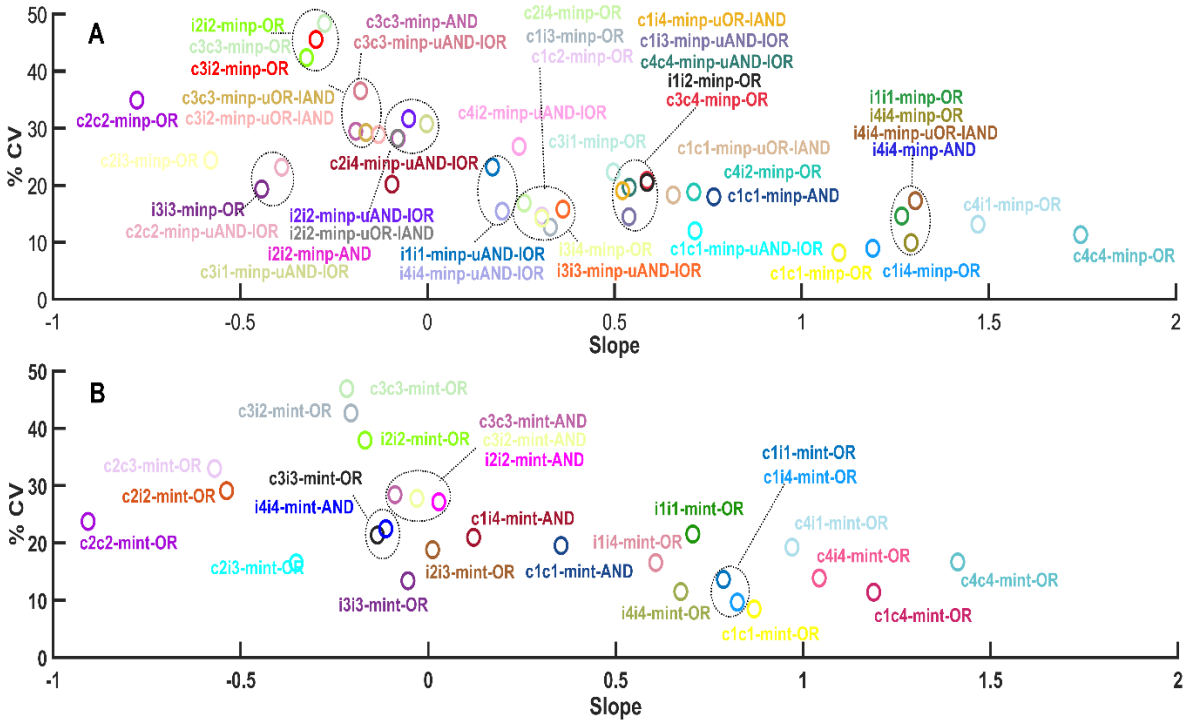

Figure 4.8: The ability of coupled FFLs to transduce signals and attenuate noise.

To demonstrate how each coupled minp-FFL (A) and mint-FFL (B) system operates in noise suppression and signal transduction, the % CV of each coupled FFL is computed at input = 6 and displayed against the slopes obtained from the correlation plots shown in Figure 4.6 and Figure 4.7. Parameter values are : $k_1=k_2=k_3=1$, $k_p=10$, $k_{pp}=40$, $k_a=5$ and one-step posttranslational modification case have been considered.

DOI:10.15774/PPKE.ITK.2023.004

4.7. Coupled FFLs vs Isolated FFLs

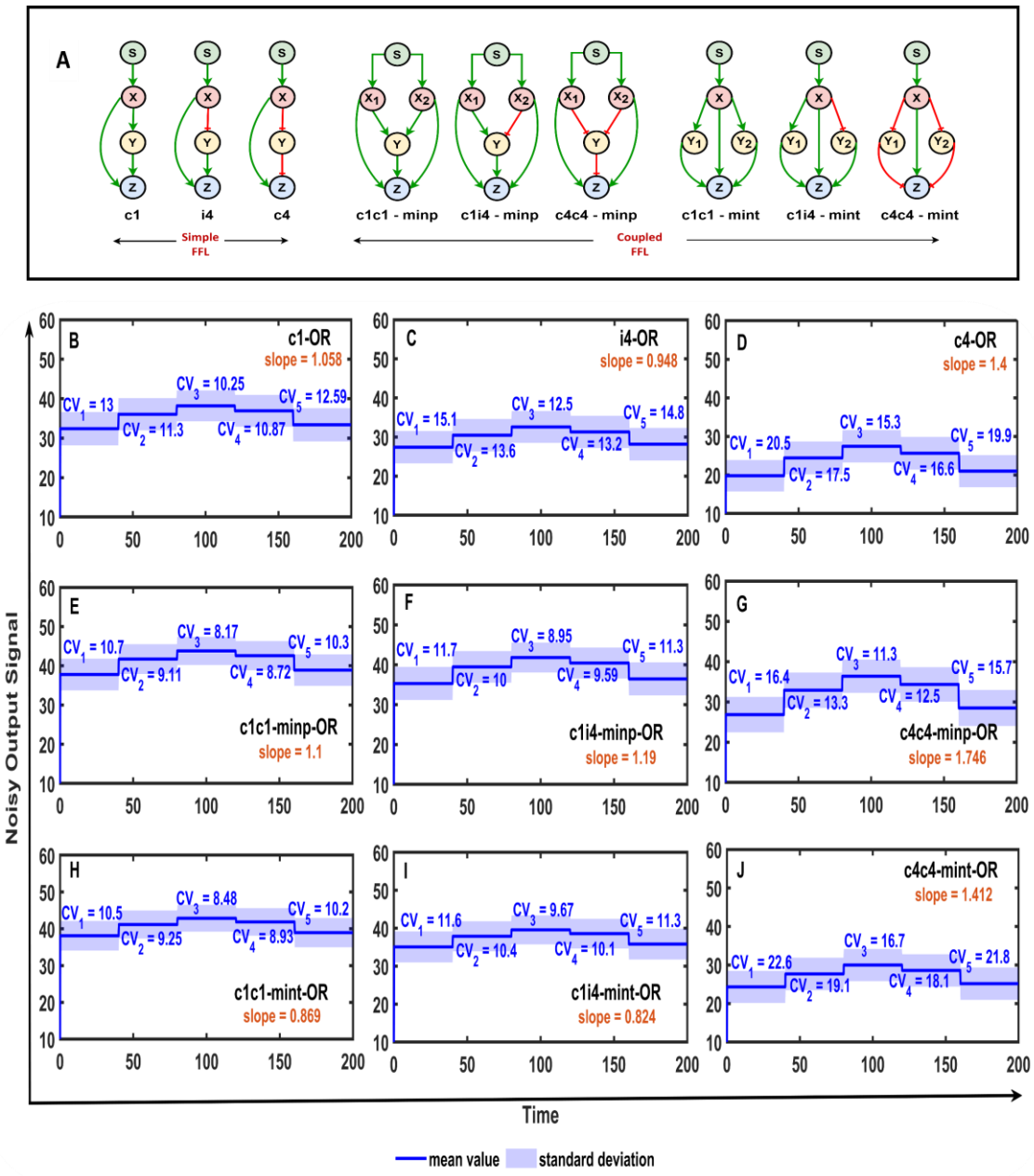

Figure 4.9: Comparison of the top performing FFL motifs in terms of noise reduction and signal transduction.

In this figure, the top performing isolated and coupled FFL networks are presented (A). The noise reduction efficacy of all of these models is presented in the panel (B-J). Figure 4.3F shows the noisy input that passed into the networks. Statistical quantities like, mean, ± standard deviations (shaded region), % CV, and slope values of all these networks' outputs are indicated in the plots. All simulations are performed using preset parameter values: $k_1=k_2=k_3=1$, $k_p=10$, $k_{pp}=40$, $k_a=5$ and one-step posttranslational modifications.

DOI:10.15774/PPKE.ITK.2023.004

The goal of this research is to determine the function of coupled FFLs in noise reduction and signal transduction capability. To come up with the best approach, I compared the noise filtering and signal transduction properties of coupled FFLs to those of isolated FFLs. When comparing Figures 4.4D and 4.8, it is clear that coupled FFLs have higher noise-reduction capabilities than isolated FFLs. To examine the top performing isolated and coupled FFL motifs in further detail (Figure 4.9A), the mean, standard deviations (shaded region), % CV, and slope values of all these networks' outputs (Figure 4.9B-J) are displayed. The usual input changes (Figure 4.3F) are implemented to all the networks in this case, and the results reveal that c1c1-minp-FFL-OR is the best noise filter (having a lowest % CV) and c4c4-minp-OR is best signal transducer (with highest value for slope). The fundamental incoherent type 4 FFL performs well too, and its many combinations with coherent type 1 FFL result in a best-performing coupled FFL when the two FFLs vary. Large negative slope values imply that inverted signal transduction is effective. Type 2 coherent FFL (c2) acts as a good signal transducer inverter and also possesses noise filtering abilities.

4.8. Good vs Bad FFLs

Among different network topologies of coupled and isolated FFLs, it is worthwhile to be able to distinguish between the networks that work well in terms of noise attenuation and signal transduction. From Figures 4.4D and 4.8, the good and the bad FFLs in terms of noise reduction can be identified. Noise analyses (% CV) in each layer of these good and bad FFLs indicate a significant differences. In good noise filters, noise decreases along the lower levels of FFLs (with minor variations in case of incoherent FFLs), but in case of poor noise filters, the intermediate layer (i.e. species Y) has the best noise reducing capacity (Figure 4.10). In this study we examined isolated FFLs: c1-OR (Figure 4.10A), c3-OR (Figure 4.10B), minp-FFLs: c1c1-minp-OR (Figure 4.10C), c3c3-minp-OR (Figure 4.10D), and mint-FFLs: c1i4-mint-OR (Figure 4.10E), c3i2-mint-OR (Figure 4.10F). This result demonstrates that networks that are thought to be poor noise reducers may still be detected in biology when significant signals are utilized for cross-talking from intermediate layers of pathways [104]. This implies that excellent noise-reducing models at the output nodes are efficient in noise attenuation since the noise decreases as the signal advances through lower levels of FFLs.

DOI:10.15774/PPKE.ITK.2023.004

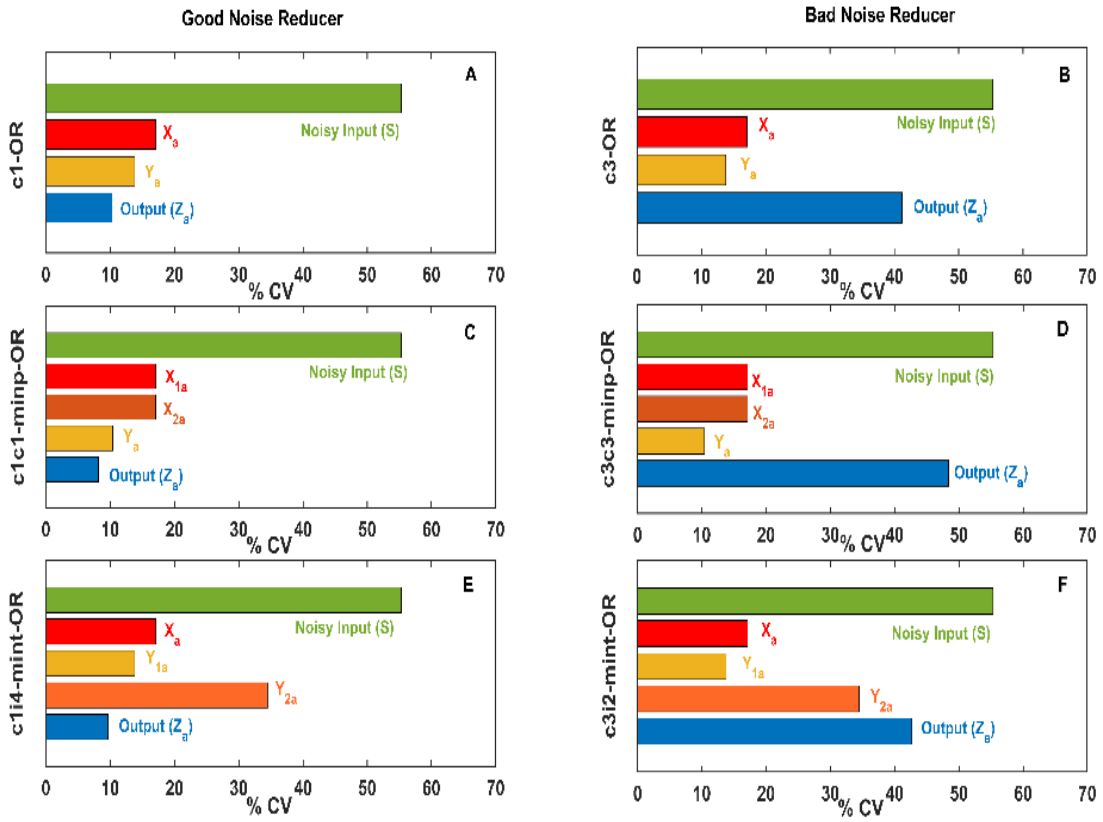

Figure 4.10: Noise filtering capabilities among good and bad performing FFLs.

When the input level equals 6, the % CV of every species associated with the best noise-filter (A,C,E) and the worst noise-filter (B,D,F) are presented in panels (A,C,E) and (B,D,F), respectively. Consider parameter values: $k_1=k_2=k_3=1$, $k_p=10$, $k_{pp}=40$, $k_a=5$ and one-step posttranslational modifications.

4.9. Studying Noise Reduction Capabilities of FFLs While Altering Level of Noise in Input

Based on the previous part, I was able to differentiate between FFLs that perform better or worse in terms of noise reduction and signal transduction capability. The next question is what causes certain FFLs to do well in noise reduction while others perform poorly in this job. That is why I perturbed the input with a greater or smaller levels of noise to comprehend the significant variations in the noisiness at the output nodes. The noisiness at the input level has been provided by a molecule that was produced in doublets, and this results in a super-Poissonian distributed noise. Later, by altering the synthesis kinetics and rate I was able to generate a lower and a higher level of noise at the input (shown below at the Increased and Decreased Scenario respectively).

DOI:10.15774/PPKE.ITK.2023.004

There are no significant differences in the level of noise for the output level when the input has been altered with smaller and larger levels of noise (Figure 4.11). When the degree of input noise is raised, three copies of S have been formed, but when it is dropped, only one copy of S has been made. The rate of production of these following reactions needs to be scaled in a manner that will hold the average input level value unchanged. This phenomenon has been described below-

Original Scenario:

A^+ -> S + S + A^+, original rate constant = 200

Decreased Scenario:

A^+ -> S + A^+, rate constant for this reaction needs to be doubled of the original rate so that the steady state value of the input remains unchanged.

Increased Scenario:

A^+ -> S + S + S + A^+, rate constant for this reaction will be 2/3 times of the original rate in order to keep the steady state value of the input same.

The figure demonstrates that the noise that occurs at each level of posttranslational modification to FFLs is a characteristic that is intrinsic to them and is not much influenced by the noise that occurs at the input nodes. This result is true for models that perform well in terms of noise reduction, but it does not hold true for models that perform poorly. For the poor noise reducer models, the intermediate nodes reduce noise more effectively than the output nodes (Figure 4.11).

DOI:10.15774/PPKE.ITK.2023.004

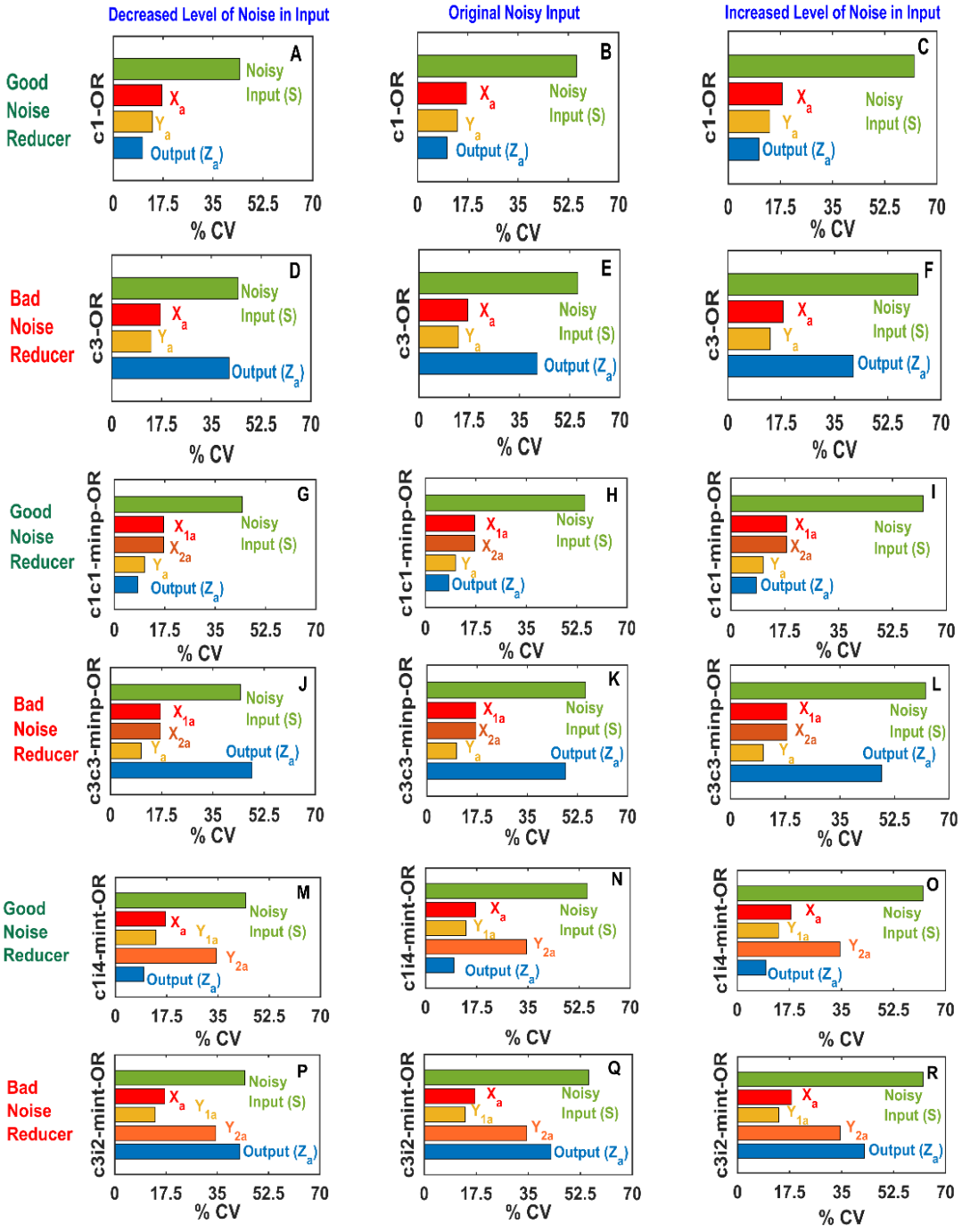

Figure 4.11: Estimated noise in every level of the best and worst noise filtering networks.

Demonstrated how noise propagates along the pathways for c1-OR (A,B,C), c3-OR (D,E,F), c1c1-minp-FFL (G,H,I), c3c3-minp-FFL (J,K,L), c1i4-mint-FFL (M,N,O), and c3i2-mint-FFL (P,Q,R) models by raising (right panel) and reducing (left panel) the degree of noise in the input and comparing it to the initial noisy input (middle panel). The estimation has been done at input = 6 and parameter set is $k_1=k_2=k_3=1$, $k_p=10$, $k_{pp}=40$, $k_a=5$. Single step posttranslational modification is considered.

DOI:10.15774/PPKE.ITK.2023.004

4.10. Comparing Noise Filtering Properties Among FFLs containing AND and OR logical Gates

I previously discussed the good and bad noise reducer FFL models. Now I would like to explore more about the type of connectivity between the network nodes that can be the key factor in controlling the noise. So, in this section, I compared FFL networks with AND or OR logical connection to see which kind of logical gates is superior for noise reduction for a certain model (Figure 4.12). It is worth noting that combined FFLs with AND logical gates have a lower noise reduction abilities than the models having OR gates (Figure 4.13, Figure 4.14). It's more difficult to observe this pattern in the busier image Figure 4.8, but the same connection holds true for all models, particularly when assessing effective and poor noise reducers (Figure 4.12). Level of noise in the input goes down to lower levels of the motif through simultaneous influence in coupled FFLs, and these correlating noises increase their combined impact when they merge at the output nodes via an AND gate. This apparent increase in the noise appears to be mitigated when the network has a OR gate.

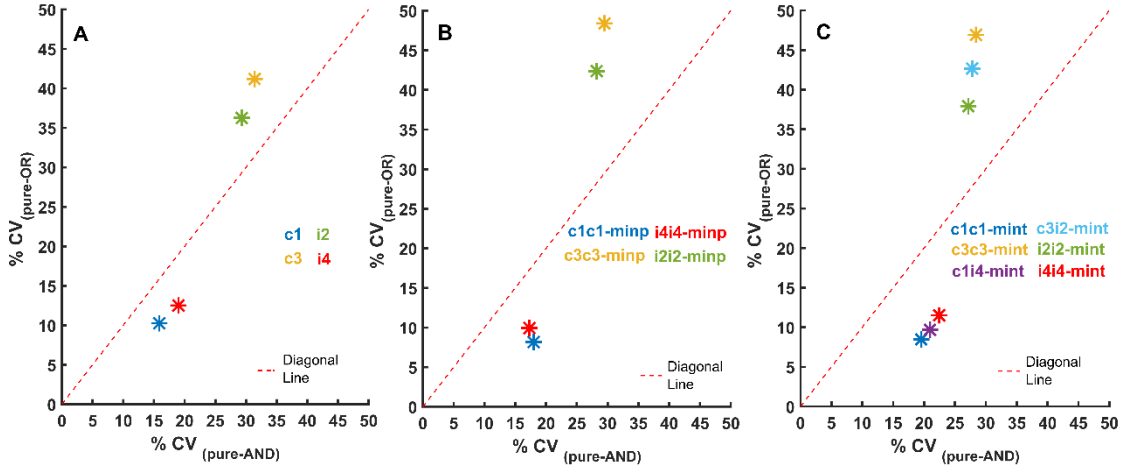

Figure 4.12: A comparison of the noise minimizing characteristics of FFLs with OR and AND logic gates.

The data from Figure 4.4D and Figure 4.8 are shown here to illustrate how the % CV of networks driven by OR gates compare to that of networks including AND gates. Networks that incorporate OR gates have a lower coefficient of variation (%CV) than those that contain AND gates (placed at the below of the diagonal). This result is valid for all types of FFLs, including isolated FFLs (A), minp-FFLs (B), and mint-FFLs (C). The models which have both the AND and OR type of connectivity is plotted here. The estimation has been done at input = 6 and parameter set is $k_1=k_2=k_3=1$, $k_p=10$, $k_{pp}=40$, $k_a=5$. Single step posttranslational modification is considered.

DOI:10.15774/PPKE.ITK.2023.004

4.11. Impact of One-Step and Two-Step Posttranslational Modification on Noise Reduction

Up until this point, I have only taken into account one -step modification process involving active and inactive states throughout all of the layers of the FFL networks. It is common for posttranslational signal transduction pathway networks to operate with several sites of modification, which may result in extremely non-linear behavior [48,49]. A version of the model has been developed in which every species passes through two-step modification and is triggered by a same activator. This version of the network will be used to assess whether or not multisite modifications increase the performance of FFLs. Based on a study of the input-output relationship slopes and the % CV generated by these motifs and comparable networks with single changes, it has been shown that multisite modification enhances both signal transduction and % CV (Figure 4.13). Therefore, the noise-reduction skills of FFLs are not improved by multisite modification (Figure 4.14), while the signal-transducing capacities of FFL motifs are improved by multisite modification.

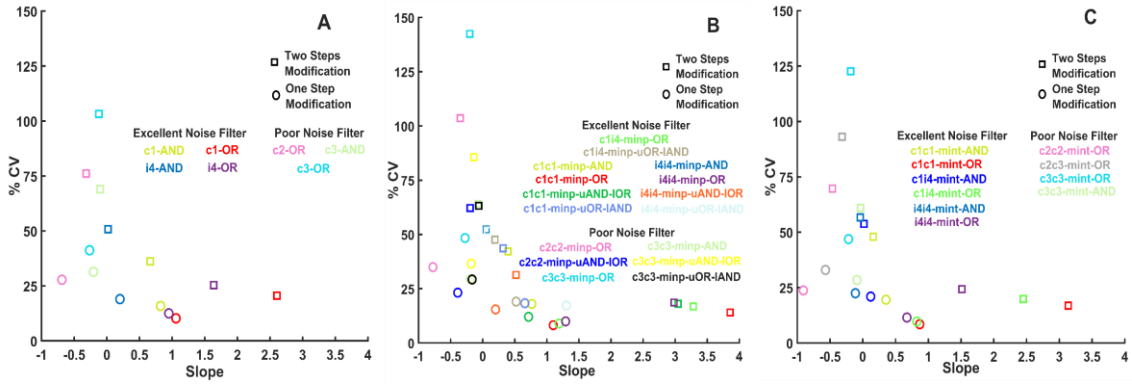

Figure 4.13: Comparison of FFLs with one-step and two-step modification.

The slope of the input-output relationship and the % CV data from Figure 4.4D and Figure 4.8 are displayed along with the comparable models that undergo two-step modification processes before being activated at each layer. Two-step modification process have a greater % CV than one-step modification for isolated FFLs (A), coupled minp-FFL (B), and coupled mint-FFL (C). The estimation has been done at input = 6 and parameter set is $k_1=k_2=k_3=1$, $k_p=10$, $k_{pp}=40$, $k_a=5$.

DOI:10.15774/PPKE.ITK.2023.004

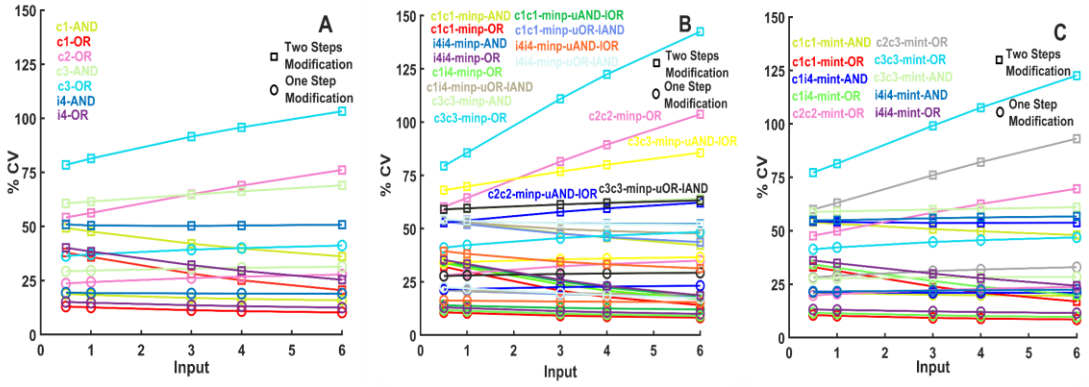

Figure 4.14: The estimated noise in one-step vs two-step posttranslational modification networks. As shown on the axis, the inputs to all of the networks have been changed, and the % CV of the output is plotted. The plot includes (A) isolated FFL, (B) minp-FFL and (C) mint-FFL networks. The parameter set is $k_1=k_2=k_3=1$, $k_p=10$, $k_{pp}=40$, $k_a=5$. Here are the outcomes of one-step (circle shaped point with solid line) and two-step (square shaped point with solid line) posttranslational modifications in each subplot. Each network is illustrated by a distinct colour, with different shaped markers.

The Figure 4.14 suggests that c1c1-minp-OR is a more effective in noise reduction than the c1c1-minp-2s-OR network (Figure 4.14B). It is also clear that OR-type of connection is less noisy than AND-type of connection. This is valid for isolated-FFL (A) as well as for coupled mint-FFL (C). In addition, it is possible to assert that the coupled minp-FFL (c1c1-minp-OR) (B) is the most effective noise filter when contrasted with the other options (A, C).

4.12. Noise Reduction and Signal Transduction Capabilities of Coupled FFLs With Varied Parameters

The noise reduction capability comparison of FFLs was performed with a parameter set, where all rates were equal to 1. I was investigating models where posttranslational modifications of molecules were considered. Each molecule was considered to be present at a total concentration of 60 AU. To ensure that noise reduction is not resulting from saturation at this level by either the active or inactive forms, I had to choose parameters (Figure 4.15B) to ensure that stochastic simulations almost never hit the maximal (Figure 4.15C) or minimal (Figure 4.15A) abundance levels. The simplest (all rates equal 1) parameter combination matched this requirement, but a random parameter search cannot be performed without running to this problem. Another parameter set could be chosen, where all rates are slowed down, but steady states do not change. An analysis with a five-

DOI:10.15774/PPKE.ITK.2023.004

fold slower rate ($k_1 = k_2 = k_3 = 0.2$) has been performed to understand how such change in parameter values impact the overall trends of coupled FFLs.

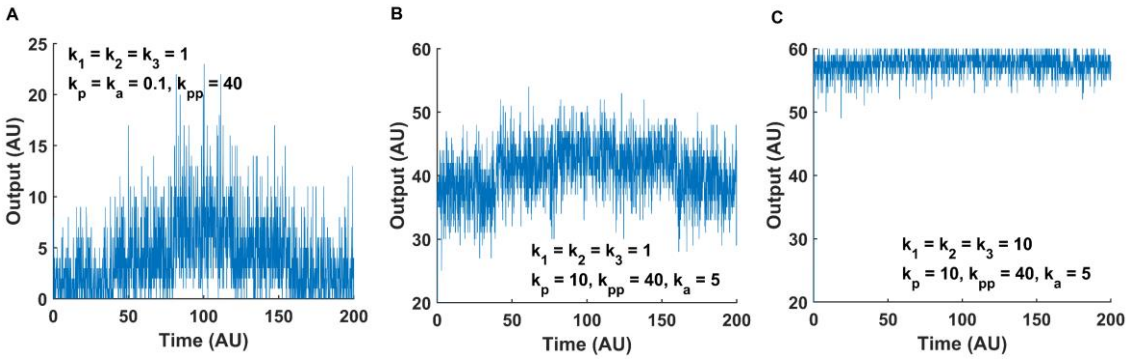

Figure 4.15: Stochastic time course analysis of a coupled FFL network.

The figure shows the stochastic time course analysis of the c1c1-minp-OR (Figure 4.1C) coupled FFL network at three distinct parameter sets, which are mentioned inside each subplot. Gillespie method was used to perform stochastic simulations. Here subplots A and C show the stochastic time course analysis of the output where the abundance hits the minimum (i.e. 0 AU) and maximum (i.e. 60 AU) levels, respectively. Subplot B depicts a stochastic time course study of the same network motif, with the output being distant from the maximum and lowest abundance levels.

When comparing the results with the original parameter set and the five-fold decreased parameter set we can see that the trend of differences between the various FFL models remain the same. In case of minp-FFL, c1c1-minp-OR is the best (with a largest slope value), and c2c2-minp-OR is the worst (with a smallest slope value) model for signal transduction at the reduced parameter values as well (Figure 4.16A). Again for minp-FFL, c1c1-minp-OR is still the best (lowest % CV), and c3c3-minp-OR is still the worst (highest % CV) model for noise attenuation (Figure 4.16B).

DOI:10.15774/PPKE.ITK.2023.004

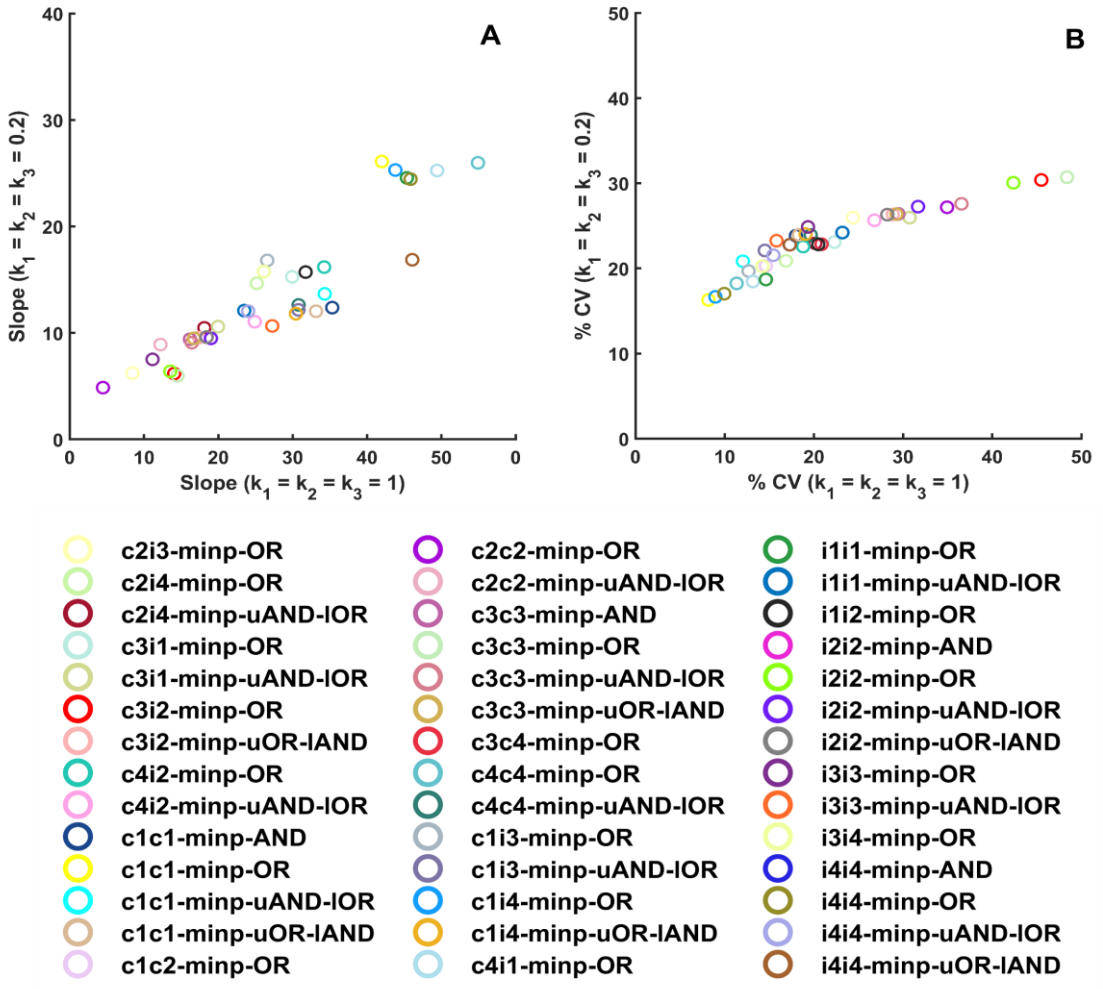

Figure 4.16: Noise reduction and signal transduction capacity of minp-FFLs.

A, slope obtained from input-output relations for two different parameter sets (k_1=k_2=k_3=1, k_p=10, k_{pp}=40, k_a=5; and k_1=k_2=k_3=0.2, k_p=10, k_{pp}=40, k_a=5) are plotted against each other for all the possible coupled minp-FFLs. At input = 6, the % CV of each combined minp-FFL has been calculated. In the panel B, calculated % CV for two different parameter sets are plotted against each other for all the possible coupled minp-FFLs.

Among mint-FFLs, the trend still remains the same, with a small change in ranking as the best model for signal transduction with reduced parameter values is c1c1-mint-OR, and the worst model is c2c2-mint-OR (Figure 4.17A). With both sets of parameter values, the best and worst models for noise reduction in the case of mint-FFL are the same, c1c1-mint-OR and c3c3-mint-OR, respectively (Figure 4.17B).

DOI:10.15774/PPKE.ITK.2023.004

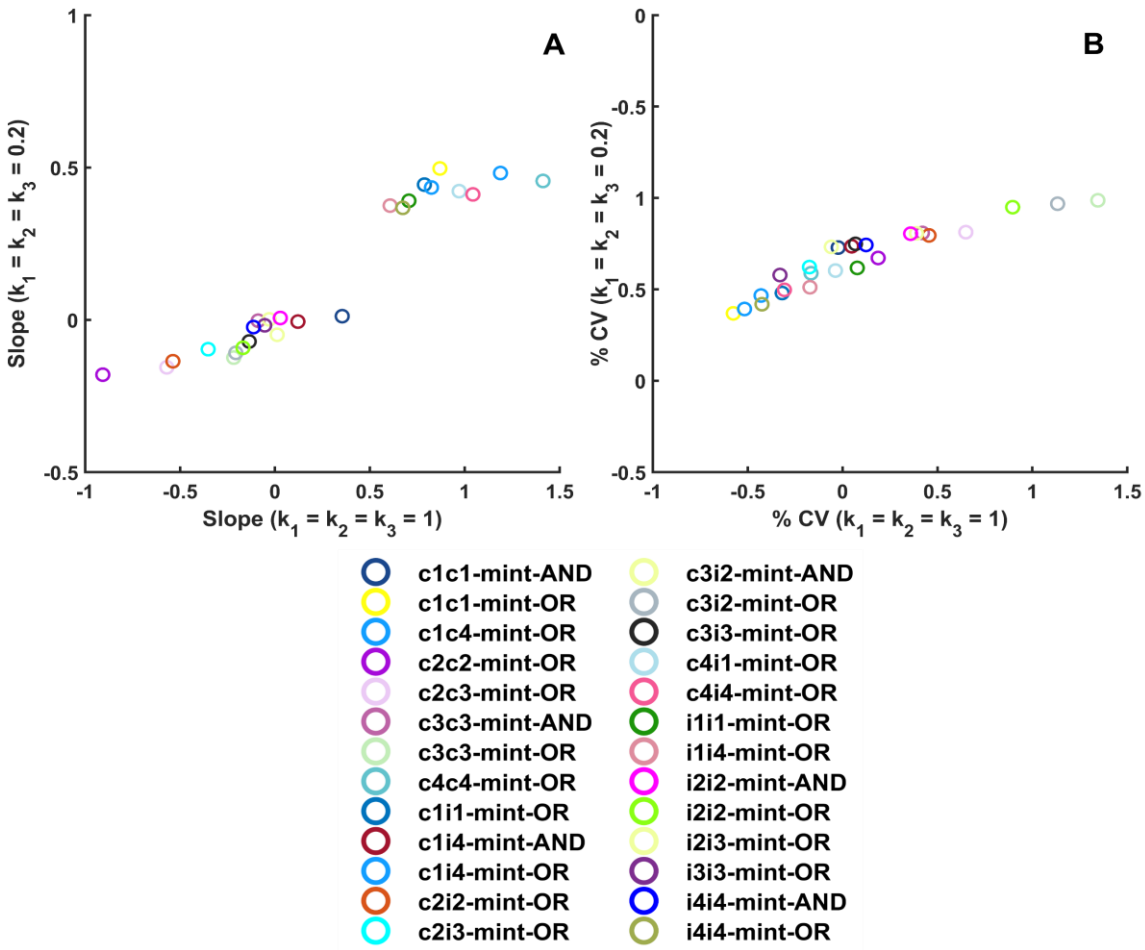

Figure 4.17: Noise reduction and signal transduction capacity of mint-FFL.

In the panel A, slope value obtained from input-output relations for two different parameter sets (k_1=k_2=k_3=1, k_p=10, k_{pp}=40, k_a=5; and k_1=k_2=k_3=0.2, k_p=10, k_{pp}=40, k_a=5) are plotted against each other for all the possible coupled mint-FFLs. At input = 6, the % CV of each coupled mint-FFL has been calculated. In the panel B, calculated % CV for two different parameter sets are plotted against each other for all the possible coupled mint-FFLs.

By changing parameter values, the general trends for noise reduction across various coupled FFLs stay the same (Figure 4.16, Figure 4.17). A slight difference can be observed in signal transduction capacity among coupled FFL (Figure 4.16, Figure 4.17). With five times slower parameter values (k_1=k_2=k_3=0.2), the c1c1-minp-OR and c1c1-mint-OR models perform best, whereas with the original values (k_1=k_2=k_3=1), the c4c4-minp-OR and c4c4-mint-OR models function best for signal transduction.

DOI:10.15774/PPKE.ITK.2023.004

4.13. Summary

Despite the fact that biological systems are noisy, they are robust and make dependable choices when incorporating environmental data [105]. By triggering posttranslational changes on downstream molecules, signaling pathways enable a quick response to ligand-extracellular receptor interaction. MAPK networks have been intensively studied by mathematical modeling [103,106,107] and its dynamical behavior and signal transduction capacities have been studied a lot. Simultaneously, FFLs were studied using comparable methods to learn about their adaptive and noise-filtering and behaviors [88,108,109]. The combination of these two ideas motivates to investigate how combined three-layer posttranslational signaling module may conduct signal transduction and noise reduction.

A thorough analysis of all potential FFL combinations revealed that connected FFLs improve the noise reducing and signal transducing ability than the corresponding isolated FFLs. This is particularly true if OR gates are used in circuits with several inputs. Posttranslational modifications include multiple states [48,103]. It has been shown that these extremely non-linear processes enhance the FFL-based signal transduction capacity, but also decrease their noise filtering capacities.

Several intriguing characteristics emerge from the analysis: The FFLs that have shown the greatest ability for signal transduction have an activatory direct path that runs from input node to output node (Figure 4.4D and Figure 4.8). This indicates that in order to achieve optimal signal transduction, node X ought to directly activate node Z. It has also been discovered that successful signal transduction may take place when the input node X inhibits the activity of at least a single copy of the intermediatory species Y and output gates obey an OR logic. All of these statements are valid for the FFLs that have the maximum capacity for signal transduction, including c4-OR, c4c4-mint-OR, c1i4-mint-OR, c4i1-minp-OR, and c4c4-minp-OR. However, effective noise reduction may be demonstrated in FFLs having the same activatory direct path between node X and node Z, but this is supplemented with a reaction in which Z is being activated by Y (Figure 4.4D and Figure 4.8) and once more, multi-input processes use an OR logic. It's found that i4-OR, c1-OR, c1i4-mint-OR, c1c1-mint-OR, c1c1-minp-OR, and c1i4-minp-OR FFLs are the best noise filters.

DOI:10.15774/PPKE.ITK.2023.004

There are various limitations to this study. It has been considered that total protein abundance at every level to be similar but even though the abundance rises at each level for the higher signal amplification [106]. The investigation was confined to the connection of two FFLs, while signalling circuits contain substantially more crosstalk [110]. The systematic research gives a comprehensive assessment of the noise lowering and signal processing capacity of coupled FFLs regardless of these constraints. According to the findings of the research, particularly combined FFLs of coherent type-1 and type-4 and incoherent type-4 with OR connectivity, have the potential to perform admirably both as the noise reducers and as the signal transducers. It is expected that the fabrication of such coupled FFL motifs might bring up new potential for better controlling signal transduction and noise in synthetic biology [111].

DOI:10.15774/PPKE.ITK.2023.004

Chapter 5

Understanding the role of positive and negative feedback loops in circadian rhythms' robustness and temperature compensation

DOI:10.15774/PPKE.ITK.2023.004

5.1. Oscillations in Biological Processes

Oscillations may be seen in both the biological and physical worlds. Biological oscillations can be seen in a variety of important biological processes [112]. To name just a few examples: cell cycles [113], the response of pacemaker cells [114–116], calcium oscillations [117], circadian rhythms [30,118,119], hormone secretion [120], responses of transcription factor [121–125], and fertility cycles [126]. The existence of a negative feedback (NFB) loop plus a delay in all these systems cause oscillations to form [76]. Oscillations need not just non-linear reaction kinetics, but also opposing chemical reactions with properly balanced timescales, as shown in a research by Novak et al. [29].

Circadian oscillations are one of the most common biological oscillation types because most organisms' internal clocks are synchronized with environmental variations in the day/night cycle. A clock that runs internally in almost all living things has a free-running period of about 24 hours [127]. The circadian clock acts as an accurate biological timekeeper despite the existence of metabolic variations [31]. An investigation into the nitrogen-fixation ability of the cyanobacterium *Synechococcus sp.* offered the first strong evidence for prokaryotic circadian rhythms [128]. Genetic studies of the *Neurospora crassa* [129], model filamentous fungus and the fruit fly *Drosophila melanogaster* [118], which were later applied to mammals [130], showed that circadian oscillations are made at the molecular level. In mammals, the fundamental clock genes (*Per1, Per2, Per3, Cry1, Cry2, Clock, Bmal1, Rev-erbα*, and *Rorα*) control rhythmic gene expression and the physiological aspects of circadian rhythms [131,132]. Three scientists (Jeffrey Hall, Michael Rosbash, and Michael Young) were awarded the 2017 Nobel Prize in Physiology or Medicine for their discoveries into the mechanisms underlying circadian clocks [17]. Maintaining a generally constant period despite changes in temperature is known as temperature compensation [18,133], and it is one of the well-known basic features of circadian period homeostasis. Another distinguishing aspect of a circadian oscillator has been its resistance to random oscillations [32,134]. The network architecture or underlying mechanisms that influence temperature compensation and circadian rhythm resilience are still largely unknown.

Researchers have come up with detailed mathematical models to explain how the circadian oscillator works. Some models include a minimal number of species and interactions to produce robust oscillations. The basic mathematical model for limit cycle

DOI:10.15774/PPKE.ITK.2023.004

oscillations due to negative feedback in gene expression was developed by Goodwin [135–137]. Further research indicates that the existence of positive feedback (PFB) in the circadian clock regulates the peak concentration of proteins [138]. Sustained oscillation may also result from the combination of a PFB and substrate depletion reaction [33]. Later research has shown that the existence of PFB promotes the resilience of circadian oscillation. PFB causes oscillation in the NFB loops without needing a large cooperativity coefficient (at least a Hill coefficient of 8, what is needed in a pure, three component NFB system) [139]. The Hill coefficient may be decreased further by including additional variables in an NFB network. Positive feedback may be classified into three types based on the underlying principle: self-activation, cross-activation, and Michaelis-Menten degradation [140]. According to Ferrell et al., a circadian oscillatory system with interconnected positive and negative feedback seems to be more suitable for producing oscillations with variable frequency and constant amplitude [113].

Many previous and contemporary studies [113,141–143] have led to a better understanding of the molecular regulatory systems that drive biological oscillations, as well as their advantageous properties such temperature compensation, robustness, tunability, and entrainment [144]. According to the Arrhenius law [72], rate of the reaction increases with temperature [72–74]. As a consequence, oscillation periods are anticipated to decrease as temperatures increase [75]. The circadian clock, on the other hand, is temperature compensated, and the period is generally independent of temperature within such a physiological range [75,145,146]. The fundamental purpose of this research is to examine essential aspects of primary circadian oscillator pathways in order to identify networks that are critical for oscillation period resilience and temperature adaptation.

5.2. Outline of Investigated Models

I describe and compare four vastly different minimalistic models for circadian oscillations to acquire a better grasp of the essential dynamical aspects of circadian rhythms. Most biological clocks [147] depend on transcriptional-translational NFB loops (TTFL), according to the literature [148,149]. In comparison, the circadian clock [131] of cyanobacteria is determined by the post-translational modifications of a single protein species. This makes the cyanobacterial clock a post-translational oscillator (PTO), which itself is regulated by a positive feedback mechanism [149,150]. This PTO is controlled

DOI:10.15774/PPKE.ITK.2023.004

by the three clock proteins in *S. elongatus*: KaiA, KaiB, and KaiC. In addition, temperature compensated oscillations may be seen when the cyanobacterial circadian clock is observed in an in vitro environment [151]. In order to achieve sustained oscillation, the components KaiA, KaiB, and KaiC as well as adenosine triphosphate (ATP) were all combined in this experiment. During the day and night, different forms of KaiC are produced, and different proteins bind to them in vivo. The KaiC subunit is a hexamer, and it has two sites where phosphorylation may take place (T432 and S431; abbreviated as T and S). Over the course of 24 hours, the phosphorylated and dephosphorylated states cycle through the following states [128]: U (two states are unphosphorylated) → T (S/pT, single state is phosphorylated) → ST (pS/pT, two states are phosphorylated) → S (pS/T, single state is phosphorylated) → U (where p holds for the phosphorylated site). KaiC autophosphorylates during the day and dephosphorylates during the night via the same active domain. Rust et al. [152] conclude that KaiA makes the auto kinase activity of KaiC go up, while KaiB makes the auto phosphatase activity go up [153,154]. Kinetic and biochemical data suggest that one of those phospho forms inhibits KaiA activity by associating with KaiB, therefore offering the essential feedback required to maintain circadian oscillations [152]. I have taken into account the complex model proposed by Rust et al., which has several PFB loops. This network is referred to as cyano-KaiABC in the rest of the chapter (Figure 5.1A).

For this theoretical analysis, I also look at the "conservative Goodwin oscillator," which is a simple and quite a well-studied example of a two-component [76] negative-feedback loop network (Figure 5.1B). The model can be also considered as the simple version of the TTFL [155]. In this particular implementation of the Two-Variable-Goodwin-NFB network, mRNA, denoted by the variable X, is first transcribed from a gene before being translated into a protein (denoted by the variable Y). The latter acts as a repressor, suppressing mRNA synthesis. I considered the modified version of two-variable Goodwin model equations in conjunction with Michaelis–Menten degradation kinetics [76] instead of zeroth-order degradation to avoid the possibility of getting negative concentration values for the variables.

Hernansaiz et al. [156] proposed an alternative for Rust's model [152] that contains all mass action reactions but a combination of positive and negative feedback to broaden the concept of positive-plus-negative feedback oscillators while simplifying the kinetics. In this concept, a single molecule goes through four distinct chemically altered states

DOI:10.15774/PPKE.ITK.2023.004

depending on the amount of modifications: none (OO), single (OP/PO), or double (PP). This core regulation connects with a two-state molecule (A and B). The oscillating network is termed combined positive-plus-negative feedback (cPNFB) (Figure 5.1C).

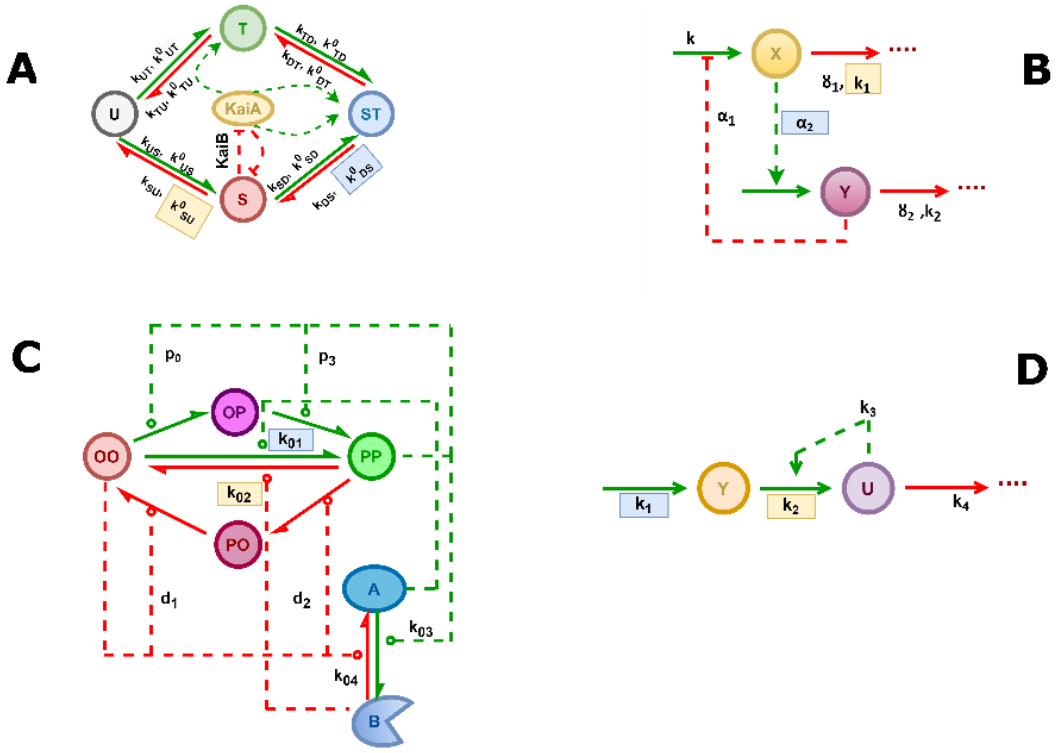

Figure 5.1: Oscillatory networks with positive and negative feedback.

Schematic illustration of Rust's cyanobacterial oscillatory system in KaiABC (cyano-KaiABC), which works through many positive feedback loops (A); Goodwin's negative feedback loop between two species (Two-Variable-Goodwin-NFB) (B); a single molecule with both positive and negative feedback that passes through four chemically changed states while communicating with an outside molecule with two states (A and B) (cPNFB) (C); and Selkov's substrate depletion oscillatory system (Selkov-PFB), which has the basic positive feedback loop and is driven by substrate depletion (D). The green and red arrows show the reactions of activation (phosphorylation) and inhibition (dephosphorylation) respectively. Processes that are inhibited are shown by arrows with flat heads, while processes that are activated are shown by arrows with pointed heads. A dual arrows in both ways represent the reversible reactions. The direct responses (synthesis/degradation, phosphorylation/dephosphorylation) are shown with solid arrows, whereas the regulatory interactions (activation/inhibition) are shown with dashed arrows. The parameters that are highlighted with blue color are the ones that have been fixed in the models shown in Figure 5.9 and yellow highlighted rates are further fixed in the analysis shown at Figure 5.14.

I studied Selkov's substrate depletion system to examine a PFB induced oscillator. I named the network Selkov-PFB (Figure 5.1D). This network displays a simple kinetics of an open single- enzyme (phosphofructokinase) that generates self-oscillations in

DOI:10.15774/PPKE.ITK.2023.004

glycolysis due to the existence of substrate suppression and product activation events [33]. I examined an oscillator that depends exclusively on positive feedback and excludes a direct NFB loop in the context of circadian clock models. Still, in this example, I see that although Y has a positive influence on U, U has a negative effect on Y (by converting it to U), resulting in the predicted opposite signed cross effects required to cause oscillations.

Figure 5.2 depicts the time course diagram for such oscillatory networks when they are subjected to a temperature of 298 K. At 298 Kelvin, the period of oscillation for each of the models is around 24 hours. When it comes to the design of regulatory networks, this will make it possible to get a deeper understanding of the impacts of the fundamental components of a circadian clock, such as the circadian clock's robustness and temperature compensation. The codes for each network have been uploaded in GitHub (https://github.com/SuchanaChakravarty/Systematic-analysis-of-NFB-PFB-loops-for-robustness-temperature-compensation-in-circadian-rhythm.git).

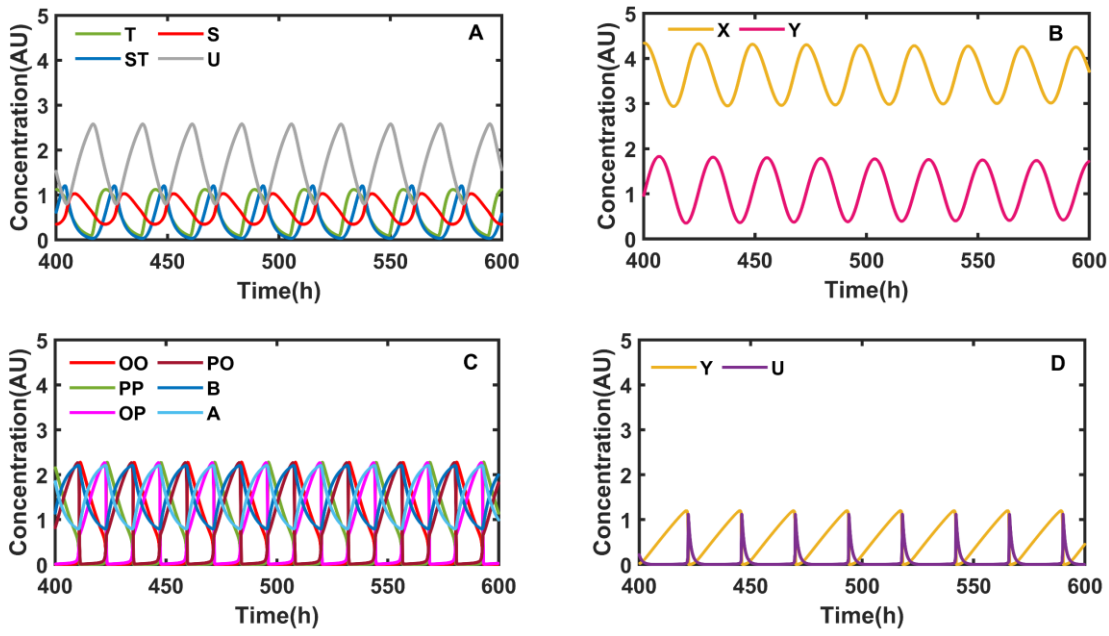

Figure 5.2: Diagram showing the time evolution for each of the four examined oscillatory networks, based on Figure 5.1.

The graph depicts the time evolution of species concentrations for such four oscillators cyano-KaiABC (A), Two-Variable-Goodwin-NFB (B), cPNFB (C), and Selkov-PFB (D). The simulations are conducted at 298 K. Table-5.1, Table-5.2, Table-5.3 and Table-5.4 show the initial concentrations of the species as well as the parameters.

DOI:10.15774/PPKE.ITK.2023.004

5.3. Mathematical Models of Four Oscillatory Networks

The mathematical equations for all these four simple circadian oscillatory networks, which include temperature dependency terms for each parameter, are provided below. All these dynamical equations are simulated in Matlab (version R2021b) using ODE45 solver tools.

5.3.1. ODE for cyano-KaiABC Model

This model's dynamical equations as well as the parameter values have been obtained from the article by Rust et al. [152].

If U refers to the unphosphorylated form, T to the threonine phosphorylated form of kaiC, D to the doubly phosphorylated form of kaiC (=ST), and S to the serine phosphorylated form of kaiC, then

$$U = kaiC - T - D - S \tag{5.1}$$

$$kaiA = A = max\,(0, A - 2 \cdot S) \tag{5.2}$$

$$k_{ij} = k_{ij}^{0} + k_{ij}^{A} \cdot \frac{A}{k_{half} + A} \tag{5.3}$$

Here, i,j ε {U,T,D,S}.

$$\frac{dT}{dt} = k_{UT} \cdot U + k_{DT} \cdot ST - k_{TU} \cdot T - k_{TD} \cdot T \tag{5.4}$$

$$\frac{dST}{dt} = k_{TD} \cdot T + k_{SD} \cdot S - k_{DT} \cdot ST - k_{DS} \cdot ST \tag{5.5}$$

$$\frac{dS}{dt} = k_{US} \cdot U + k_{DS} \cdot ST - k_{SU} \cdot S - k_{SD} \cdot S \tag{5.6}$$

DOI:10.15774/PPKE.ITK.2023.004

5.3.2. ODE for Two-Variable-Goodwin-NFB Model

These dynamical equations are obtained from Gonze et al. [76], which is credited as the original source. The network's parameters are altered so that the oscillation period is 24 hours at a temperature of 298 K.

$$\frac{dX}{dt} = \frac{\alpha_1 \cdot k}{k + Y} - \frac{8_1 \cdot X}{k_1 + X} \tag{5.7}$$

$$\frac{dY}{dt} = \alpha_2 \cdot X - \frac{8_2 \cdot Y}{k_2 + Y} \tag{5.8}$$

5.3.3. ODE for cPNFB Model

These ODEs are obtained from the article by Hernansaiz et al. [156]. The network's parameters are altered in such a manner that the oscillation period is now 24 hours at a temperature of 298 K.

$$\frac{dOO}{dt} = k_{02} \cdot B \cdot PP + d_1 \cdot OO \cdot PO - k_{01} \cdot A \cdot OO - p_0 \cdot OO \cdot PP \tag{5.9}$$

$$\frac{dPP}{dt} = k_{01} \cdot A \cdot OO + p_3 \cdot OP \cdot PP - k_{02} \cdot B \cdot PP - d_2 \cdot OO \cdot PP \tag{5.10}$$

$$\frac{dOP}{dt} = p_0 \cdot OO \cdot PP - p_3 \cdot OP \cdot PP \tag{5.11}$$

$$\frac{dPO}{dt} = d_2 \cdot OO \cdot PP - d_1 \cdot OO \cdot PO \tag{5.12}$$

$$\frac{dB}{dt} = k_{03} \cdot A \cdot PP - k_{04} \cdot B \cdot OO \tag{5.13}$$

$$\frac{dA}{dt} = k_{04} \cdot B \cdot OO - k_{03} \cdot A \cdot PP \tag{5.14}$$

DOI:10.15774/PPKE.ITK.2023.004

5.3.4. ODE for Selkov-PFB Model

The ODEs for this model are adapted from SEL'KOV's original publication [33]. The parameters of this model were adjusted such that the oscillation period is 24 hours at 298 K.

$$\frac{dY}{dt} = k_1 - k_2 \cdot Y - k_3 \cdot U^2 \cdot Y \tag{5.15}$$

$$\frac{dU}{dt} = k_2 \cdot Y + k_3 \cdot U^2 \cdot Y - k_4 \cdot U \tag{5.16}$$

5.4. Parameters Relevant for Models Discussed in Chapter 5

The temperature dependency of the reaction rates can be represented in the form of Arrhenius equations, as follows:

$$rate = A_e \cdot e^{\frac{-E}{R \cdot T}} \tag{5.17}$$

Here, for all the reaction rates A_e is the pre-exponential factor, and A_e = 383.83 (Arbitrary Unit, 'AU') [18]. For robustness study the value of A_e is randomly selected. R is the universal gas constant and R = 8.3144598 $J.K^{-1}.mol^{-1}$. Also, T = Temperature in Kelvin.

Table-5.1: Parameter combinations for cyano-KaiABC network.

Parameter values are for the corresponding equations 5.1-5.6.

i. Activation Energy (E) in KJ/mol				
$\mathbf{k_{half}}$	$\mathbf{k_{UT}^A}$	$\mathbf{k_{DT}^A}$	$\mathbf{k_{TU}^0}$	$\mathbf{k_{TU}^A}$
16.83	16.57	19.09	18.61	21.00
$\mathbf{k_{SD}^A}$	$\mathbf{k_{DS}^0}$	$\mathbf{k_{US}^A}$	$\mathbf{k_{SU}^0}$	$\mathbf{k_{TD}^A}$
16.43	17.64	22.01	20.21	18.57
Rates (AU)				
$\mathbf{k_{UT}^0}$	$\mathbf{k_{DT}^0}$	$\mathbf{k_{TD}^0}$	$\mathbf{k_{SD}^0}$	$\mathbf{k_{US}^0}$
0	0	0	0	0

ii. Activation Energy (E) in KJ/mol	
$\mathbf{k_{DS}^A}$	$\mathbf{k_{SU}^A}$
17.57	19.74

DOI:10.15774/PPKE.ITK.2023.004

Rust et al. [152] made the suggestion that their model should include some negative rates. In order to account for them, the Arrhenius equation has to be modified to read as follows:

$rate = A_e \cdot (-e^{\frac{-E}{R.T}})$ (highlighted boxes indicated, Table-5.1-ii)

(5.18)

iii. Initial Concentration (AU)				
KaiC	**KaiA**	**T**	**ST**	**S**
3.4	1.3	0.68	1.36	0.34

At a temperature of 298 Kelvin, the true reaction rates for the cyano-KaiABC motif may be expressed as follows:

iv. Reaction Rate (AU) at temperature 298 K								
$\mathbf{k_{half}}$	$\mathbf{k_{UT}^{A}}$	$\mathbf{k_{DT}^{A}}$	$\mathbf{k_{TU}^{0}}$	$\mathbf{k_{TU}^{A}}$	$\mathbf{k_{SD}^{A}}$	$\mathbf{k_{DS}^{0}}$	$\mathbf{k_{US}^{A}}$	$\mathbf{k_{SU}^{0}}$
0.4302	0.4793	0.1731	0.2101	0.0799	0.5059	0.3101	0.0533	0.11
$\mathbf{k_{TD}^{A}}$	$\mathbf{k_{UT}^{0}}$	$\mathbf{k_{DT}^{0}}$	$\mathbf{k_{TD}^{0}}$	$\mathbf{k_{SD}^{0}}$	$\mathbf{k_{US}^{0}}$	$\mathbf{k_{DS}^{A}}$	$\mathbf{k_{SU}^{A}}$	
0.2130	0	0	0	0	0	-0.3195	-0.1331	

Table-5.2: Parameter combinations for Two-Variable-Goodwin-NFB network.

Parameter values are for the corresponding equations 5.7-5.8.

i. Activation Energy (E) in KJ/mol						
$\mathbf{k_1}$	$\mathbf{k_2}$	$\mathbf{\delta_1}$	$\mathbf{\delta_2}$	**k**	$\mathbf{\alpha_1}$	$\mathbf{\alpha_2}$
31.8565	31.8565	14.7420	14.7420	12	14.01	17.9420

At a temperature of 298 Kelvin, the real reaction rate for this Two-Variable-Goodwin-NFB network may be expressed as follows:

ii. Reaction Rate (AU) at temperature 298 K						
$\mathbf{k_1}$	$\mathbf{k_2}$	$\mathbf{\delta_1}$	$\mathbf{\delta_2}$	**k**	$\mathbf{\alpha_1}$	$\mathbf{\alpha_2}$
0.001	0.001	1.0003	1.0003	3.0253	1.3442	0.2749

iii. Initial Concentration (AU)	
X	**Y**
1	0

DOI:10.15774/PPKE.ITK.2023.004

Table-5.3: Parameter combinations for cPNFB network.

Parameter values are for the corresponding equations 5.9-5.14.

i. Activation Energy (E) in KJ/mol							
p_0	p_3	d_1	d_2	k_{01}	k_{02}	k_{03}	k_{04}
6.45	10	10	6.45	21.55	21.55	21.55	21.55

At a temperature of 298 Kelvin, the real reaction rate for this cPNFB network may be expressed as follows:

ii. Reaction Rate (AU) at temperature 298 K							
p_0	p_3	d_1	d_2	k_{01}	k_{02}	k_{03}	k_{04}
28.417	6.7816	6.7816	28.417	0.0641	0.0641	0.0641	0.0641

iii. Initial Concentrations (AU)					
OO	**PP**	**OP**	**PO**	**B**	**A**
2	1	0	0	2	1

Table-5.4: Parameter combinations for Selkov-PFB network.

Parameter values are for the corresponding equations 5.15-5.16.

i. Activation Energy (E) in KJ/mol			
k_1	k_2	k_3	k_4
21.5	27.5	5.1768	14.8691

At a temperature of 298 Kelvin, the true reaction rates for the Selkov-PFB motif may be expressed as follows:

ii. Reaction Rate (AU) at temperature 298 K			
k_1	k_2	k_3	k_4
0.0654	0.0058	47.5057	0.9503

iii. Initial Concentration (AU)	
Y	**U**
0.48	0.0075

5.5. Studying the Robustness of Four Oscillatory Models

To generate oscillations with a duration of 24 hours, the four examined models need unique parameter combinations (Table-5.1, Table-5.2, Table-5.3 and Table-5.4). Maintaining this time in a noisy biochemical environment is critical from a physiological

DOI:10.15774/PPKE.ITK.2023.004

standpoint. I explore how the durations of oscillations react to parameter changes in the four analyzed models. In order to measure the robustness of biological systems against the extrinsic fluctuations in parameters, I have generated 1000 random parameter combinations from a log normal distribution of all of the models' parameters (randomly chosen multiplicative factor from a log normal distribution with mean value equals to 1 and standard deviation equals to 0.0142 for all parameters). This was done in order to follow earlier ideas [157,158] regarding the measurement of the robustness of biological networks.

5.5.1. Incorporation of Variability into the Models

For all rates in each model, I picked 1000 random pre-exponential components (A_e) from a log normal distribution with a mean value of 383.83 (AU) and a variance equals to 30 ($(AU)^2$).

The following MATLAB code (https://www.mathworks.com/help/stats/lognrnd.html) is provided for this purpose:

```
% Log-Normal Distribution with Variance = 30 (A.U)^2 and mean = 383.83 (A.U)
m = 383.83;   % mean value of Ae
v = 30;    % variance of Ae
mu = log((m^2)/sqrt(v+m^2))  % mean of the logarithmic values
sigma = sqrt(log(v/(m^2)+1))   % standard deviation of the logarithmic values
% For generating random numbers
r = lognrnd(mu,sigma,[1000, 1]);
% end
```

Adding a multiplicative factor to the pre-exponential value results in a degree of uncertainty in the reaction rates, as shown in Figure 5.3. I applied the ratio of these randomly chosen pre-exponential values to the average pre-exponential value to calculate these multiplicative factors. Small differences in all of these multiplicative components (mean ± standard deviation, 1 ± 0.0142) may add up to a large overall variance for all response rates.

DOI:10.15774/PPKE.ITK.2023.004

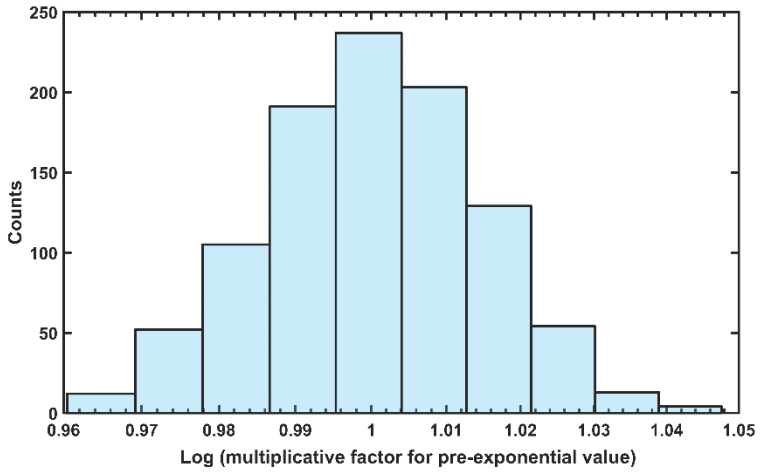

Figure 5.3: A multiplicative factor histogram for pre-exponential values is drawn randomly from a log normal distribution.

A log normal distribution is used to choose pre-exponential (A_e) values arbitrarily. Above, in blue, is a histogram depicting the logarithmic scale of the multiplicative factors used to the average pre-exponential value for generating random numbers.

5.5.2. Estimation of Noise

I have estimated total parameter variation by following the research [157,158] that appeared earlier and the Bayesian Information Criterion (BIC) in order to assess the noise that is present in each oscillatory networks.

5.5.2.1. Estimation of Total Parameter Variation

I figured out how much the random choice of parameters changed the total parameter variation by taking the arithmetic mean of how far each parameter was from its nominal value (marked as true below) [157]:

$$Total\ Parameter\ Variation = \frac{\sum_{i=1}^{k} \left| \frac{Rate_{random_i} - Rate_{true_i}}{Rate_{true_i}} \right|}{\mathrm{k}} \tag{5.19}$$

Here, k equals the total number of parameters in each oscillatory model.

DOI:10.15774/PPKE.ITK.2023.004

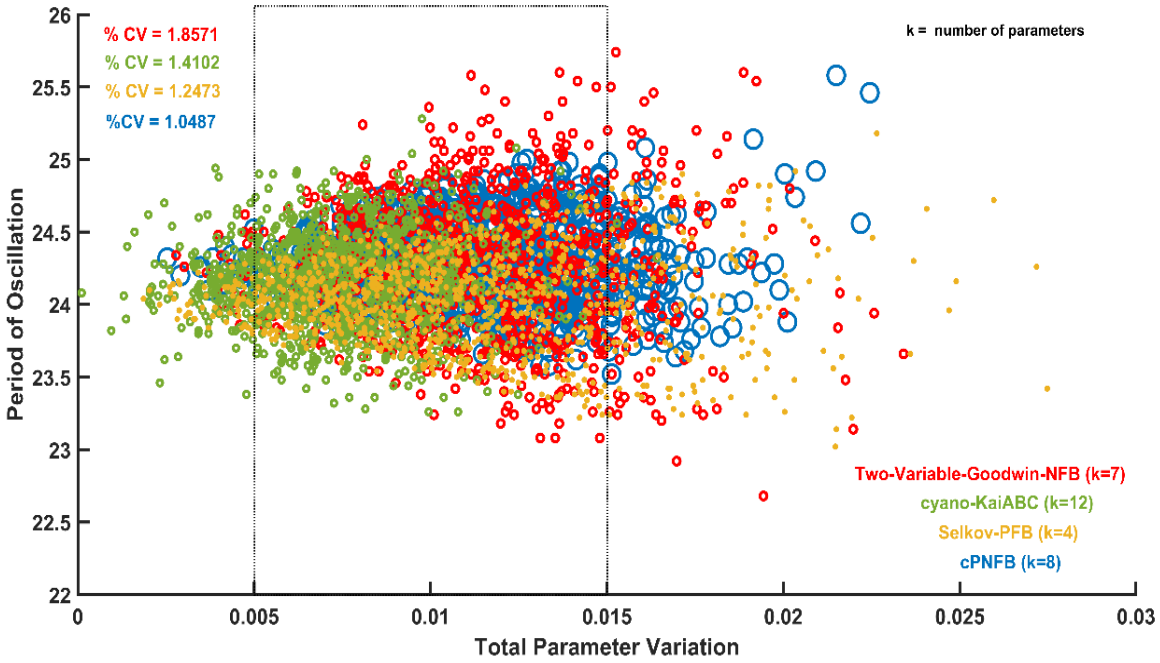

Figure 5.4: Period of oscillation in relation to the total parameter fluctuations for the four types of oscillatory systems.

The figure shows how the duration of oscillations varies in accordance with the total parameter changes for the four separate oscillatory systems shown in Figure 5.1. For 1000 randomly chosen parameter combinations, at 298K, the four distinct models are plotted in different colors. The inset on the upper left records the percentage value of the co-efficient of variation (% CV) along with the matching colors for all networks for 200 sampled parameter sets for each between 0.005 and 0.015 (0.005 < Total parameter variation < 0.015 , shown by the dashed rectangular box). Table-5.1, Table-5.2, Table-5.3 and Table-5.4 provide descriptions of the various parameters.

Since the arithmetic mean is expressed in this case as a ratio, it is effectively a unitless quantity whose value relies upon this number of parameters perturbed.

In Figure 5.4, the arithmetic mean of these reaction rates is plotted against the oscillation periods, and the figure reveals that Two-Variable-Goodwin-NFB model has a larger distribution, but the cPNFB model has a smaller distribution with regard to the period of oscillation.

In order to make a more accurate quantitative comparison of the networks' ability to tolerate extrinsic noise, I have computed the percentage coefficient variation (% CV) of period of oscillations across a small range of parameter variations. According to the percentage value of the coefficient of variation (% CV), the Two-Variable-Goodwin-NFB system is the noisiest network (% CV = 1.8571).

DOI:10.15774/PPKE.ITK.2023.004

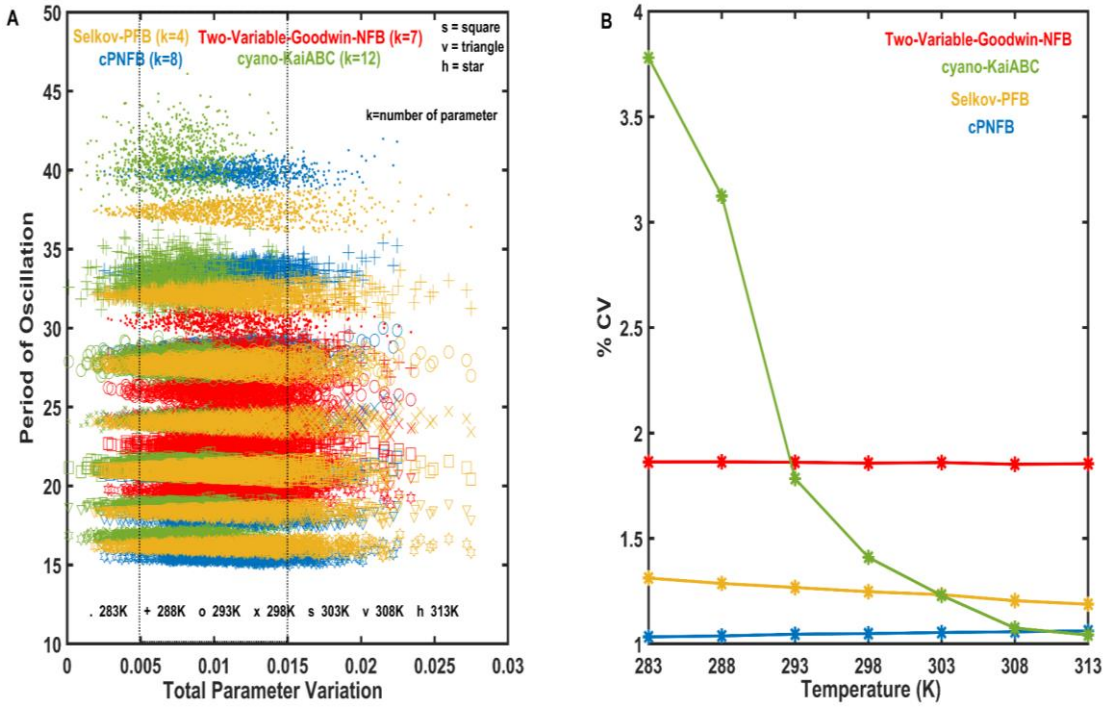

Figure 5.5: Examining the robustness of the four oscillatory networks.

Column (A) depicts the how the oscillation period changes in relation to the total parameter changes in four oscillatory models (Figure 5.1) with 1000 randomly selected points at 7 distinct temperatures. The models are identified by 4 different colors, and the seven varied temperatures are denoted by distinct shaped markers. Table-5.1, Table-5.2, Table-5.3 and Table-5.4 have a listing of the initial concentrations of each of the substances as well as the parameters. The fluctuation of the percentage coefficient of variation (% CV, also known as standard deviation over the mean) with temperature is shown in panel B. This change is shown for each of these four oscillatory networks (Figure 5.1). The percentage coefficient of variation, also known as % CV, has been estimated based on the period of oscillation shown in Figure 5.5A for a total of 200 sampled parameter sets, each of which fell between 0.005 and 0.015 (0.005 < Total parameter variation < 0.015 , shown by the dashed rectangular box).

To put it another way, the Two-Variable-Goodwin-NFB network with the lowest level of robustness, while the combined positive and negative feedback (cPNFB) network has the highest level of robustness. In addition to this, I have broadened the scope of my study of the oscillation period in terms of total parameter variation to include seven distinct temperatures ranging between 283K and 313K (Figure 5.5A).

Because my investigation did not concentrate on any one organism, I used a broad range of temperatures. Cyanobacteria, for example, can withstand a wide variety of temperatures [159–161]. In Figure 5.5B, I demonstrate how the percentile coefficient of variation (% CV) of oscillation period changes relates to temperature variations in four distinct oscillatory networks (displayed in Figure 5.1).

DOI:10.15774/PPKE.ITK.2023.004

Throughout all the temperatures, the cPNFB model has the least variation in periods, whereas the Two-Variable-Goodwin-NFB network has the most variation in oscillation periods. This is valid for all the parameter fluctuations between 283 K and 313 K temperature. Just the robustness of cyano-KaiABC motif is temperature sensitive, whilst others seem to be temperature independent (Figure 5.5B).

5.5.2.2. Estimation of Bayesian Information Criterion (BIC)

Even though they have different numbers of parameters, the Selkov-PFB model (which has the lowest number of total parameters, 4) and the cyano-KaiABC model (which has the greatest number of total parameters, at 12) have similar distributions (shown in Figure 5.4). I questioned if the total parameter numbers had an impact on a model's ability to cancel out noise. It's indeed common practice to compare motifs with different parameter numbers using the Bayesian Information Criterion (BIC). It is primarily employed to evaluate models and determine which one best fits an observation while taking into account the number of fitted parameters in each model. As a result, BIC is a strategy that punishes more complicated models by applying a penalty based on the total number of parameters the model evaluates. When parameters are randomly chosen, a model with a lower BIC value exhibits lower variations from the mean response, making up for the possibility that bigger models are more noise-resistant.

The BIC was determined using the following method:

$$BIC = n \cdot \log(SSE) - n \cdot \log(n) + k \cdot \log(n) \tag{5.20}$$

Here k is the total number of parameters in a model, n is the sample size (I have taken into account n = 200 random parameter sets in a constrained total parameter variation domain), and SSE is the sum squared error. I determined the SSE to be as follows:

$$SSE = \sum_{i=1}^{n} (Y_{random} - Y_{average})^2 \tag{5.21}$$

Pursuing this thought, I investigated the relationship between the BIC of several models meeting the specified 24 hour period of oscillations at various temperatures (Figure 5.6).

DOI:10.15774/PPKE.ITK.2023.004

Regardless of its difference in size from others, the Two-Variable-Goodwin-NFB network is still the noisiest at the most values of temperatures (shows the largest value of BIC). In this investigation, the tiny Selkov-PFB and cPNFB models exhibit the smallest noise to parameter alterations. As a result, although the number of parameters seems to have no effect on the robustness evaluation, it seems that the existence of positive feedback in a system leads to a decreased level of noise (Figure 5.6). This contradicts conventional assertions about the function of negative and positive feedback loops in noise reduction and increase, respectively [162]. Despite the fact that negative feedback is recognized to be a noise-reducing model [4], it has been found that the Two-Variable-Goodwin-NFB network is the least resilient. In the next sections, I will explore if negative feedback may aid in the temperature compensation property of a circadian clock network.

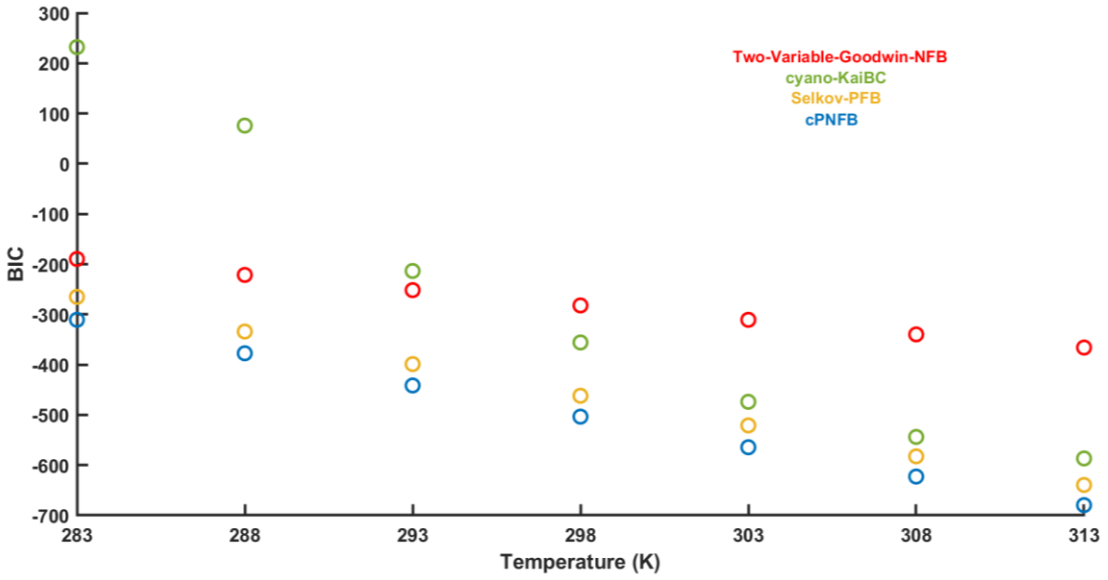

Figure 5.6: The Bayesian Information Criterion (BIC) of these four networks has been examined at different temperatures.

The BIC has been shown against different temperatures for every model (Figure 5.1). The Two-Variable-Goodwin-NFB network has the highest value of BIC above 298K. The analysis sample size is 200, and each set correlates to 0.005 < Total parameter variation < 0.015 (displayed in Figure 5.4 and Figure 5.5). Table-5.1, Table-5.2, Table-5.3 and Table-5.4 show the initial concentrations of the elements as well as the parameters.

DOI:10.15774/PPKE.ITK.2023.004

5.6. Studying the Temperature Compensation Characteristics of Four Oscillatory Models

When I examine the temperature dependency of robustness (Figure 5.5), I observe that the networks' average period changes with changes in temperature, but the magnitude of this shift varies amongst the four models. I have measured the values of these biological oscillators' temperature coefficients (Q_{10}) in order to get an assessment of the temperature compensation capabilities that they possess [163,164]. Simplifying the computation allows us to focus on variations in period duration, as shown below [164]-

$$Q_{10} = \frac{Period\ of\ oscillation\ at\ temperature\ T\ (in\ K)}{Period\ of\ oscillation\ at\ temperature\ (T+10)\ (in\ K)} \quad \textbf{(5.22)}$$

It is necessary for circadian oscillators to have temperature compensation built into them so that they can keep their period of around 24 hours. I have displayed, for each of the four models, how the oscillation periods vary in response to changes in temperature (Figure 5.7). Although I can see how all of these networks compensate for temperature variations, I still see a significant influence of temperature fluctuations on the periods of oscillation.

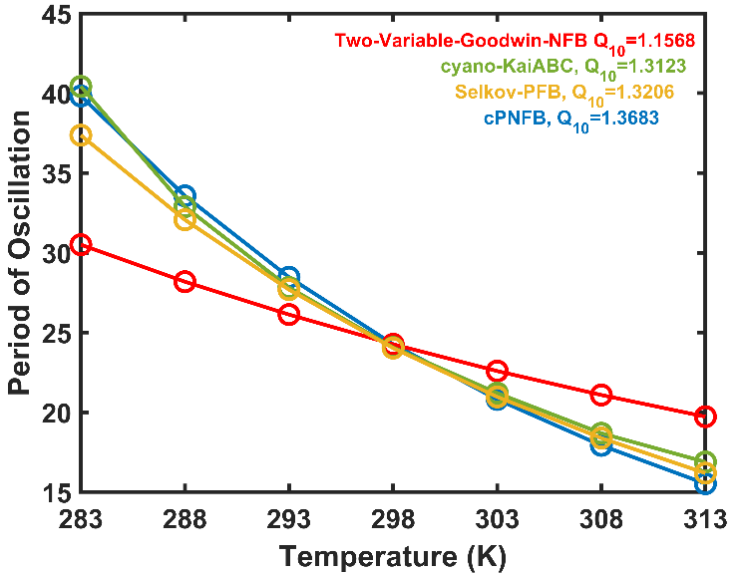

Figure 5.7: Temperature dependence of oscillation period.

In all four models (shown in Figure 5.1), the oscillation period decreases as the temperature increases. The Q_{10} values between the temperature 293K and 303K for every motif are also included in the table inset on the upper right. The parameters are presented in the Table-5.1, Table-5.2, Table-5.3 and Table-5.4.

DOI:10.15774/PPKE.ITK.2023.004

The Two-Variable-Goodwin-NFB network has the least Q_{10} value in Figure 5.7, indicating that it is greater temperature compensated compared to the other 3 models. The pattern also reveals that as the temperature increases, the length of the period for all four motifs reduces. Two-Variable-Goodwin-NFB succeeds at temperature compensation but fails miserably at robustness (Figure 5.4). Given that all of the models are inadequately temperature compensated, further claims may need to be evaluated.

5.6.1. Temperature Insensitive Individual Reactions

Rather than expecting kinetic rate responses to temperature changes to compensate for oscillation period changes [165], I assume that a single reaction could be temperature insensitive, resulting in a significant impact on compensating period alterations [18,73,166]. Adapting concepts from Hong et al. [167] and observations that a crucial circadian clock reaction is insensitive to temperature changes [168,169], I have examined what occurs when I fix the rates of one reaction but letting all others to react to a change in temperature.

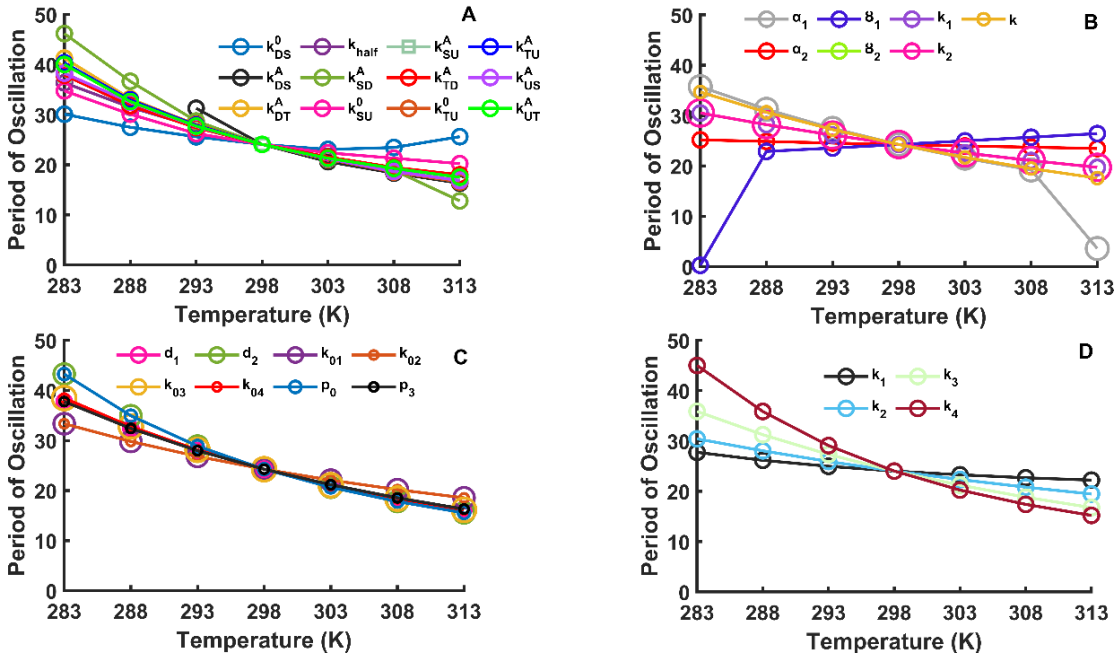

Figure 5.8: Temperature dependence of periods of oscillation if a single reaction is independent of temperature.

The graph depicts how periods of oscillation fluctuate with temperature in each of the four oscillatory models (Figure 5.1) when such rate of a single reaction gets fixed (as specified in the legend), but all others are allowed to response to temperature variations. Each of these reactions connected with each motif are analyzed. Table-5.1, Table-5.2, Table-5.3 and Table-5.4 show the initial concentrations of the elements as

DOI:10.15774/PPKE.ITK.2023.004

well as the parameters. Some of the models fail to depict oscillations at high and low temperatures, resulting in periods of zero.

Finding the reactions that could be in charge of temperature compensation in different oscillatory networks is the aim of this study. When a single reaction rate is constant, I have investigated how much the oscillation periods vary with temperature in pure NFB and pure PFB motifs (plotted in Figure 5.8B and Figure 5.8D, respectively). I have also tested this in complicated oscillatory networks with various combinations of negative and positive feedback loops (Figures 5.8A and 5.8C).

Figure 5.9 displays the best-performing models in which a single rate is considered to be independent of temperature while the rest react to changes in temperature. When the α_2 rate of the Two-Variable-Goodwin-NFB motif, is temperature resistant, it is possible to draw the conclusion that this model performs better than the others (Figure 5.9). The pace at which the activator X causes the production of its own inhibitor, Y, is known as the α_2 reaction rate (highlighted with blue color on Figure 5.1B).

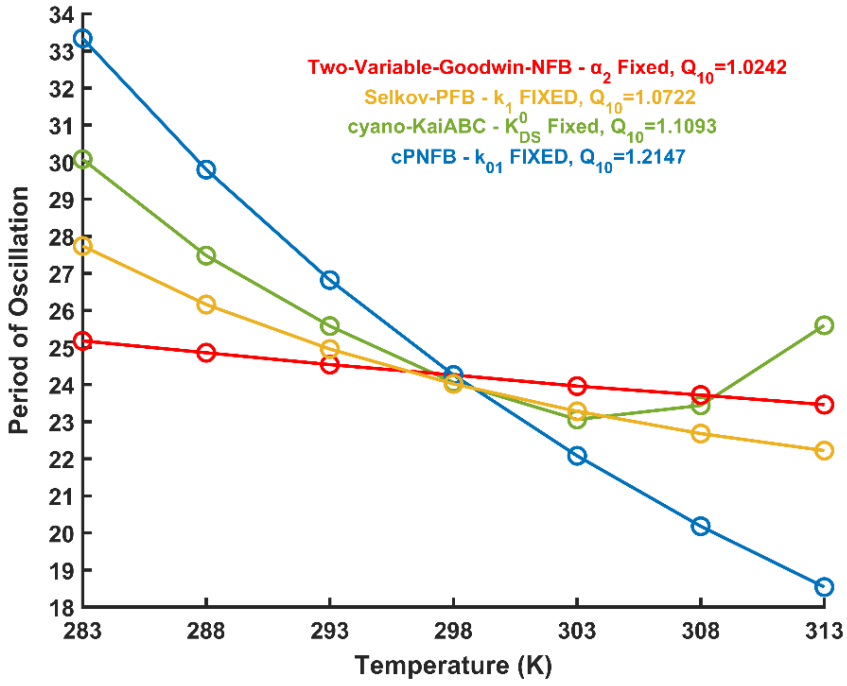

Figure 5.9: Dependency of periods of oscillation if the rate of a single reaction is independent of temperature.

The graph shows how much the periods of oscillation vary with temperature across all four analyzed oscillatory networks (Figure 5.1), during which a single reaction rate is fixed (indicated in the legend), while all other rates are responsive to temperature variations. The parameters are shown in Table-5.1,

DOI:10.15774/PPKE.ITK.2023.004

Table-5.2, Table-5.3 and Table-5.4. The image also depicts the Q_{10} values for each model, which range from 293K to 303K. Figure 5.1 depicts the fixed parameters which are shaded with blue color boxes.

Even if they have progressed on their Q_{10} values, the other models are still very sensitive to variations in temperature. With rate k_{DS}^{0} constant (the rate at which the dual phosphorylated state 'ST' switches to the single phosphorylated state 'S', highlighted with blue color in Figure 5.1A), Rust's cyanobacterial circadian oscillator network shows a temperature dependency curve with a rise in the length of the period at higher temperatures.

5.6.2. Considering Two Temperature Independent reactions

Considering the two reaction rates to be temperature independent, I believe that oscillator periods will be strongly temperature compensated. For Two-Variable-Goodwin-NFB model, cyano-KaiABC model, cPNFB model, and Selkov-PFB model, Figures 5.10-5.13 illustrate all conceivable combinations of two temperature compensated parameters.

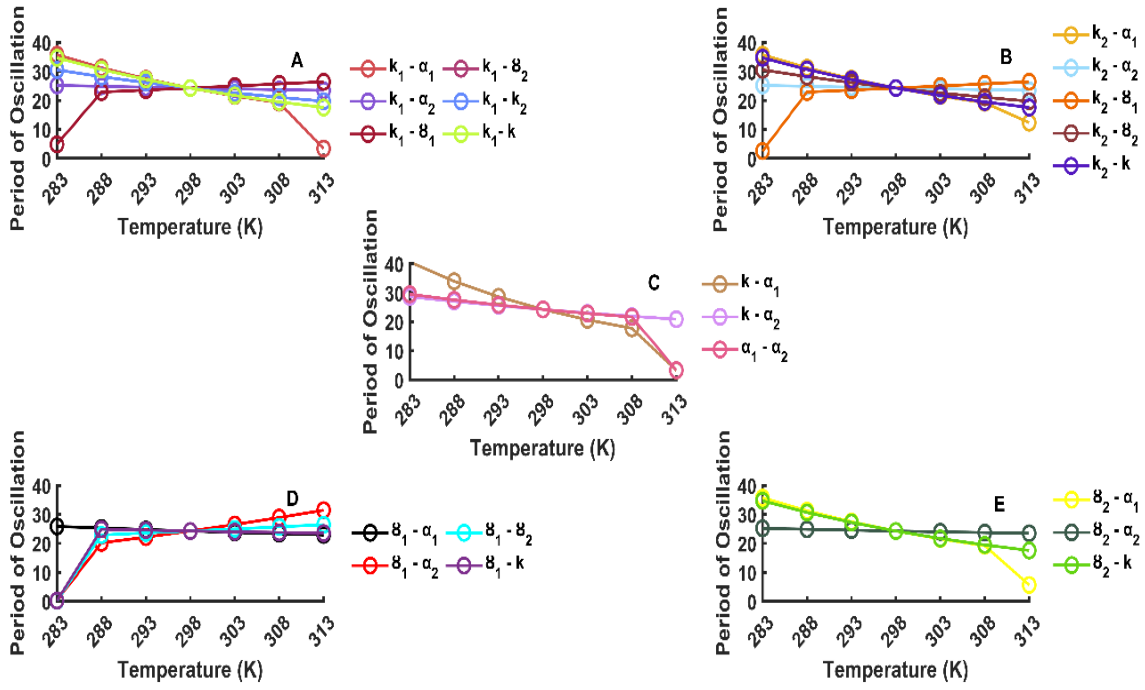

Figure 5.10: Oscillation Periods for the Two-Variable-Goodwin-NFB model where two reaction rates remain temperature independent.

The figures (A-E) show how much the durations of oscillations in Two-Variable-Goodwin-NFB model fluctuate with temperature when the two rates are independent of temperature (as mentioned in the legend) and the others are permitted to respond to changes in temperature. All feasible reaction rate

DOI:10.15774/PPKE.ITK.2023.004

combinations connected with this model are analyzed. Table-5.2 lists the initial concentrations of components as well as the parameters.

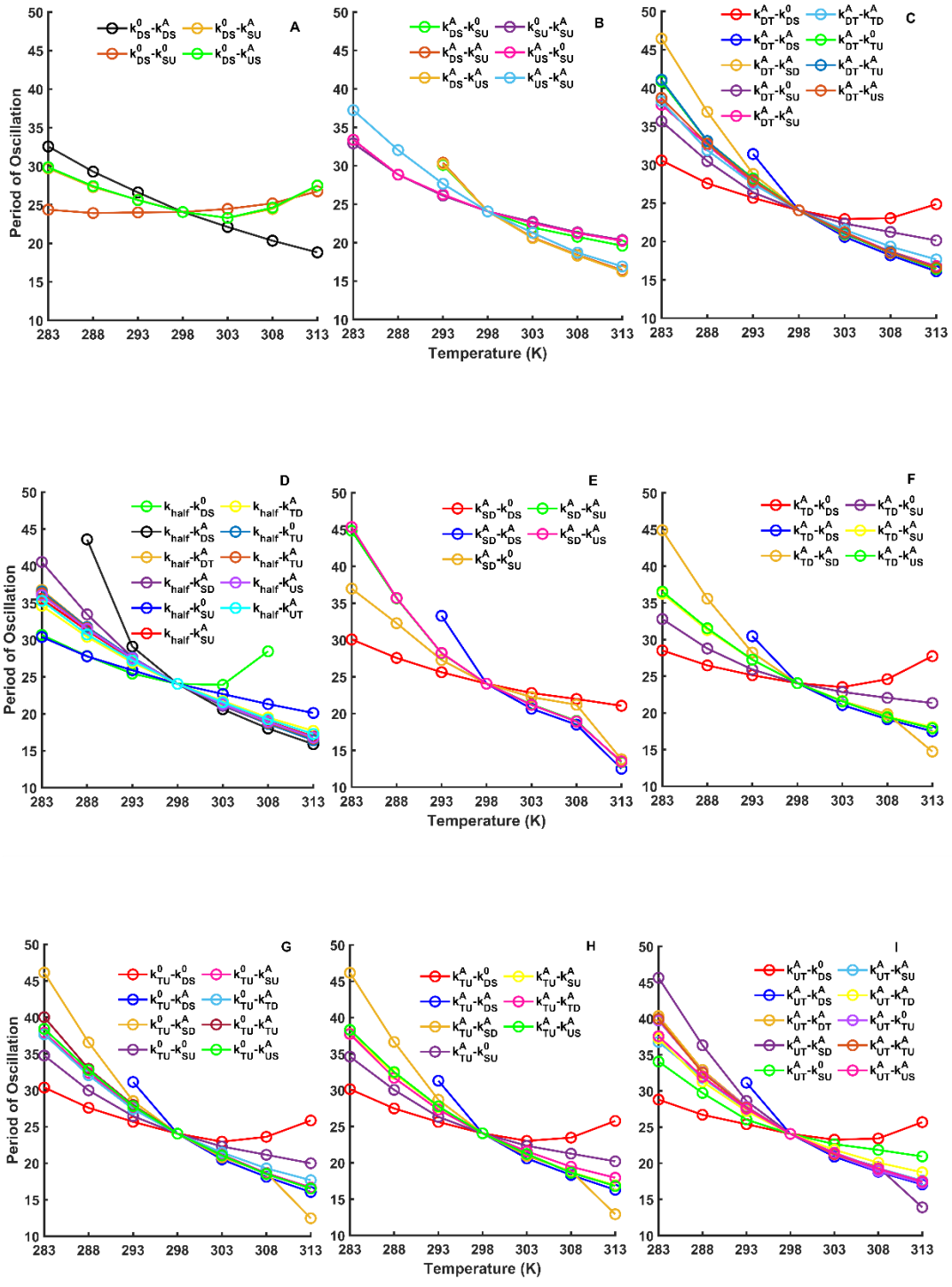

Figure 5.11: Oscillation Periods for the cyano-KaiABC model where two reaction rates remain temperature independent.

The subfigures (A-I) show how much the durations of oscillations in cyano-KaiABC model fluctuate with temperature when the two rates are independent of temperature (as mentioned in the legend) and the others are permitted to respond to changes in temperature. All feasible reaction rate combinations connected with

DOI:10.15774/PPKE.ITK.2023.004

this model are analyzed. Table-5.1 lists the initial concentrations of components as well as the parameters. A few systems fail to show oscillations at high or low temperatures, resulting in missing points on Figure 5.12.

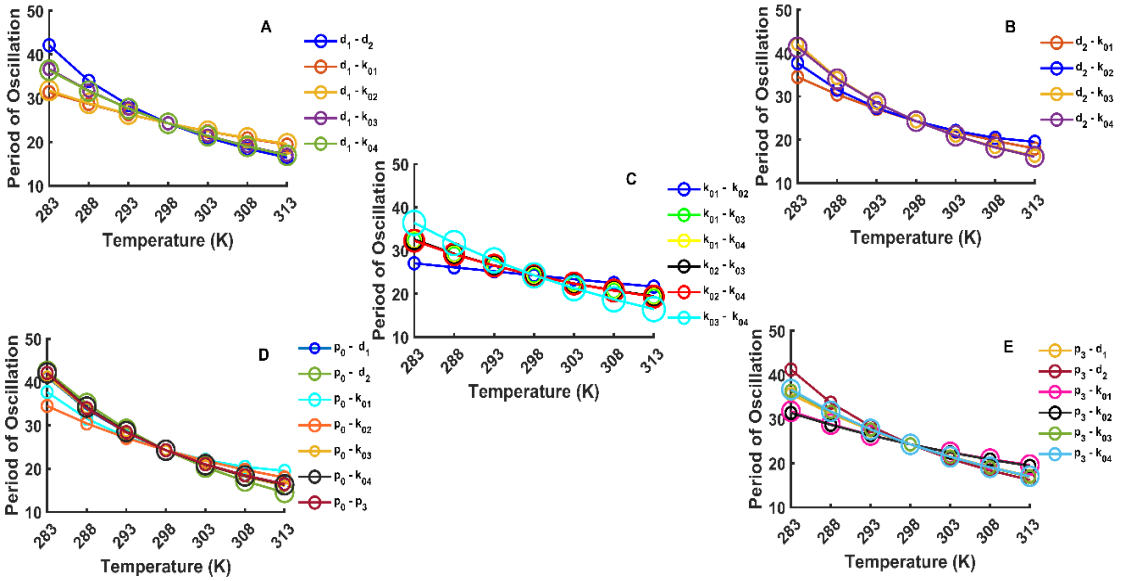

Figure 5.12: Oscillation Periods for the cPNFB model where two reaction rates remain temperature independent.

The subfigures (A-E) show how much the durations of oscillations in cPNFB model fluctuate with temperature when the two rates are independent of temperature (as mentioned in the legend) and the others are permitted to respond to changes in temperature. All feasible reaction rate combinations connected with this model are analyzed. Table-5.3 lists the initial concentrations of components as well as the parameters.

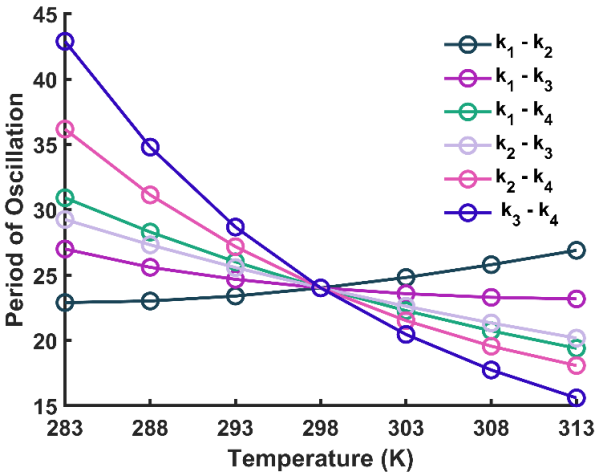

Figure 5.13: Oscillation Periods for the Selkov-PFB model where two reaction rates remain temperature independent.

The figure shows how much the durations of oscillations in Selkov-PFB model fluctuate with temperature when the two rates are independent of temperature (as mentioned in the legend) and the others are

DOI:10.15774/PPKE.ITK.2023.004

permitted to respond to changes in temperature. All feasible reaction rate combinations connected with this model are analyzed. Table-5.4 lists the initial concentrations of components as well as the parameters.

Only such parameter combinations that result in the lowest Q_{10} values have been shown in Figure 5.14, which uses data from Figures 5.10-5.13 as its source material.

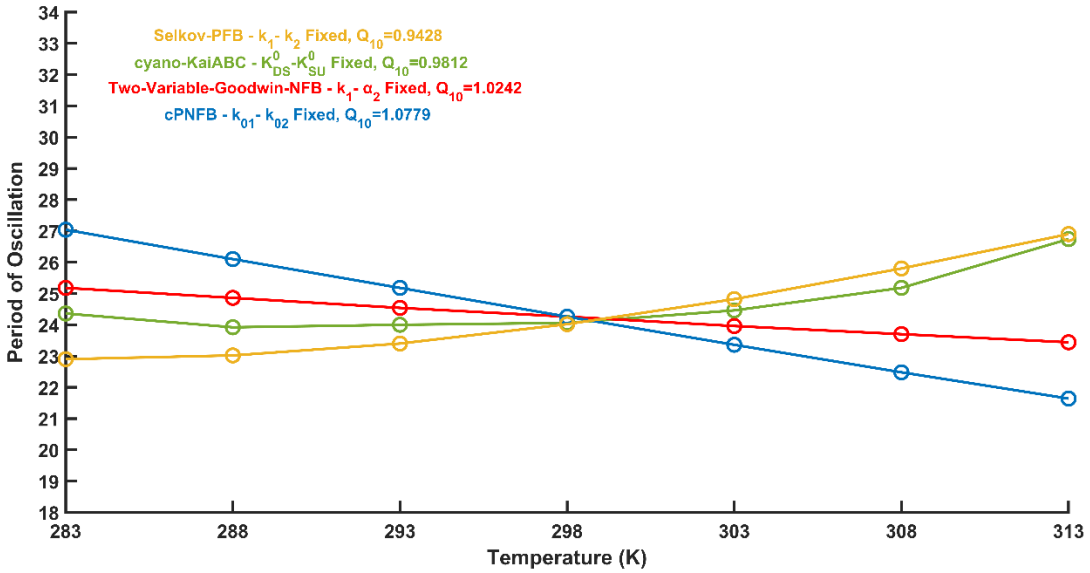

Figure 5.14: If two processes are temperature change resistant, the temperature dependence of the oscillation periods.

When the rates of chemical reactions are concurrently fixed (as stated in the legend), but the others are free to adjust to temperature changes, the picture illustrates how much the period of oscillations in the four oscillatory motifs (Figure 5.1) varies with temperature. Only the parameter combinations that result in the lowest Q_{10} values are displayed here. Table-5.1, Table-5.2, Table-5.3 and Table-5.4 include parameters. The second and principal fixed parameters (Figure 5.9) are shown in the Figure 5.1 with the yellow and blue colored boxes, respectively.

Two-Variable-Goodwin-NFB (illustrated in the red color) and cPNFB (illustrated in the blue color) plots show the projected reduction in the period for the temperature rise (Figure 5.14). The Selkov-PFB model (illustrated in yellow), on the other hand, has just 4 parameters, and it appears that if I set two of them, the other two may be pretty adequately temperature compensated, although the period grows as a function of the temperature. The cyano-KaiABC network (plotted in green) is the most complex network in this investigation, with a complicated temperature sensitivity that indicates a minimum at 24 hours. The cyano-KaiABC network works well between temperatures of 283K and 298K; however, at 303K, the oscillation period starts to diverge considerably from 24 hours.

DOI:10.15774/PPKE.ITK.2023.004

By considering Figures 5.9 and 5.14, it can be seen that the Two-Variable-Goodwin-NFB model with the single temperature insensitive parameter (α_2) performs almost equally to such two-parameter fixed scenario (k_1-α_2) whereas the other three networks show additional gains for second rate fixing (the reaction rates are labeled by blue and yellow colors on Figure 5.1). It can be shown that the Two-Variable-Goodwin-NFB model's α_2 rate controls the negative feedback loop directly. For the cyano-KaiABC and cPNFB networks, the rate of the reaction, which must be temperature independent, is also negative feedback loop controllers. Since there is no NFB loop in the Selkov-PFB, so the most important parameter appears to be the one that governs the synthesis of the PFB loop's substrate. Even yet, some gains in temperature adjustment can be noted across all models because to the addition of a second biochemical reaction rate. Because of the lower values of Q_{10} shown in Figure 5.14, the oscillation periods are more temperature compensated than those shown in Figure 5.9, where only a single rate was held constant throughout all of the models.

5.7. Differentiating the Impacts of Negative and Positive Feedbacks

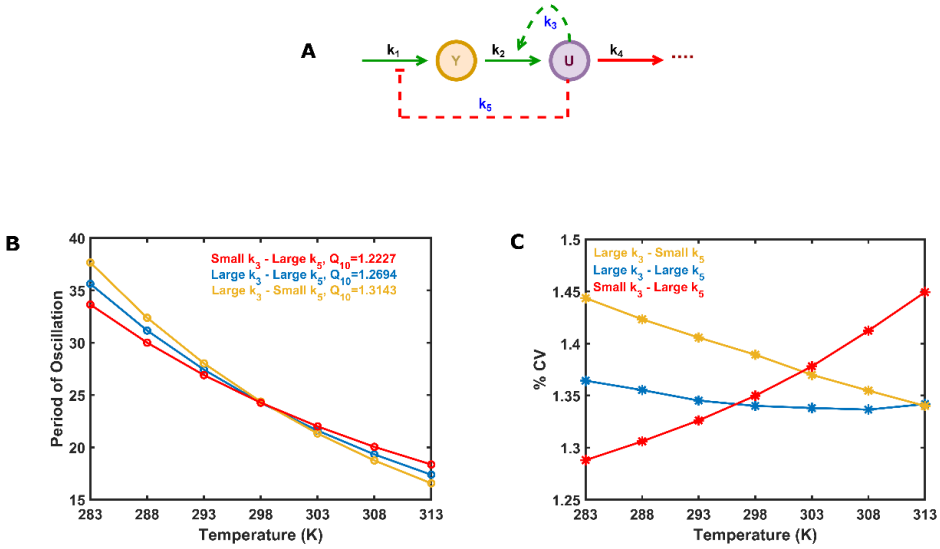

Figure 5.15: PFB oscillator in the Selkov model with an extra NFB loop.

The oscillatory network's schematic diagram (A). The dotted green arrowhead (k_3) represents the intrinsic autocatalytic positive feedback in a Selkov model, while the dotted red line with a blunt head represents the external extra negative feedback (k_5). k_3 and k_5 rates are marked in blue because they were changed. (B) Oscillation period varies with temperature in the instances of strong NFB - weak PFB (red), weak NFB - strong PFB (yellow), and strong NFB - strong PFB (blue). (C) Robustness, expressed in terms of

DOI:10.15774/PPKE.ITK.2023.004

percentile coefficient of variation (%CV) at different temperatures for the three separate examples described in panel B. Table-5.5 contains a list of parameters.

Because the four examined networks have varying kinetics and complexity (Figure 5.1), the research has been extended with the Selkov-like PFB-based network with an extra NFB loop in order to establish a systematic method for understanding the function of negative and positive feedback in the temperature compensation and robustness analysis of circadian clock models (Figure 5.15A).

5.7.1. ODE for Selkov-like PFB Framework With an Extra NFB Loop

The following is the mathematical representation of the Selkov-like PFB framework with an extra NFB loop (Figure 5.15A):

$$\frac{dY}{dt} = \frac{k_1}{1 + k_5 \cdot U} - k_2 \cdot Y - k_3 \cdot U^2 \cdot Y \tag{5.23}$$

$$\frac{dU}{dt} = k_2 \cdot Y + k_3 \cdot U^2 \cdot Y - k_4 \cdot U \tag{5.24}$$

In this case, the conventional Selkov model's intrinsic activatory autocatalytic positive-feedback action on the species U is represented by k_3 (Figure 5.1D). By preventing the synthesis of substance Y at a rate equal to k_5, U displays an additional NFB. The total number of parameters (k) in this model is equal to 5 as a result of the extra NFB.

The preceding mathematical equation may be represented in terms of the number of molecules by including a scaling factor (V_s) on both sides of the equation. For the robustness analysis shown in Figure 5.17, I used the Gillespie technique [59] and the corresponding equation:

$$\frac{dN_Y}{dt} = \frac{k_1 \cdot {V_s}^2}{V_s + k_5 \cdot N_U} - k_2 \cdot N_Y - k_3 \cdot \left(\frac{N_U}{V_s}\right)^2 \cdot N_Y \tag{5.25}$$

$$\frac{dN_U}{dt} = k_2 \cdot N_Y + k_3 \cdot \left(\frac{N_U}{V_s}\right)^2 \cdot N_Y - k_4 \cdot N_U \tag{5.26}$$

DOI:10.15774/PPKE.ITK.2023.004

5.7.2. Parameter values for Selkov-like PFB Framework With an Extra NFB Loop

Low k_3 or k_5 values result in estimated response rates that are typically one-fifteenth of those for higher k_3 or k_5 values. The system will have a dominant NFB (strong NFB - weak PFB) if k_3 is low and k_5 is high, while the system will possess a dominant PFB if k_3 is big and k_5 is low (weak NFB – strong PFB). The system will reflect the combined impact of a PFB and an NFB when both rates are high and equal (strong NFB – strong PFB).

Table-5.5: Parameter combinations for Selkov-like PFB Framework with an Extra NFB Loop network.

The parameters for the 3 examples shown in Figures 5.15B-C, 5.16, and 5.17 taking into account the Arrhenius rate law presented in Section 5.4, are listed here.

Cases	**i.** Activation Energy (E) in KJ/mol				
Small k_3 - Large k_5	**k_1**	**k_2**	**k_3**	**k_4**	**k_5**
	16.35	27.5	12.0203	14.8691	5.17
Large k_3 - Small k_5	**k_1**	**k_2**	**k_3**	**k_4**	**k_5**
	21.5	27.5	5.17	14.8691	12.0203
Large k_3 - Large k_5	**k_1**	**k_2**	**k_3**	**k_4**	**k_5**
	20.877	27.5	5.17	14.8691	5.17

Cases	**ii.** Reaction Rate (AU) at temperature 298 K				
Small k_3 - Large k_5	**k_1**	**k_2**	**k_3**	**k_4**	**k_5**
	0.2325	0.0058	3	0.9503	47.63
Large k_3 - Small k_5	**k_1**	**k_2**	**k_3**	**k_4**	**k_5**
	0.0691	0.0058	47.63	0.9503	3
Large k_3 - Large k_5	**k_1**	**k_2**	**k_3**	**k_4**	**k_5**
	0.0841	0.0058	47.63	0.9503	47.63

iii. Initial Concentration (AU)	
Y	**U**
0.48	0.0075

DOI:10.15774/PPKE.ITK.2023.004

5.7.3. Robustness and Temperature Compensation Analysis for Selkov-like PFB Framework With an Extra NFB Loop

The four explored models had different sizes (in Figure 5.1), which indicates ambiguity toward robustness analysis (Figure 5.4, Figure 5.5, Figure 5.6). To guarantee that the compared models have comparable size and kinetics, I maintain the network size constant and alter the intensity of a single rate for the positive (k_3) and negative feedback loops (k_5) (parameter values are shown in the Table-5.5, and rate constants at 298K are indicated in the Table-5.5).

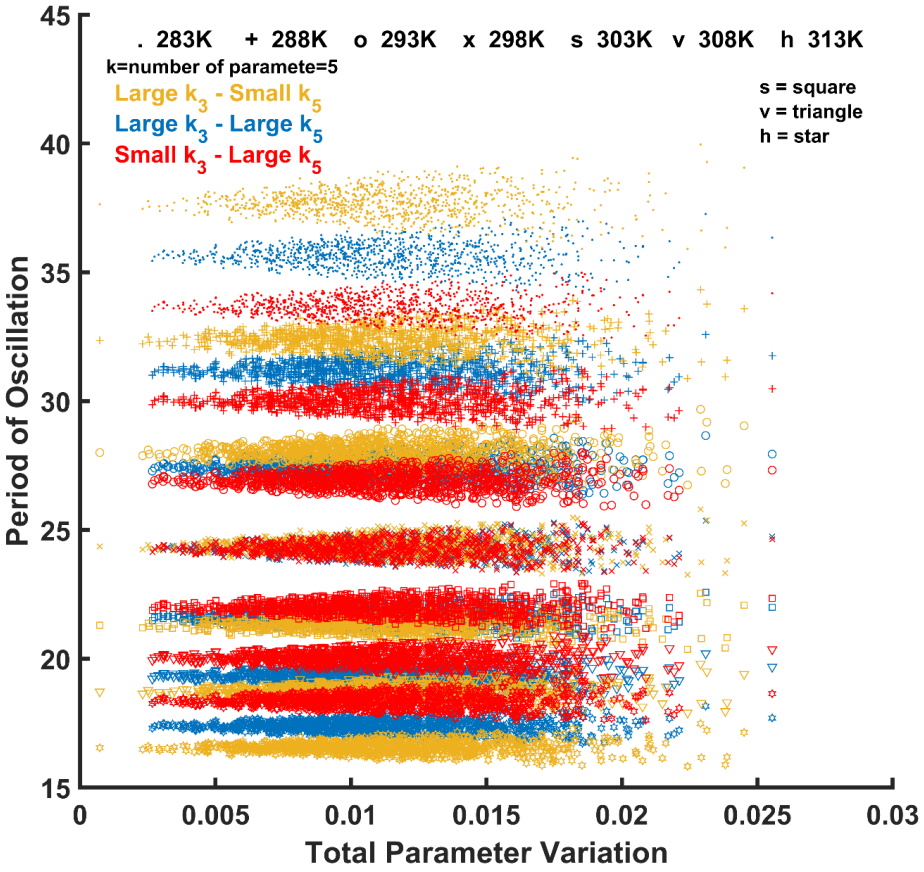

Figure 5.16: The connection among total parameter variations and period of oscillation for a Selkov-like PFB framework with an extra NFB loop.

The graph demonstrates how the oscillation periods change in relation to total parameter variations (Section 5.5.2.1.) in an oscillatory system (Figure 5.15A) for 1000 randomly selected points at 7 distinct temperatures. The three distinct examples (Table-5.5) that correspond to the system (Figure 5.15A) are denoted by three distinct colors, and the different 7 temperatures are denoted with differently shaped markers. Table-5.5 shows the initial concentrations of molecules as well as the parameters.

DOI:10.15774/PPKE.ITK.2023.004

The temperature compensation study of the combined network (Figure 5.15B) reveals that combining the strong NFB with the weak PFB (the small k_3-large k_5 instance, displayed in red line) results in better temperature compensation (lower Q_{10} values) than any of the other possible combinations (Figure 5.15B). This is consistent with the previous results (Figure 5.7), which show that negative feedback enhances temperature compensation.

A robustness study in presence of extrinsic noise [51] (Figure 5.15C, Figure 5.16) reveals that network robustness is strongly temperature dependent. The coupling between positive and negative feedback loops (in blue color) has the lowest temperature dependency on noise, but the strong PFB solely (large k_3-small k_5 instance, with yellow line) exhibits less robustness.

An intriguing result is that at higher temperatures, strong NFB (small k_3-large k_5 instance, using red line) is less robust (Figure 5.15C). This is most likely because at higher temperatures, quicker response rates lower feedback loop delays, resulting in a more difficult to sustain period.

The result that negative feedback may increase noise contradicts previous studies that indicated negative feedback loops might reduce noise [4]. However, they were previously examined for inherent intrinsic noise [51], not extrinsic noise, what was studied here. To check the effects of intrinsic noise on the studied model, the equations of the coupled Selkov-like positive-negative feedback model (Figure 5.15A) were converted to individual reactions and the model simulated by a Gillespie solver (Methods Section 3.1.2., Example-3). Stochastic simulations of such a system at different low molecular abundance levels show that at 298 K, a strong NFB with a weak PFB (small k_3-large k_5) combination is the most resilient against the intrinsic noise generated by smaller molecular abundances (displayed in Figure 5.17). It can be concluded that in the presence of intrinsic noise, NFB reduces noise better, whereas in the presence of extrinsic noise, it seems PFB is a better noise reducer.

DOI:10.15774/PPKE.ITK.2023.004

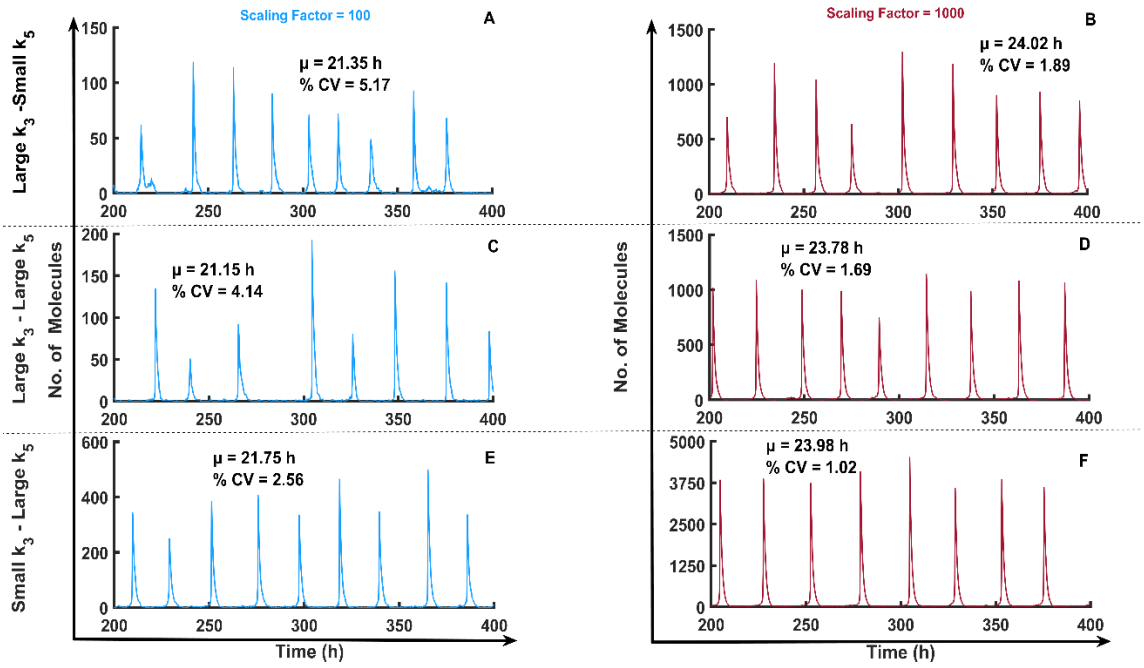

Figure 5.17: Analysis of such Selkov-like positive feedback oscillator model with an extra negative feedback loop, taking into account the effects of intrinsic noise.

Time course trajectory examples of species U (Figure 5.15A) with involved scaling factor of Gillespie simulation fixed to 100 and (B, D, F) or 1000 at temperature 298 K. For 100 cycles, the percentage of co-efficient of variations (%CV) and mean period (μ) at 298 K were determined and shown at the top of each panel. Table-5.5 contains a list of parameters.

5.8. Summary

The processes of temperature compensation in biological oscillators are still not fully understood. This study has shown that temperature compensation and resilience of circadian oscillators are mutually exclusive properties of circadian clocks. Figure 5.4 and Figure 5.7 make it abundantly evident that the Two-Variable-Goodwin-NFB model is the least resilient for parameter variations (it holds a high % CV value for oscillation periods), but it is better in temperature compensation (it has a lower Q_{10} value) compared to the other models. The cPNFB circadian oscillatory network, in contrast, provides the most robustness and least temperature compensation (Figures 5.4, 5.5 and 5.7). These are the two extreme instances of resilience and temperature compensation among the four oscillatory models that I have analyzed. Based on this systematic study of coupled positive and negative feedback systems (Figure 5.15), it can be concluded that pure NFB cannot effectively reduce extrinsic noise in a system (Two-Variable-Goodwin-NFB), whereas the availability of a PFB enhances the robustness of a system (at high temperatures) without greatly lowering the temperature compensating

DOI:10.15774/PPKE.ITK.2023.004

capabilities of a negative feedback loop, in presence of extrinsic noise. In contrast, NFB enhances the system's resiliency against intrinsic noise (Figure 5.17) [4,51].

The cyano-KaiABC model that was developed by Rust et al. [152] is a very complicated model that includes highly non-linear dynamics, as well as both negative and positive feedbacks. This model does a fair job of compensating for temperature when both k_{DS}^{0} and k_{SU}^{0} are held constant (Figure 5.14), but despite having the maximum number of parameters (k=12), it is neither the most temperature compensated or best robust system available. In addition, it is assumed that such linear mass action kinetics in the case of a cPNFB circadian oscillatory system might be the differentiating factor for its behavior that is the least noisy, especially in comparison to the other models, which have non-linear terms that might amplify any noise that is present in the network (Section 5.3.1. and 5.3.3.). Even at low input signal levels, mass-action kinetics gives accuracy, but non-linear dynamics like Hill or Michaelis-Menten fail accuracy owing to overly complex combinations and scaling factors of multiple reaction rates utilized to describe the kinetics [170].

Avello et al. [171] explored temperature compensation using minimalistic models of plant circadian clock with varying levels of complexity. This comprehensive study uncovered that negative feedback loops are required for adequate temperature compensation, and that combining positive and negative feedback loops might result in decreased noise in circadian clocks. It can also be observed that temperature independent reactions, which is critical for negative feedback loops, may assist the whole system in driving temperature compensated oscillations. These findings may help clarify why the circadian clock in higher eukaryotes is driven by a conventional delayed negative feedback loop, whereas the circadian oscillator in cyanobacteria in-vitro is positive feedback-based KaiC system, and temperature compensation is accomplished through the temperature independent key reactions in that system [165]. These findings also confirm previous findings that positive feedback might strengthen the circadian clock [113,167].

On the molecular level, feedback loops may be built in a variety of ways [172]. Feedback may either promote activation or inhibition processes, or both. Furthermore, the exact dynamics of oscillators may be affected by reaction kinetics. I studied a large range of such systems here, but only one combination model was rigorously validated (Figures

DOI:10.15774/PPKE.ITK.2023.004

5.15, 5.17). Thus, my approach has limits and might be broadened by investigating the impacts of different kinetics, regulatory effects, and baseline reaction rates.

Despite these constraints, the suggested model engineering and comparison methodologies may be effective in the design of synthetic circuits that must withstand environmental perturbations such as temperature changes. This might be applicable to cyanobacteria species engineering strategies for biomass production, incorporating light harvesting [173]. This work is expected to help this growing scientific area even more.

DOI:10.15774/PPKE.ITK.2023.004

Chapter 6

Conclusions

DOI:10.15774/PPKE.ITK.2023.004

In this dissertation, I looked into how different types of feedforward and feedback loops can lead to robust responses. I showed that, when it comes to noise reduction and signal transduction, combined FFLs are better than isolated FFLs.
I studied unique properties of circadian oscillations, such as temperature compensation and noise attenuation. I also took steps to find the key controllers of the circadian oscillatory network that allow temperature compensation.

This section summarizes the key contributions of this study. The potential pathways for further investigation have been also suggested. For each thesis point, the appropriate section, figure number, and corresponding publications are indicated.

6.1. New Scientific Results

Thesis 1a. I have discovered that coupled feedforward loops (FFLs) outperformed isolated feedforward loops in terms of robustness and signal transduction.

Related publications: [J1], [C1], [C2], [C3]

I performed LNA simulations with two different kinds of FFLs: coupled and isolated. The percentile coefficient of variation (% CV) measures noise, and the slope values of the networks (Figure 4.1) generated from the input-output plots (Figures 4.4C, 4.5, 4.6, and 4.7) assess signal transduction capability. Interestingly, there is a typical inverse relationship between the percentage CV and the slope values. A greater % CV indicates inadequate noise reduction, but a higher slope value indicates improved signal transduction capabilities. I demonstrated that coupled FFLs are better at reducing noise than isolated FFLs by comparing Figures 4.4D and 4.8. I've shown in Figure 4.9 that coupled FFLs transmit signals more effectively than isolated FFLs.

Thesis 1b. I have been able to distinguish between FFLs that perform better at minimizing noise and signal transduction based on their network architecture.

Related publications: [J1], [C1], [C2], [C3]

I have shown a number of fascinating traits that come out of the analysis: All of the FFLs (Figure 4.1) with the higher signal transduction capacity have an activatory direct connection between the input and output nodes (Figure 4.4D and Figure 4.8). This suggests that node X should directly activate the node Z to provide the best signal transduction. Successful signal transduction occurs when input node X suppresses at least

DOI:10.15774/PPKE.ITK.2023.004

one copy of intermediate species Y and output gates follow OR logic. All of these claims are true for FFLs with maximal signal transduction capability, including c4-OR, c4c4-mint-OR, c1i4-mint-OR, and c4i1-minp-OR.

Effective noise reduction may be shown in FFLs with the same activatory direct channel between nodes X and Z, but this is augmented by a reaction in which Z is activated by Y (Figure 4.4D and Figure 4.8) and follows OR logic. The best FFLs are i4-OR, c1-OR, c1i4-mint-OR, c1c1-mint-OR, and c1i4-minp-OR.

In excellent noise filters, noise reduces down the lower levels of FFLs (with slight differences in incoherent FFLs), while in bad noise filters, species Y has the highest noise-reducing performance (Figure 4.10). Excellent noise-reducing models at output nodes are effective in noise removal because noise lowers as the signal progresses through lower levels of FFLs.

Based on this study, coherent type-1 and type-4 and incoherent type-4 with OR connection can perform well as noise reducers and signal transducers. Figure 4.10 depicts the best and worst FFLs in regard to their noise reduction capacity. In this scenario, the standard input alterations (Figure 4.3F) are applied to all networks, and the results show that c1c1-minp-FFL-OR is the best noise filter (with the lowest % CV) and c4c4-minp-OR is the best signal transducer (with highest value for slope).

Thesis 1c. I discovered that the FFLs' noise reducing capability trends remained unchanged even with the addition of stochastic input signal.

Related publications: [J1], [C1], [C2], [C3]

Noise through each level of posttranslational modification to FFLs is inherent and unaffected by noise at the input nodes. Therefore, changing the input noise level maintains the conclusion's consistency (Thesis 1a., Thesis 1b.) at all levels of the models (Figure 4.11).

Thesis 1d. I discovered that OR gates in FFLs are better than AND gates in terms of noise reduction.

Related publications: [J1], [C1], [C2], [C3]

FFLs with AND logical gates reduce noise less than those with OR gates (Figure 4.13, Figure 4.14). This trend is harder to see in Figure 4.8, but it remains true for all models,

DOI:10.15774/PPKE.ITK.2023.004

especially when comparing successful and ineffective noise reducers (Figure 4.12). Through simultaneous effect in coupled FFLs, the degree of noise in the input decreases to lower levels of the motif, and these associated noises enhance their overall effect when they integrate at the output nodes through an AND gate. When the network has an OR gate, this apparent rise in noise seems to be minimized.

Thesis 1e. I evaluated one-step and two-step post translational modification in FFLs and discovered that multisite modification improves signal transduction but decrease noise reduction capability.

Related publications: [J1], [C1], [C2], [C3]

I have shown that multisite alteration improves both signal transduction and % CV based on an analysis of the input-output correlation slopes and the % CV produced by these motifs and equivalent networks with single modifications (Figure 4.13). As a result, multisite alteration does not increase FFLs' noise-reduction abilities (Figure 4.14), but it does improve FFL motifs' signal transducing abilities.

Thesis 2a. I have investigated four distinct oscillatory modules and identified that the delayed negative feedback loop model is the least robust, while a model combining positive and negative feedbacks is the most robust among the four investigated ones.

Related publications: [J2], [C4], [C5]

In Figures 5.4 and 5.5B, I have demonstrated that the Two-Variable-Goodwin-NFB network (delayed NFB model) is the least resistant (it has a high% CV value for oscillation periods), while cPNFB models (which is a combination of positive and negative feedback loops) have the lowest noise to parameter changes. Irrespective of the size, the Two-Variable-Goodwin-NFB architecture is the noisiest at the majority of temperature values (which indicates the highest value of BIC). In this study, parameter changes cause the least amount of noise in the Selkov-PFB and cPNFB models, which are smaller in size.

DOI:10.15774/PPKE.ITK.2023.004

Thesis 2b. I have discovered that the delayed negative feedback loop model is better at temperature compensation, while the model combining positive and negative feedbacks shows the least temperature compensation from the four investigated models.

Related publications: [J2], [C4], [C5]

In Figure 5.7, I showed that the Two-Variable-Goodwin-NFB model is better at temperature compensation because its Q_{10} value is lower, while the cPNFB circadian oscillatory network is the worst at temperature compensation because its Q_{10} value is higher.

Thesis 2c. I have found that in all the investigated cases, temperature-insensitive parameters are either direct or indirect controllers of negative feedback.

Related publications: [J2], [C4], [C5]

I have shown, with the help of Figures 5.9, that the temperature insensitive rate (the α_2 rate) of the Two-Variable-Goodwin-NFB model directly controls the negative feedback loop. The parameter, which must be temperature insensitive, is also a negative feedback loop controller for both the cyano-KaiABC (the k_{DS}^0 rate) and cPNFB (the k_{01}) networks. Since the Selkov-PFB lacks an NFB loop, the most essential parameter is the PFB loop's substrate synthesis (k_1 rate).

I also observed that the Two-Variable-Goodwin-NFB model with a single temperature insensitive parameter (α_2) performs nearly as well as a two-parameter fixed scenario (k_1-α_2), while the other three networks exhibit extra improvements for second rate fixing. According to Figure 5.14's lower Q_{10} values, the oscillation periods are more temperature compensated than in Figure 5.9, when only one rate was temperature independent throughout all models.

6.2. Future Perspectives

In this thesis, I have thoroughly investigated and performed systematic analysis of network motifs comprising of feedforward and feedback loops to study their diverse dynamical behaviors. Using mathematical modeling and computer simulations, I have explored the noise reduction and signal transduction properties of isolated and coupled feedforward loops which is explained in detail in Chapter 4 in this thesis. I found that the

DOI:10.15774/PPKE.ITK.2023.004

coupled feedforward loops are more efficient in noise reduction as well as in signal transduction compared to the isolated networks. In future, one could expand these networks by increasing the number of coupling units in the feedforward loops and explore their properties in noise reduction and signal transduction. It is essential to comprehend the dynamical characteristics of several larger physiological pathways, and this knowledge can be gained by looking at smaller regulatory network motifs. The resilience of the system's ability to operate in the face of chemical noise precisely and effectively is greatly influenced by the architecture of the regulatory motifs.

I have also investigated the properties of various feedback loops involved in the circadian oscillatory system in terms of their ability to robustness to noise and temperature compensation which I have discussed in detail in Chapter 5. This prospective topic of research might focus on the synthetic development of these oscillatory systems as well as the importance of in vivo systems in understanding circadian clocks in living organisms, particularly mammals. One might investigate how effectively a circadian oscillator can be modified in terms of robustness and temperature compensation in vivo by altering the relevant biological reaction rates mentioned in Chapter 5. The answers to these fundamental problems, which were derived from the previous theoretical study, may be found in a wet research laboratory. Feedback may either activate or inhibit processes, or both. Furthermore, response kinetics may influence the precise dynamics of oscillators. Future work will be able to forecast the robustness analysis and temperature compensation studies for negative feedbacks with different kinds of connection and kinetics. The next stage of this study might be a comparison of linear and non-linear kinetics systems while changing the decay rates and introducing delay to the system.

As discussed previously, regulatory network motifs form the basic functional unit of the large complex molecular network of a biological system. It is therefore crucial to study and explore the architectural significance of regulatory network motifs in order to acquire insights into the mechanisms of biological systems, including industrial and clinical biosensing applications, human disease, and thereby uncover new therapeutic approaches. I hope that my findings will aid in the advancement of these scientific domains and the creation of broadly used reverse engineering application.

References

1. Klein C, Marino A, Sagot M-F, Vieira Milreu P, Brilli M. Structural and dynamical analysis of biological networks. Brief Funct Genomics. 2012;11: 420–433. doi:10.1093/bfgp/els030

2. Groß A, Kracher B, Kraus JM, Kühlwein SD, Pfister AS, Wiese S, et al. Representing dynamic biological networks with multi-scale probabilistic models. Commun Biol. 2019;2: 21. doi:10.1038/s42003-018-0268-3

3. Sontag ED. Molecular Systems Biology and Control. Eur J Control. 2005;11: 396–435. doi:10.3166/ejc.11.396-435

4. Alon U. Network motifs: theory and experimental approaches. Nat Rev Genet. 2007;8: 450–461. doi:10.1038/nrg2102

5. Milo R, Shen-Orr S, Itzkovitz S, Kashtan N, Chklovskii D, Alon U. Network Motifs: Simple Building Blocks of Complex Networks. Science (80-). 2002;298: 824–827. doi:10.1126/science.298.5594.824

6. Gillespie DT. Exact stochastic simulation of coupled chemical reactions. J Phys Chem. 1977;81: 2340–2361. doi:10.1021/j100540a008

7. Gillespie DT. Stochastic Simulation of Chemical Kinetics. Annu Rev Phys Chem. 2007;58: 35–55. doi:10.1146/annurev.physchem.58.032806.104637

8. Gunawardena J. Models in biology: ‘accurate descriptions of our pathetic thinking.’ BMC Biol. 2014;12: 29. doi:10.1186/1741-7007-12-29

9. Radhakrishnan K, Halász A, Vlachos D, Edwards JS. Quantitative understanding of cell signaling: the importance of membrane organization. Curr Opin Biotechnol. 2010;21: 677–682. doi:10.1016/j.copbio.2010.08.006

10. Baltoumas FA, Zafeiropoulou S, Karatzas E, Koutrouli M, Thanati F, Voutsadaki K, et al. Biomolecule and Bioentity Interaction Databases in Systems Biology: A Comprehensive Review. Biomolecules. 2021;11. doi:10.3390/biom11081245

11. Leite M, Wang Y. Multistability, oscillations and bifurcations in feedback loops.

Math Biosci Eng. 2010;7: 83–97. doi:10.3934/mbe.2010.7.83

12. Barik D, Ball DA, Peccoud J, Tyson JJ. A Stochastic Model of the Yeast Cell Cycle Reveals Roles for Feedback Regulation in Limiting Cellular Variability. You L, editor. PLOS Comput Biol. 2016;12: e1005230. doi:10.1371/journal.pcbi.1005230

13. Atay O, Doncic A, Skotheim JM. Switch-like transitions insulate network motifs to modularize biological networks. Cell Syst. 2016;3: 121–132.

14. Gyorgy A, Del Vecchio D. Modular Composition of Gene Transcription Networks. PLOS Comput Biol. 2014;10: 1–16. doi:10.1371/journal.pcbi.1003486

15. Buri G, Zelleke GM, Ndifon W. Dynamic Regulation of T Cell Activation by Coupled Feedforward Loops. In: Teboh-Ewungkem MI, Ngwa GA, editors. Infectious Diseases and Our Planet. Cham: Springer International Publishing; 2021. pp. 241–255. doi:10.1007/978-3-030-50826-5_9

16. Keifer J, Houk JC. Modeling signal transduction in classical conditioning with network motifs. Front Mol Neurosci. 2011;4: 9.

17. Callaway E, Ledford H. Medicine Nobel awarded for work on circadian clocks. Nature. England; 2017. p. 18. doi:10.1038/nature.2017.22736

18. Ruoff P. Introducing temperature-compensation in any reaction kinetic oscillator model. J Interdiscipl Cycle Res. 1992;23: 92–99. doi:10.1080/09291019209360133

19. Ferrell JE. Q&A: Systems biology. J Biol. 2009;8: 2. doi:10.1186/jbiol107

20. Cardelli L, Csikász-Nagy A. The Cell Cycle Switch Computes Approximate Majority. Sci Rep. 2012;2: 656. doi:10.1038/srep00656

21. Cardelli L, Hernansaiz-Ballesteros RD, Dalchau N, Csikász-Nagy A. Efficient Switches in Biology and Computer Science. PLOS Comput Biol. 2017;13: 1–16. doi:10.1371/journal.pcbi.1005100

22. Thomas R, Thieffry D, Kaufman M. Dynamical behaviour of biological regulatory networks—I. Biological role of feedback loops and practical use of

the concept of the loop-characteristic state. Bull Math Biol. 1995;57: 247–276. doi:10.1007/BF02460618

23. Tyson JJ, Chen KC, Novak B. Sniffers, buzzers, toggles and blinkers: dynamics of regulatory and signaling pathways in the cell. Curr Opin Cell Biol. 2003;15: 221–231. doi:10.1016/S0955-0674(03)00017-6

24. Tyson JJ, Novák B. Functional Motifs in Biochemical Reaction Networks. Annu Rev Phys Chem. 2010;61: 219–240. doi:10.1146/annurev.physchem.012809.103457

25. Pavlopoulos GA, Secrier M, Moschopoulos CN, Soldatos TG, Kossida S, Aerts J, et al. Using graph theory to analyze biological networks. BioData Min. 2011;4: 10. doi:10.1186/1756-0381-4-10

26. Strogatz SH. Nonlinear Dynamics and Chaos. Nonlinear Dynamics and Chaos. CRC Press; 2018. doi:10.1201/9780429492563

27. Ingalls BP. Mathematical modeling in systems biology: an introduction. Choice Reviews Online. MIT Press; 2013. Available: https://www.goodreads.com/en/book/show/17471031-mathematical-modeling-in-systems-biology

28. Chakravarty S, Barik D. Steady state statistical correlations predict bistability in reaction motifs. Mol Biosyst. 2017;13: 775–784. doi:10.1039/C7MB00052A

29. Novák B, Tyson JJ. Design principles of biochemical oscillators. Nat Rev Mol Cell Biol. 2008;9: 981–991. doi:10.1038/nrm2530

30. Bargiello TA, Jackson FR, Young MW. Restoration of circadian behavioural rhythms by gene transfer in Drosophila. Nature. 1984;312: 752–754. doi:10.1038/312752a0

31. Csikász-Nagy A, Dalchau N. What makes a biological clock efficient? Evolution of biological clocks. Essays Luca Cardelli Fest. Essays for. Microsoft Research; 2014 Sep. Available: http://research.microsoft.com/apps/pubs/default.aspx?id=230889

32. Gonze D, Halloy J, Goldbeter A. Robustness of circadian rhythms with respect to molecular noise. Proc Natl Acad Sci. 2002;99: 673–678.

doi:10.1073/pnas.022628299

33. SEL'KOV EE. Self-Oscillations in Glycolysis 1. A Simple Kinetic Model. Eur J Biochem. 1968;4: 79–86. doi:https://doi.org/10.1111/j.1432-1033.1968.tb00175.x

34. Thattai M, van Oudenaarden A. Attenuation of noise in ultrasensitive signaling cascades. Biophys J. 2002;82: 2943–2950. doi:10.1016/S0006-3495(02)75635-X

35. Ghosh B, Karmakar R, Bose I. Noise characteristics of feed forward loops. Phys Biol. 2005;2: 36. doi:10.1088/1478-3967/2/1/005

36. Gui R, Liu Q, Yao Y, Deng H, Ma C, Jia Y, et al. Noise decomposition principle in a coherent feed-forward transcriptional regulatory loop. Front Physiol. 2016;7: 600.

37. Cardelli L. Morphisms of reaction networks that couple structure to function. BMC Syst Biol. 2014;8: 84. doi:10.1186/1752-0509-8-84

38. Feliu E, Wiuf C. Simplifying biochemical models with intermediate species. J R Soc Interface. 2013;10: 20130484. doi:10.1098/rsif.2013.0484

39. Brijder R. Computing with chemical reaction networks: a tutorial. Nat Comput. 2019;18: 119–137. doi:10.1007/s11047-018-9723-9

40. Waage P, Gulberg CM. Studies concerning affinity. J Chem Educ. 1986;63: 1044. doi:10.1021/ed063p1044

41. Ferner RE, Aronson JK. Cato Guldberg and Peter Waage, the history of the Law of Mass Action, and its relevance to clinical pharmacology. Br J Clin Pharmacol. 2016;81: 52–55. doi:https://doi.org/10.1111/bcp.12721

42. Johnson KA, Goody RS. The Original Michaelis Constant: Translation of the 1913 Michaelis–Menten Paper. Biochemistry. 2011;50: 8264–8269. doi:10.1021/bi201284u

43. Goutelle S, Maurin M, Rougier F, Barbaut X, Bourguignon L, Ducher M, et al. The Hill equation: a review of its capabilities in pharmacological modelling. Fundam Clin Pharmacol. 2008;22: 633–648. doi:10.1111/j.1472-8206.2008.00633.x

44. Weiss JN. The Hill equation revisited: uses and misuses. FASEB J. 1997;11: 835–841. doi:10.1096/fasebj.11.11.9285481

45. Ferrell JEJ. Tripping the switch fantastic: how a protein kinase cascade can convert graded inputs into switch-like outputs. Trends Biochem Sci. 1996;21: 460–466. doi:10.1016/s0968-0004(96)20026-x

46. Gunawardena J. Multisite protein phosphorylation makes a good threshold but can be a poor switch. Proc Natl Acad Sci. 2005;102: 14617–14622.

47. Kapuy O, Barik D, Domingo Sananes MR, Tyson JJ, Novák B. Bistability by multiple phosphorylation of regulatory proteins. Prog Biophys Mol Biol. 2009;100: 47–56. doi:https://doi.org/10.1016/j.pbiomolbio.2009.06.004

48. Markevich NI, Hoek JB, Kholodenko BN. Signaling switches and bistability arising from multisite phosphorylation in protein kinase cascades. J Cell Biol. 2004;164: 353–359. doi:10.1083/jcb.200308060

49. Salazar C, Höfer T. Multisite protein phosphorylation--from molecular mechanisms to kinetic models. FEBS J. 2009;276: 3177–3198. doi:10.1111/j.1742-4658.2009.07027.x

50. Raser JM, O'Shea EK. Control of stochasticity in eukaryotic gene expression. Science. 2004;304: 1811–1814. doi:10.1126/science.1098641

51. Elowitz MB, Levine AJ, Siggia ED, Swain PS. Stochastic gene expression in a single cell. Science. 2002;297: 1183–1186. doi:10.1126/science.1070919

52. Chabot JR, Pedraza JM, Luitel P, van Oudenaarden A. Stochastic gene expression out-of-steady-state in the cyanobacterial circadian clock. Nature. 2007;450: 1249–1252. doi:10.1038/nature06395

53. Newman JRS, Ghaemmaghami S, Ihmels J, Breslow DK, Noble M, DeRisi JL, et al. Single-cell proteomic analysis of S. cerevisiae reveals the architecture of biological noise. Nature. 2006;441: 840–846. doi:10.1038/nature04785

54. Ozbudak EM, Thattai M, Kurtser I, Grossman AD, van Oudenaarden A. Regulation of noise in the expression of a single gene. Nat Genet. 2002;31: 69–73. doi:10.1038/ng869

55. Ramsey S, Ozinsky A, Clark A, Smith KD, de Atauri P, Thorsson V, et al. Transcriptional noise and cellular heterogeneity in mammalian macrophages. Philos Trans R Soc London Ser B, Biol Sci. 2006;361: 495–506. doi:10.1098/rstb.2005.1808

56. Gillespie DT. The chemical Langevin equation. J Chem Phys. 2000;113: 297–306. doi:10.1063/1.481811

57. Lei J. Stochastic modeling in systems biology. J Adv Math Appl. 2012;1: 76–88.

58. Gillespie DT. A rigorous derivation of the chemical master equation. Phys A Stat Mech its Appl. 1992;188: 404–425. doi:https://doi.org/10.1016/0378-4371(92)90283-V

59. Gillespie DT. A general method for numerically simulating the stochastic time evolution of coupled chemical reactions. J Comput Phys. 1976;22: 403–434. doi:https://doi.org/10.1016/0021-9991(76)90041-3

60. Palanichamy J, Becker T, Spiller M, Köngeter J, Mohan S. Multicomponent reaction modelling using a stochastic algorithm. Comput Vis Sci. 2009;12: 51–61. doi:10.1007/s00791-007-0080-y

61. van Parijs FRD, Morreel K, Ralph J, Boerjan W, Merks RMH. Modeling Lignin Polymerization. I. Simulation Model of Dehydrogenation Polymers . Plant Physiol. 2010;153: 1332–1344. doi:10.1104/pp.110.154468

62. Schnoerr D, Sanguinetti G, Grima R. The complex chemical Langevin equation. J Chem Phys. 2014;141: 24103. doi:10.1063/1.4885345

63. Wallace EWJ, Gillespie DT, Sanft KR, Petzold LR. Linear noise approximation is valid over limited times for any chemical system that is sufficiently large. IET Syst Biol. 2012;6: 102–115. doi:10.1049/iet-syb.2011.0038

64. Grima R, Thomas P, Straube A V. How accurate are the nonlinear chemical Fokker-Planck and chemical Langevin equations? J Chem Phys. 2011;135: 84103. doi:10.1063/1.3625958

65. Cardelli L, Kwiatkowska M, Laurenti L. Stochastic analysis of Chemical Reaction Networks using Linear Noise Approximation. Biosystems. 2016;149: 26–33. doi:https://doi.org/10.1016/j.biosystems.2016.09.004

66. Wallace EWJ. A simplified derivation of the Linear Noise Approximation. arXiv Stat Mech. 2010.

67. Bureš V. Comparative analysis of system dynamics software packages. Int Rev Model Simulations. 2015;8: 245–255.

68. Suresh NT, Ashok S. Comparative Strategy for the Statistical & Network based Analysis of Biological Networks. Procedia Comput Sci. 2018;143: 165–180. doi:https://doi.org/10.1016/j.procs.2018.10.373

69. Cardelli L. Kaemika App: Integrating Protocols and Chemical Simulation: Integrating Protocols and Chemical Simulation. Computational Methods in Systems Biology: 18th International Conference, CMSB 2020, Konstanz, Germany, September 23--25, 2020, Proceedings. 2020. pp. 373–379.

70. Zheng L, Chen M, Nie Q. External noise control in inherently stochastic biological systems. J Math Phys. 2012;53: 115616. doi:10.1063/1.4762825

71. Houcque D, others. Introduction to Matlab for engineering students. Northwest Univ. 2005.

72. Laidler KJ. The development of the Arrhenius equation. J Chem Educ. 1984;61: 494. doi:10.1021/ed061p494

73. Ruoff P, Rensing L, Kommedal R, Mohsenzadeh S. Modeling temperature compensation in chemical and biological oscillators. Chronobiol Int. 1997;14: 499–510. doi:10.3109/07420529709001471

74. Balzer I, Hardeland R. Influence of temperature on biological rhythms. Int J Biometeorol. 1988;32: 231–241. doi:10.1007/BF01080021

75. Kurosawa G, Iwasa Y. Temperature compensation in circadian clock models. J Theor Biol. 2005;233: 453–468. doi:10.1016/j.jtbi.2004.10.012

76. Gonze D, Ruoff P. The Goodwin Oscillator and its Legacy. Acta Biotheor. 2021;69: 857–874. doi:10.1007/s10441-020-09379-8

77. Gonze D, Halloy J, Leloup J-C, Goldbeter A. Stochastic models for circadian rhythms: effect of molecular noise on periodic and chaotic behaviour. C R Biol. 2003;326: 189–203. doi:10.1016/s1631-0691(03)00016-7

78. Raj A, Rifkin SA, Andersen E, van Oudenaarden A. Variability in gene expression underlies incomplete penetrance. Nature. 2010;463: 913–918. doi:10.1038/nature08781

79. Holloway DM. Experimental and Modeling Approaches for Understanding the Effect of Gene Expression Noise in Biological Development. Front Phys. 2018;6: 36.

80. Fraser HB, Hirsh AE, Giaever G, Kumm J, Eisen MB. Noise Minimization in Eukaryotic Gene Expression. PLOS Biol. 2004;2: e137. Available: https://doi.org/10.1371/journal.pbio.0020137

81. Becskei A, Kaufmann BB, van Oudenaarden A. Contributions of low molecule number and chromosomal positioning to stochastic gene expression. Nat Genet. 2005;37: 937–944. doi:10.1038/ng1616

82. Thomas P. Intrinsic and extrinsic noise of gene expression in lineage trees. Sci Rep. 2019;9: 474. doi:10.1038/s41598-018-35927-x

83. Pedraza JM, Paulsson J. Effects of Molecular Memory and Bursting on Fluctuations in Gene Expression. Science (80-). 2008;319: 339–343. doi:10.1126/science.1144331

84. Swain PS, Elowitz MB, Siggia ED. Intrinsic and extrinsic contributions to stochasticity in gene expression. Proc Natl Acad Sci. 2002;99: 12795–12800. doi:10.1073/pnas.162041399

85. Paulsson J. Models of stochastic gene expression. Phys Life Rev. 2005;2: 157–175. doi:https://doi.org/10.1016/j.plrev.2005.03.003

86. Dobrin R, Beg QK, Barabási A-L, Oltvai ZN. Aggregation of topological motifs in the Escherichia coli transcriptional regulatory network. BMC Bioinformatics. 2004;5: 10. doi:10.1186/1471-2105-5-10

87. Laurenti L, Csikasz-Nagy A, Kwiatkowska M, Cardelli L. Molecular Filters for Noise Reduction. Biophys J. 2018;114: 3000–3011. doi:https://doi.org/10.1016/j.bpj.2018.05.009

88. Mangan S, Alon U. Structure and function of the feed-forward loop network motif. Proc Natl Acad Sci. 2003;100: 11980 LP – 11985.

doi:10.1073/pnas.2133841100

89. Csikász-Nagy A, Cardelli L, Soyer OS. Response dynamics of phosphorelays suggest their potential utility in cell signalling. J R Soc Interface. 2011;8: 480–488. doi:10.1098/rsif.2010.0336

90. Goldbeter A, Koshland DE. An amplified sensitivity arising from covalent modification in biological systems. Proc Natl Acad Sci. 1981;78: 6840–6844. doi:10.1073/pnas.78.11.6840

91. Tsimring LS. Noise in biology. Reports Prog Phys. 2014;77: 26601. doi:10.1088/0034-4885/77/2/026601

92. Becskei A, Serrano L. Engineering stability in gene networks by autoregulation. Nature. 2000;405: 590–593. doi:10.1038/35014651

93. Nevozhay D, Adams RM, Murphy KF, Josic K, Balázsi G. Negative autoregulation linearizes the dose-response and suppresses the heterogeneity of gene expression. Proc Natl Acad Sci U S A. 2009;106: 5123–5128. doi:10.1073/pnas.0809901106

94. Schmiedel JM, Klemm SL, Zheng Y, Sahay A, Blüthgen N, Marks DS, et al. MicroRNA control of protein expression noise. Science (80-). 2015;348: 128–132. doi:10.1126/science.aaa1738

95. Dhananjaneyulu V, Sagar P VN, Kumar G, Viswanathan GA. Noise propagation in two-step series MAPK cascade. PLoS One. 2012;7: e35958. doi:10.1371/journal.pone.0035958

96. Maity AK, Bandyopadhyay A, Chattopadhyay S, Chaudhuri JR, Metzler R, Chaudhury P, et al. Quantification of noise in bifunctionality-induced post-translational modification. Phys Rev E Stat Nonlin Soft Matter Phys. 2013;88: 32716. doi:10.1103/PhysRevE.88.032716

97. Cooper MB, Loose M, Brookfield JFY. Evolutionary modelling of feed forward loops in gene regulatory networks. Biosystems. 2008;91: 231–244. doi:10.1016/j.biosystems.2007.09.004

98. Mc Mahon SS, Sim A, Filippi S, Johnson R, Liepe J, Smith D, et al. Information theory and signal transduction systems: from molecular information processing

to network inference. Semin Cell Dev Biol. 2014;35: 98–108. doi:10.1016/j.semcdb.2014.06.011

99. Momin MSA, Biswas A, Banik SK. Coherent feed-forward loop acts as an efficient information transmitting motif. Phys Rev E. 2020;101: 22407. doi:10.1103/PhysRevE.101.022407

100. Rao C V, Wolf DM, Arkin AP. Control, exploitation and tolerance of intracellular noise. Nature. 2002;420: 231–237. doi:10.1038/nature01258

101. Arriaga E. Determining biological noise via single cell analysis. Anal Bioanal Chem. 2008;393: 73–80. doi:10.1007/s00216-008-2431-z

102. Shen-Orr SS, Milo R, Mangan S, Alon U. Network motifs in the transcriptional regulation network of Escherichia coli. Nat Genet. 2002;31: 64–68. doi:10.1038/ng881

103. Huang CY, Ferrell JE. Ultrasensitivity in the mitogen-activated protein kinase cascade. Proc Natl Acad Sci. 1996;93: 10078–10083. doi:10.1073/pnas.93.19.10078

104. Korcsmáros T, Farkas IJ, Szalay MS, Rovó P, Fazekas D, Spiró Z, et al. Uniformly curated signaling pathways reveal tissue-specific cross-talks and support drug target discovery. Bioinformatics. 2010;26: 2042–2050. doi:10.1093/bioinformatics/btq310

105. Balázsi G, van Oudenaarden A, Collins JJ. Cellular decision making and biological noise: from microbes to mammals. Cell. 2011;144: 910–925. doi:10.1016/j.cell.2011.01.030

106. Sturm OE, Orton R, Grindlay J, Birtwistle M, Vyshemirsky V, Gilbert D, et al. The mammalian MAPK/ERK pathway exhibits properties of a negative feedback amplifier. Sci Signal. 2010;3: ra90. doi:10.1126/scisignal.2001212

107. Fritsche-Guenther R, Witzel F, Sieber A, Herr R, Schmidt N, Braun S, et al. Strong negative feedback from Erk to Raf confers robustness to MAPK signalling. Mol Syst Biol. 2011;7: 489. doi:10.1038/msb.2011.27

108. Goentoro L, Shoval O, Kirschner MW, Alon U. The incoherent feedforward loop can provide fold-change detection in gene regulation. Mol Cell. 2009;36:

894–899. doi:10.1016/j.molcel.2009.11.018

109. Osella M, Bosia C, Corá D, Caselle M. The Role of Incoherent MicroRNA-Mediated Feedforward Loops in Noise Buffering. PLOS Comput Biol. 2011;7: e1001101. Available: https://doi.org/10.1371/journal.pcbi.1001101

110. Oda K, Matsuoka Y, Funahashi A, Kitano H. A comprehensive pathway map of epidermal growth factor receptor signaling. Mol Syst Biol. 2005;1: 2005.0010. doi:10.1038/msb4100014

111. Zechner C, Seelig G, Rullan M, Khammash M. Molecular circuits for dynamic noise filtering. Proc Natl Acad Sci. 2016;113: 4729–4734. doi:10.1073/pnas.1517109113

112. Heltberg ML, Krishna S, Kadanoff LP, Jensen MH. A tale of two rhythms: Locked clocks and chaos in biology. Cell Syst. 2021;12: 291–303. doi:https://doi.org/10.1016/j.cels.2021.03.003

113. Tsai TY-C, Choi YS, Ma W, Pomerening JR, Tang C, Ferrell JEJ. Robust, tunable biological oscillations from interlinked positive and negative feedback loops. Science. 2008;321: 126–129. doi:10.1126/science.1156951

114. O'Rourke B, Ramza BM, Marban E. Oscillations of membrane current and excitability driven by metabolic oscillations in heart cells. Science. 1994;265: 962–966. doi:10.1126/science.8052856

115. Ganitkevich V, Mattea V, Benndorf K. Glycolytic oscillations in single ischemic cardiomyocytes at near anoxia. J Gen Physiol. 2010;135: 307–319. doi:10.1085/jgp.200910332

116. Weiss JN, Yang J-H. Oscillations at odds in the heart. J Gen Physiol. 2010;135: 303–305. doi:10.1085/jgp.201010422

117. Goldbeter A. Computational approaches to cellular rhythms. Nature. 2002;420: 238–245. doi:10.1038/nature01259

118. Hardin PE, Hall JC, Rosbash M. Feedback of the Drosophila period gene product on circadian cycling of its messenger RNA levels. Nature. 1990;343: 536–540. doi:10.1038/343536a0

119. Thommen Q, Pfeuty B, Morant P-E, Corellou F, Bouget F-Y, Lefranc M. Robustness of Circadian Clocks to Daylight Fluctuations: Hints from the Picoeucaryote Ostreococcus tauri. PLOS Comput Biol. 2010;6: e1000990. Available: https://doi.org/10.1371/journal.pcbi.1000990

120. Waite E, Kershaw Y, Spiga F, Lightman SL. A glucocorticoid sensitive biphasic rhythm of testosterone secretion. J Neuroendocrinol. 2009;21: 737–741. doi:10.1111/j.1365-2826.2009.01900.x

121. Hoffmann A, Levchenko A, Scott ML, Baltimore D. The IkappaB-NF-kappaB signaling module: temporal control and selective gene activation. Science. 2002;298: 1241–1245. doi:10.1126/science.1071914

122. Lahav G, Rosenfeld N, Sigal A, Geva-Zatorsky N, Levine AJ, Elowitz MB, et al. Dynamics of the p53-Mdm2 feedback loop in individual cells. Nat Genet. 2004;36: 147–150. doi:10.1038/ng1293

123. Nelson DE, Ihekwaba AEC, Elliott M, Johnson JR, Gibney CA, Foreman BE, et al. Oscillations in NF-kappaB signaling control the dynamics of gene expression. Science. 2004;306: 704–708. doi:10.1126/science.1099962

124. Krishna S, Jensen MH, Sneppen K. Minimal model of spiky oscillations in NF-κB signaling. Proc Natl Acad Sci. 2006;103: 10840–10845. doi:10.1073/pnas.0604085103

125. Zhang Z-B, Wang Q-Y, Ke Y-X, Liu S-Y, Ju J-Q, Lim WA, et al. Design of Tunable Oscillatory Dynamics in a Synthetic NF-κB Signaling Circuit. Cell Syst. 2017;5: 460-470.e5. doi:10.1016/j.cels.2017.09.016

126. Baker FC, Driver HS. Circadian rhythms, sleep, and the menstrual cycle. Sleep Med. 2007;8: 613–622. doi:10.1016/j.sleep.2006.09.011

127. Gérard C, Gonze D, Goldbeter A. Dependence of the period on the rate of protein degradation in minimal models for circadian oscillations. Philos Trans Ser A, Math Phys Eng Sci. 2009;367: 4665–4683. doi:10.1098/rsta.2009.0133

128. Johnson CH, Egli M. Metabolic compensation and circadian resilience in prokaryotic cyanobacteria. Annu Rev Biochem. 2014;83: 221–247. doi:10.1146/annurev-biochem-060713-035632

129. Aronson BD, Johnson KA, Loros JJ, Dunlap JC. Negative feedback defining a circadian clock: autoregulation of the clock gene frequency. Science. 1994;263: 1578–1584. doi:10.1126/science.8128244

130. Buhr ED, Takahashi JS. Molecular components of the Mammalian circadian clock. Handb Exp Pharmacol. 2013; 3–27. doi:10.1007/978-3-642-25950-0_1

131. Dunlap JC. Molecular bases for circadian clocks. Cell. 1999;96: 271–290. doi:10.1016/s0092-8674(00)80566-8

132. Mirsky HP, Liu AC, Welsh DK, Kay SA, Doyle FJ 3rd. A model of the cell-autonomous mammalian circadian clock. Proc Natl Acad Sci U S A. 2009;106: 11107–11112. doi:10.1073/pnas.0904837106

133. Ruoff P, Rensing L. The Temperature-Compensated Goodwin Model Simulates Many Circadian Clock Properties. J Theor Biol. 1996;179: 275–285.

134. Caicedo-Casso A, Kang H-W, Lim S, Hong CI. Robustness and period sensitivity analysis of minimal models for biochemical oscillators. Sci Rep. 2015;5: 13161. doi:10.1038/srep13161

135. Goodwin BC. Oscillatory behavior in enzymatic control processes. Adv Enzyme Regul. 1965;3: 425–437. doi:https://doi.org/10.1016/0065-2571(65)90067-1

136. Gonze D, Abou-Jaoudé W. The Goodwin Model: Behind the Hill Function. PLoS One. 2013;8. doi:10.1371/journal.pone.0069573

137. Ruoff P, Vinsjevik M, Monnerjahn C, Rensing L. The Goodwin oscillator: on the importance of degradation reactions in the circadian clock. J Biol Rhythms. 1999;14: 469–479. doi:10.1177/074873099129001037

138. Zhang Y, Chen J, Li G. Analysis of Biological Smooth Oscillators Inspired by the Relay Control Tuning Method. IFAC Proc Vol. 2014;47: 4382–4387. doi:https://doi.org/10.3182/20140824-6-ZA-1003.02092

139. Griffith JS. Mathematics of cellular control processes. I. Negative feedback to one gene. J Theor Biol. 1968;20: 202–208. doi:10.1016/0022-5193(68)90189-6

140. Ananthasubramaniam B, Herzel H. Positive Feedback Promotes Oscillations in Negative Feedback Loops. PLoS One. 2014;9: e104761. Available:

https://doi.org/10.1371/journal.pone.0104761

141. Maeda K, Kurata H. A Symmetric Dual Feedback System Provides a Robust and Entrainable Oscillator. PLoS One. 2012;7: 1–11. doi:10.1371/journal.pone.0030489

142. Kim JK, Forger DB. A mechanism for robust circadian timekeeping via stoichiometric balance. Mol Syst Biol. 2012;8: 630. doi:10.1038/msb.2012.62

143. Hafner M, Koeppl H, Gonze D. Effect of Network Architecture on Synchronization and Entrainment Properties of the Circadian Oscillations in the Suprachiasmatic Nucleus. PLOS Comput Biol. 2012;8: 1–16. doi:10.1371/journal.pcbi.1002419

144. Tyson JJ, Csikasz-Nagy A, Gonze D, Kim JK, Santos S, Wolf J. Time-keeping and decision-making in living cells: Part I. Interface Focus. 2022;12: 20220011. doi:10.1098/rsfs.2022.0011

145. Ruoff P. Temperature-Compensation in Biological Clocks: Models and Experiments. In: Deutsch A, Howard J, Falcke M, Zimmermann W, editors. Function and Regulation of Cellular Systems. Basel: Birkhäuser Basel; 2004. pp. 19–29. doi:10.1007/978-3-0348-7895-1_3

146. Hatakeyama TS, Kaneko K. Generic temperature compensation of biological clocks by autonomous regulation of catalyst concentration. Proc Natl Acad Sci. 2012;109: 8109–8114. doi:10.1073/pnas.1120711109

147. Tyson JJ, Albert R, Goldbeter A, Ruoff P, Sible J. Biological switches and clocks. J R Soc Interface. 2008;5: S1–S8. doi:10.1098/rsif.2008.0179.focus

148. Partch CL, Green CB, Takahashi JS. Molecular architecture of the mammalian circadian clock. Trends Cell Biol. 2014;24: 90–99. doi:10.1016/j.tcb.2013.07.002

149. Hurley JM, Loros JJ, Dunlap JC. Circadian Oscillators: Around the Transcription-Translation Feedback Loop and on to Output. Trends Biochem Sci. 2016;41: 834–846. doi:10.1016/j.tibs.2016.07.009

150. Tomita J, Nakajima M, Kondo T, Iwasaki H. No transcription-translation feedback in circadian rhythm of KaiC phosphorylation. Science. 2005;307:

251–254. doi:10.1126/science.1102540

151. Nakajima M, Imai K, Ito H, Nishiwaki T, Murayama Y, Iwasaki H, et al. Reconstitution of circadian oscillation of cyanobacterial KaiC phosphorylation in vitro. Science. 2005;308: 414–415. doi:10.1126/science.1108451

152. Rust MJ, Markson JS, Lane WS, Fisher DS, O'Shea EK. Ordered phosphorylation governs oscillation of a three-protein circadian clock. Science. 2007;318: 809–812. doi:10.1126/science.1148596

153. Li S, Fang Y. Modelling circadian rhythms of protein KaiA, KaiB and KaiC interactions in cyanobacteria. Biol Rhythm Res. 2007;38: 43–53. doi:10.1080/09291010600832198

154. Kitayama Y, Iwasaki H, Nishiwaki T, Kondo T. KaiB functions as an attenuator of KaiC phosphorylation in the cyanobacterial circadian clock system. EMBO J. 2003;22: 2127–2134. doi:https://doi.org/10.1093/emboj/cdg212

155. Leloup J-C. Circadian clocks and phosphorylation: Insights from computational modeling. Open Life Sci. 2009;4: 290–303. doi:10.2478/s11535-009-0025-1

156. Hernansaiz-Ballesteros RD, Cardelli L, Csikász-Nagy A. Single molecules can operate as primitive biological sensors, switches and oscillators. BMC Syst Biol. 2018;12: 70. doi:10.1186/s12918-018-0596-4

157. Barkai N, Leibler S. Robustness in simple biochemical networks. Nature. 1997;387: 913–917. doi:10.1038/43199

158. Romanel A, Jensen LJ, Cardelli L, Csikász-Nagy A. Transcriptional Regulation Is a Major Controller of Cell Cycle Transition Dynamics. PLoS One. 2012;7: 1–9. doi:10.1371/journal.pone.0029716

159. Waterbury JB. The Cyanobacteria---Isolation, Purification and Identification. In: Dworkin M, Falkow S, Rosenberg E, Schleifer K-H, Stackebrandt E, editors. The Prokaryotes: Volume 4: Bacteria: Firmicutes, Cyanobacteria. New York, NY: Springer US; 2006. pp. 1053–1073. doi:10.1007/0-387-30744-3_38

160. Munkes B, Löptien U, Dietze H. Cyanobacteria blooms in the Baltic Sea: a review of models and facts. Biogeosciences. 2021;18: 2347–2378. doi:10.5194/bg-18-2347-2021

161. Rohrlack T. Low temperatures can promote cyanobacterial bloom formation by providing refuge from microbial antagonists. AIMS Microbiol. 2018;4: 304–318. doi:10.3934/microbiol.2018.2.304

162. Alon U. An Introduction to Systems Biology. 1st ed. An Introduction to Systems Biology. Chapman and Hall/CRC; 2006. doi:10.1201/9781420011432

163. Kurosawa G, Fujioka A, Koinuma S, Mochizuki A, Shigeyoshi Y. Temperature–amplitude coupling for stable biological rhythms at different temperatures. PLOS Comput Biol. 2017;13: 1–16. doi:10.1371/journal.pcbi.1005501

164. Nagao R, Epstein IR, Gonzalez ER, Varela H. Temperature (over)compensation in an oscillatory surface reaction. J Phys Chem A. 2008;112: 4617–4624. doi:10.1021/jp801361j

165. Shinohara Y, Koyama YM, Ukai-Tadenuma M, Hirokawa T, Kikuchi M, Yamada RG, et al. Temperature-Sensitive Substrate and Product Binding Underlie Temperature-Compensated Phosphorylation in the Clock. Mol Cell. 2017;67: 783-798.e20. doi:10.1016/j.molcel.2017.08.009

166. Ni XY, Drengstig T, Ruoff P. The control of the controller: molecular mechanisms for robust perfect adaptation and temperature compensation. Biophys J. 2009;97: 1244–1253. doi:10.1016/j.bpj.2009.06.030

167. Hong CI, Conrad ED, Tyson JJ. A proposal for robust temperature compensation of circadian rhythms. Proc Natl Acad Sci. 2007;104: 1195–1200. doi:10.1073/pnas.0601378104

168. Isojima Y, Nakajima M, Ukai H, Fujishima H, Yamada RG, Masumoto K, et al. CKIε/δ-dependent phosphorylation is a temperature-insensitive, period-determining process in the mammalian circadian clock. Proc Natl Acad Sci. 2009;106: 15744–15749. doi:10.1073/pnas.0908733106

169. Terauchi K, Kitayama Y, Nishiwaki T, Miwa K, Murayama Y, Oyama T, et al. ATPase activity of KaiC determines the basic timing for circadian clock of cyanobacteria. Proc Natl Acad Sci. 2007;104: 16377–16381. doi:10.1073/pnas.0706292104

170. Frank SA. Input-output relations in biological systems: measurement,

information and the Hill equation. Biol Direct. 2013;8: 31. doi:10.1186/1745-6150-8-31

171. Avello P, Davis SJ, Pitchford JW. Temperature robustness in Arabidopsis circadian clock models is facilitated by repressive interactions, autoregulation, and three-node feedbacks. J Theor Biol. 2021;509: 110495. doi:10.1016/j.jtbi.2020.110495

172. Fjeld G, Thorsen K, Drengstig T, Ruoff P. Performance of Homeostatic Controller Motifs Dealing with Perturbations of Rapid Growth and Depletion. J Phys Chem B. 2017;121: 6097–6107. doi:10.1021/acs.jpcb.7b01989

173. Abed RMM, Dobretsov S, Sudesh K. Applications of cyanobacteria in biotechnology. J Appl Microbiol. 2009;106: 1–12. doi:10.1111/j.1365-2672.2008.03918.x